EXPERIMENTS ON NUCLIDES DECAYING BY POSITON EMISSION AND ELECTRON CAPTURE

PROEFSCHRIFT

TER VERKRIJGING VAN DE GRAAD VAN DOCTOR IN DE TECHNISCHE WETENSCHAP AAN DE TECHNISCHE HOGESCHOOL TE DELFT, OP GEZAG VAN DE RECTOR MAGNIFICUS Dr. O. BOTTEMA, HOOGLERAAR IN DE AFDELING DER ALGEMENE WETENSCHAPPEN VOOR EEN COMMISSIE UIT DE SENAAT TE VERDEDIGEN OP
WOENSDAG 24 SEPTEMBER 1958
DES NAMIDDAGS TE 4 UUR

DOOR

JOSEPH KONIJN
NATUURKUNDIG INGENIEUR
GEBOREN TE BERLIJN

Dit proefschrift is goedgekeurd door de
PROMOTOR PROF. DR. A. H. WAPSTRA

Aan mijn Ouders
Aan Mien

CONTENTS

INTRODUCTION

The investigations reported in this thesis may be divided into two groups, one of which is concerned with the elucidation of the decay schemes of ^{57}Ni, ^{52}Mn and ^{86}Y (Chapters 3, 4 and 5), while the other deals with the measurements of the ratio of electron capture to positon emission in some beta transitions (^{22}Na, ^{44}Sc, ^{48}V, ^{52}Mn, ^{58}Co, ^{57}Ni, ^{84}Rb).

The investigation into decay schemes is designed to obtain the excitation energies of nuclear levels, the spins and parities of these levels, and various properties of the transitions between them. Some of these data can be obtained from nuclear reaction measurements (e.g. the measurements of the ^{55}Mn(p,α)^{52}Cr and ^{52}Cr(p,p')^{52}Cr reactions discussed in Chapter 3). This thesis contains only beta and gamma ray spectroscopical investigations.

Data such as the half-life of the radio-active parent, and the number, energies and relative intensities of the beta ray and gamma ray transitions are obtained by means of a scintillation spectrometer, a beta ray spectrometer, and a proportional counter. Energy measurements of beta ray and gamma ray transitions give the differences in energy between nuclear levels. A technique offering valuable help for arranging these energy differences in a level scheme is the so-called "coincidence" analysis which, by using suitable electronic equipment, determines which radiations produced in a given decay occur simultaneously (in coincidence) within the resolving time of the equipment.

Spin and parity assignments can be made only if more information is available. Information about the differences in spins and parities between the initial and final states of a beta ray or a gamma ray transition can be obtained from measurements of:

1) The half-lives, intensities, and energies of the beta ray or gamma ray transitions;

2) The form (shape) of the beta spectral distributions;

3) The intensities of the internal conversion lines of the gamma rays, and their intensities as compared with the gamma ray intensities (conversion coefficients);

4) The angular correlations between successive gamma rays;

5) The electron capture to positon emission ratios in transitions feeding nuclear levels.

The investigation into electron capture to positon emission ratios may yield more interesting information. Theoretically, these ratios should be uniquely determined in allowed and first forbidden transitions, if no Fierz term is present. (In non-unique forbidden transitions, these ratios depend on the values of some nuclear matrix elements and interaction constants).

Measurements of allowed or unique transitions can therefore be used to set limits to the magnitude of the Fierz term and thus yield interesting information on the beta decay interaction constants (see Chapter 2). As discussed below, the influence of this term is very small. Moreover, measurements of electron capture to positon emission ratios can be used to check the degree of forbiddenness of beta ray transitions. In non-unique transitions, such measurements may give information about nuclear matrix elements.

CHAPTER 1

EQUIPMENT FOR NUCLEAR SPECTROSCOPY

The term beta and gamma ray spectroscopy usually covers a wide variety of investigations relevant to the study of beta decay of radio-active nuclei. Though information on nuclear properties can be obtained by means of a great variety of equipment, the beta ray spectrometer is one of the basic instruments, as is indicated by the large number of different types of beta ray spectrometers developed in the past fifteen years. Experience has shown that the use of only one kind of instrument is not sufficient for working out all details of a complicated disintegration scheme, as each instrument has its advantages and its disadvantages. Therefore, apart from the various types of beta ray spectrometers, other instruments have been developed, such as scintillation spectrometers, proportional counters and gamma ray diffraction spectrometers. In addition, methods have been devised for the measurement of coincidences and angular correlations between the different radiations.

§ 1. The magnetic long lens beta ray spectrometer

Most beta ray spectrometers are based upon the deflection of charged particles in a magnetic field. The energies of these particles can be determined by the use of magnetic fields, since the curvature of the trajectory of a beta particle moving in a magnetic field depends upon its momentum. The magnetic beta ray spectroscopes are divided into two fairly distinct groups: "Flat" spectrometers, in which the direction of the magnetic lines of force is mainly perpendicular to the electron paths, and "Helical" (or lens) spectrometers, where the direction of the lines of force is mainly parallel to the electron paths.

The two main characteristics of a spectrometer are the collecting power and the resolution. The problem is to collect as many electrons as possible and to achieve maximum energy resolution. In addition to these two characteristics, a number of other important

features must be considered when choosing a particular type of spectrometer. A review of the various types of beta ray spectrometers is given by SIEGBAHN (Si 55) and by GERHOLM (Ge 56).

The beta ray spectrometer described below was designed by DE RAAD (Ra 54), and was originally intended for the detection of beta and gamma rays produced by nuclear reactions in the Van de Graaff accelerator. The preference for high transmission in conjunction with low price and reasonable dimensions of the apparatus led to the choice of a magnetic lens spectrometer.

§ 2. SOME BASIC RELATIONS IN BETA RAY SPECTROSCOPY

Some basic relations in beta ray spectroscopy are given below. Only simple formulae applicable to a homogeneous field are shown because the spectrometer described in paragraph 3 has a magnetic field that deviates only slightly ($\sim 5\%$) from a homogeneous magnetic field.

An electron (rest mass $= m_o$, charge $= e$, velocity $= v$) moving in a homogeneous magnetic field B in a plane perpendicular to the lines of force describes a circular path with radius ρ. The motion of the electrons is given by the relativistic equation:

$$\frac{d}{dt}\,(m\underline{v}) = -\,e\,[\underline{v} \times \underline{B}] \tag{1.1}$$

which reduces to:

$$\frac{mv^2}{\rho} = Bev \tag{1.2}$$

in the plane perpendicular to the lines of force, where

$$m = m_o/\sqrt{1 - \frac{v^2}{c^2}} \tag{1.3}$$

The momentum is:

$$p = mv = eB\rho \tag{1.4}$$

It is convenient to express the momentum of the electrons in terms of its $B\rho$ value. This value tells us immediately what magnitude of magnetic field and apparatus dimensions are required to keep the electrons within the spectrometer.

In this thesis the momentum and energy are frequently expressed in relativistic units:

$$\eta = p/m_oc = B\rho/1704.45 \tag{1.5}$$

$$W = (E/m_0c^2) + 1 = (E/510.984) + 1 \qquad (1.6)$$

in which E is expressed in keV, and $B\rho$, in gauss cm. The relation between η and W has the simple form:

$$W^2 = \eta^2 + 1 \qquad (1.7)$$

The relation between the energy E in keV and the momentum $B\rho$ in gauss cm is, therefore:

$$E = (510.984 \pm 0.016) \left\{ \sqrt{(3442.2 \pm 0.2) \times 10^{-10}(B\rho)^2 + 1} - 1 \right\} \qquad (1.8)$$

Both short and long coils can be used as magnetic lenses, as has long been known. The close analogy between the optics of light and that of electrons was first pointed out by BUSCH (Bu 26). He showed that the lens formula $1/a + 1/b = 1/f$ could be applied also to magnetic lenses. The electron optics of magnetic lenses can be found in several publications (Ve 51, Si 55, Ge 56).

We shall consider the case in which the magnetic field is homogeneous and the z-axis is in the direction of the lines of force. Using cylindrical co-ordinates, and assuming that the electron starts on the z-axis at $z = 0$ (Fig. 1,1), the path of the electron will be

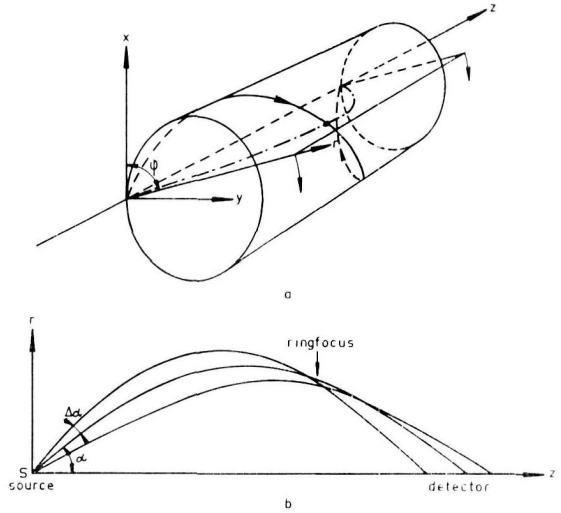

FIG. 1,1

Electron paths in a homogeneous magnetic field.
a: Perspective drawing. b: Projection on r-z plane.

a helix. The radial part of the movement is then easily found to be:

$$r = 2\rho \sin\alpha \sin\left[\frac{z}{2\rho \cos\alpha}\right] \tag{1.9}$$

where

$$\rho = \frac{(B\rho)}{B} = \frac{mv}{eB} \tag{1.10}$$

α being the angle with the z-axis at which the electron is emitted. Evidently the radius of the circle described by an electron with $\alpha = \frac{\pi}{2}$ is ρ. In the r-z plane, the electron path is obviously a sine curve with amplitude $2\rho \sin\alpha$; the half-period is therefore $2\pi\rho \cos\alpha$, corresponding to the distance between source and image.

Lens type spectrometers with an inhomogeneous field are not essentially different from those with a homogeneous field.

§ 3. Technical description of the beta ray spectrometer

A schematic drawing of the beta ray spectrometer is given in Fig. 1,2. The main features of the apparatus are as follows. The spectrometer is of the long lens type, with a magnetic field shaped to obtain low spherical aberration (Zü 48). The magnetic field is given the form as indicated in Fig. 1,2, with decreasing field at the ends of the spectrometer and with a dip in the field ($0.87 \times B_{max.}$) in the middle of the spectrometer, thus reducing the spherical aberration. The principle of ring focusing is used. The spectrometer is able to focus 6.6 MeV beta particles. The transmission of this instrument can easily be varied from about 1 to 5%, and is therefore suitable for measuring beta-gamma ray coincidences.

The magnet consists of two coils, each 33 cm in length, and with a gap of 11 cm between them. The magnet coils are built up from 44 pancakes, each constructed by putting together two layers of 14 turns, wound of double cotton covered copper wire, 6×3 mm^2. The total length of the copper wire is 1750 m. The total resistance of the coils at room temperature is 1.6 Ω. The coils are cooled by 46 copper plates alternately 0.7 and 1.5 mm thick. Along the exterior of the cooling plates, small pipes of 4 mm internal diameter are soldered. These pipes are all connected parallel to the central cooling pipe which is situated in the spacing between the two coils. Oiled paper is stuck on these cooling fins in order to improve the

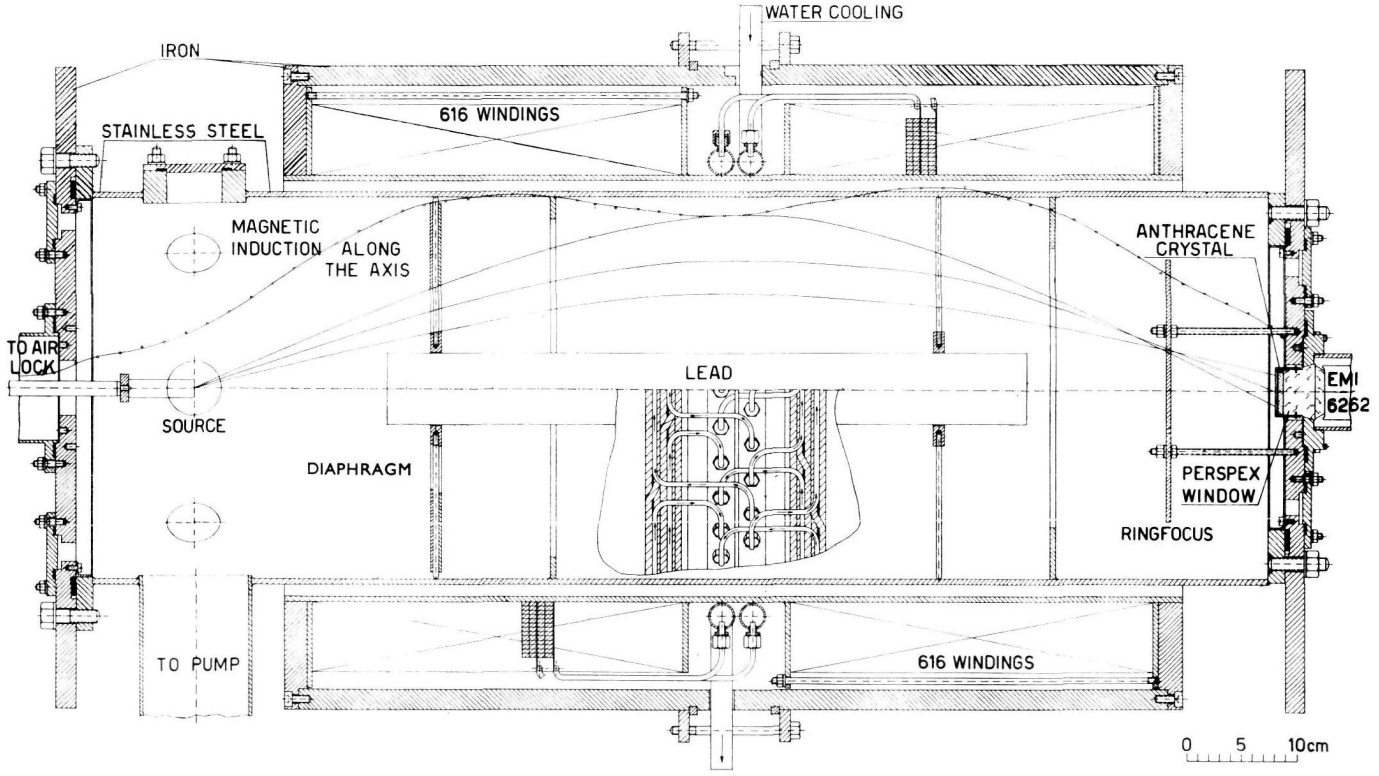

FIG. 1,2

Schematic drawing of the magnetic long lens beta ray spectrometer.

electric insulation. Each winding is thus on one side pressed to a cooling fin. The maximum power of the magnet is 17 kW (90 A, allowing the focusing of 6.6 MeV electrons). The temperature of the cooling water then rises 10 °C if 25 l/min. is consumed. The temperature of the coils stays below 70 °C.

The cooling fins change the self-induction of the lens. Without these fins a value of 0.5 henry is calculated. Fins and magnet coil together form a transformer; the fins form a secondary, short-circuited coil, reducing the impedance of the lens coil. The lens behaves as an impedance of 15 Ω for a 50 cycles alternating current.

The coils are surrounded by an iron yoke. The frame is 18 mm thick and has a diameter of 59 cm; the flanges are 20 mm thick.

The vacuum tank is a cylinder made of austenitic stainless steel. The iron flanges are welded to the tank in such a way that the coils can be pushed round the tank. The end plates of the tank are also made of iron. Their diameter is equal to that of the iron yoke around the coils. Together with this yoke they help to keep the magnetic field within the spectrometer. They decrease the power consumption of the coils for a given magnetic field by only 5%. Their most important function is to ensure that external fields (for instance the earth's magnetic field) are effectively shielded, and that iron masses in the neighbourhood of the spectrometer do not disturb the symmetry of the field. Furthermore, the low, stray magnetic field makes it possible to use photomultiplier tubes in the immediate vicinity of the spectrometer (e.g. for measurements of beta-gamma coincidences). The axis of the tank can be adjusted relative to the magnet coils as described in § 4 of this chapter.

In most vacuum seals O-rings are used. The spectrometer tank is evacuated through an opening 50 mm in diameter, by means of an oil diffusion pump, a mercury diffusion pump and a rotary pump connected in series. The oil diffusion pump is a Philips 0.21.4 with a pumping velocity of 350 l/sec. at 10^{-3} mm Hg pressure, and 50 l/sec. at 10^{-5} mm Hg, and is able to pump against 10^{-2} mm Hg. The mercury diffusion pump is a Leybold HG 12 and has a velocity of 12 l/sec. at 10^{-1} to 10^{-2} mm Hg, and can pump against 5 mm Hg. A pressure of about 10^{-5} mm Hg is obtained in about 30 minutes, starting from atmospheric pressure. The pressure in the tank is measured with the aid of a Penning manometer (Philips gauge).

A vacuum lock is mounted on the end plate (on the left-hand side

in Fig. 1,2). The central rod of the source holder can enter this lock through two O-rings. The vacuum lock is connected to the tank by a vacuum valve with an opening 50 mm in diameter. A small aluminium ring ($\varnothing = 2$ cm), carrying the radio-active source, is fitted between three brass wires (length 60 mm; $\varnothing = 1.5$ mm). These wires are soldered to a brass ring which can be screwed onto the central rod. The source is placed at a distance of 108 mm from the end plate, to minimize reflection and scattering of the electrons. These effects are further reduced by lining the end plates and walls of the tank with aluminium.

A lead cylinder 60 cm in length and 6 cm in diameter is placed on the spectrometer axis in order to prevent gamma radiation reaching the detector directly (see Fig. 1,2). Both ends of this cylinder rest in brass rings supported by four spokes.

The spectrometer rests on an iron trestle. This support does not seriously affect the magnetic field owing to the iron yoke of the magnet. The total weight of the spectrometer is slightly over 1000 kg.

§ 4. Adjustment of the beta ray spectrometer

The source and diaphragms must be carefully aligned to the axis of the magnetic field. Beta spectrometer coils are usually wound directly on the vacuum tank, especially for long lens beta ray spectrometers. In this case, the diaphragms are adjusted relative to the tank. The baffles can also be fastened to the tank. This has certain advantages. A leak in the tank is now easier to repair since the magnetic coils can be readily removed. This arrangement is also simpler and easier to construct. The tank can be adjusted relative to the magnetic field axis by two sets of bolts, fixed on both sides of the magnet yoke. Supporting plates, welded to the vacuum tank, rest on these bolts. The construction is based on the so-called cinematic principle. A fifth bolt regulates the position of the vacuum tank relative to the direction of the z-axis.

The following experimental procedure was followed in order to align the magnetic field axis to the source and diaphragms. A 2 kV electron gun was used as an electron source. The position of electrons produced by this gun were rendered visible by means of a zinc sulphide screen placed in the tank. This screen was made by dredging zinc sulphide on a glass or perspex plate, wetted with plastic glue.

Essentially, the electron gun consists of a tungsten wire, the cathode, brought under a tension of —2 kV, behind a little hole in an earthed metallic plate, the anode. In order to obtain a divergent electron beam with a top angle of about 30°, the cathode was constructed of 8 tungsten wires (diameter: 50μ) at a distance of 3 mm behind a hole of 6 mm in a brass plate. The electron gun was mounted on the rod of the source holder. The influence of possible anisotropy of the emitted electrons can be studied by revolving the source rod. The emission current of the cathode was about 1 mA.

By pushing a ring diaphragm along the z-axis it was found that the electrons leaving the source at an angle α larger than 29° get stuck in the tank. The minimum diameter of the beam at the place of the detector was 3 cm. At the corresponding position of the ring diaphragm, the ring focus was 108 mm from the end plate. This distance was found to be critical within 3 mm.

The tank was so adjusted that the ring focus was concentric with the z-axis. A photograph of the ring focus is shown in Fig. 1,3, in which the internal conversion electrons from the F line in the decay of Th B have been used. The current was adjusted in the following way: First the spectrum was measured with a diaphragm at the place of the ring focus. The current was adjusted to the top counting rate. The focus diaphragm was then removed and replaced by a sensitive film. The diameter of the source was 3 mm. The external diameter of the ring focus was found to be 79 mm, and the thickness of the ring, 6 mm. The eight radial spokes in Fig. 1,3 are the supports of the central lead cylinder (see § 3 of this chapter).

§ 5. Construction of a helical baffle

It is sometimes necessary to separate positons from negatons, as for instance, when investigating isotopes which decay by positon emission as well as by negaton emission (e.g. the decay of ^{84}Rb, Chapter 6), or when both internal conversion lines and a positon distribution are present (e.g. the decay of ^{86}Y, Chapter 5). Such a separation can be performed by making use of the fact that positons and negatons describe helical paths with opposite spirality. To this end, a helical baffle was constructed, a brief description of which is given below.

In § 2 of this chapter, the path of an electron moving in a homogeneous magnetic field along the z-axis has been given by equation

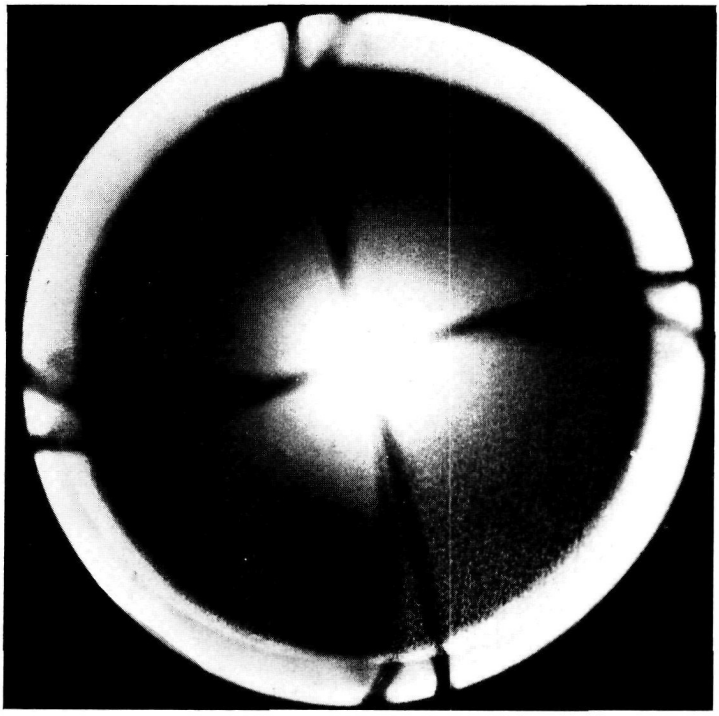

FIG. 1,3

Photograph of the ring focus. The beta ray spectrometer was adjusted to the maximum of the internal conversion peak of the F line in the decay of Th B.

Opposite page 18

(1.9). The projections on the different planes of such a trajectory are shown in Fig. 1,4. The electron paths, as given by equation

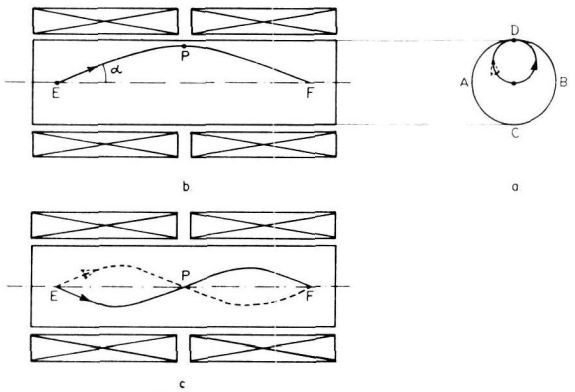

FIG. 1,4

The trajectory of an electron, moving in a homogeneous magnetic field along the z-axis. The projections of the electron path on the different planes are represented by a drawn line, that of a positon by a dotted line.

a: Projection on the r-φ plane. b: Projection on the r-z plane through D-C. c: Projection on the r-z plane through A-B.

(1.9), are situated on cylindrical surfaces, enclosing the z-axis as generating line. The drawn line in Fig. 1,4 represents the path of an electron with momentum η, the intersected line, that of a positon with the same momentum, and the same direction of the magnetic field. The two trajectories of the electron and the positon will meet half-way, intersecting each other at an angle of 2α.

When a plate is placed at point P in the direction of the electron path (making angle α with the z-axis), the electrons pass whereas the baffle stops the positons. Several plates around the circumference of a circle perpendicular to the z-axis at P are required to obtain a complete separation of positons and electrons. The construction of the baffle is shown by a perspective drawing in Fig. 1,5.

The plates are mounted on two brass rings; each plate is connected by one pin to each of the rings. One ring is fastened to the tank, the other can turn relative to the first, thus enabling all the plates to be brought into the right position, simultaneously. The second ring is turned by means of a small lever. The position of the baffles is indicated by a scale on one of the rings.

The plates of the baffle are made of 1 mm thick brass; 1 mm thick aluminium covers are riveted to each side of the brass plate

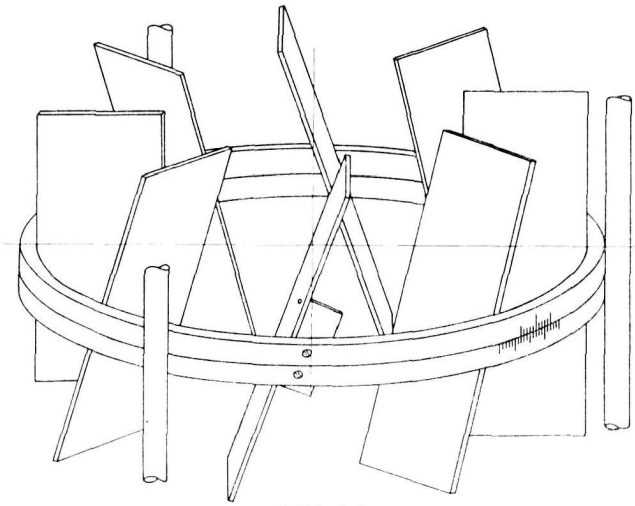

FIG. 1,5

Perspective drawing of the helical baffle. The plates are mounted on two brass rings; one ring is fastened to the tank, the other can turn relative to the first in order to bring the plates into the right position.

in order to reduce the scattering of electrons on the plates, which are thick enough to stop all beta rays with energies of less than 2 MeV. The plates can be replaced by thicker ones if necessary. The baffle contains 32 plates, each 75 mm in height and 60 mm in width. Each brass ring (14×14 mm^2; diameter 315 mm) is cut into two half circles, in order to enable the baffle to be mounted in the spectrometer without removing the other baffles.

The adjustment of the helical baffle is done experimentally by recording the internal ^{137}Ba conversion electrons with different baffle positions. The transmission of the beta ray spectrometer was reduced by only about 20% after mounting the baffle, whereas the intensity with the magnetic field in the "wrong" direction was smaller than 0.01% of that with the field in opposite direction. The resolution of the spectrometer was only slightly affected.

§ 6. The electron detector and gamma ray detector of the beta ray spectrometer

The electron detector of the beta ray spectrometer is an anthracene scintillation counter. The cylindrical crystal (height: 5 mm; diameter: 4 cm) is optically coupled to a photomultiplier, E.M.I. 6262, by means of a short perspex window.

The crystal is thick enough to stop all electrons with energies of less than 1.2 MeV. A few formvar films, rendered conductive by evaporating aluminium on their backing, cover the anthracene crystal. These foils prevent the evaporation of anthracene in vacuum and provide a reflective layer on the crystal.

A ring of perspex, fixed with a bayonet-joint, presses the crystal against the perspex window. Between this ring and the crystal a rubber ring is inserted to prevent the crystal breaking. The perspex light guide is about 5 cm in length.

The photomultiplier, fitted into a socket with spring suspension, is mounted in a mu-metal shield. The E.M.I. 6262 photomultiplier was chosen since it is less sensitive to external magnetic fields than electrostatically focused photomultipliers.

The magnetic stray field has some influence on the amplification of the multiplier. The variation in amplification as a function of the energy of the focused electrons was found by recording the position of the Compton edge produced by ^{60}Co gamma rays. The result of this measurement is shown in Fig. 1,6. The half-width

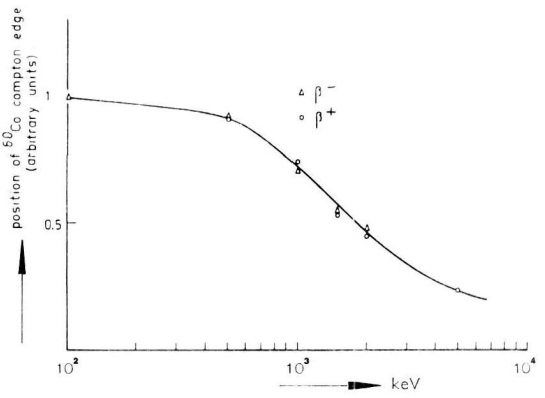

FIG. 1,6

Influence of the magnetic stray field on the amplification of the E.M.I. 6262 photomultiplier tube in the anthracene scintillation detector of the beta ray spectrometer.

of a mono-energetic electron line of 624 keV (from the decay of ^{137}Cs to ^{137}Ba) was recorded as 30%, in this arrangement. If necessary the half-width could probably be decreased to about 20%, provided the perspex window was more carefully designed.

In order to check whether the efficiency of the anthracene counter

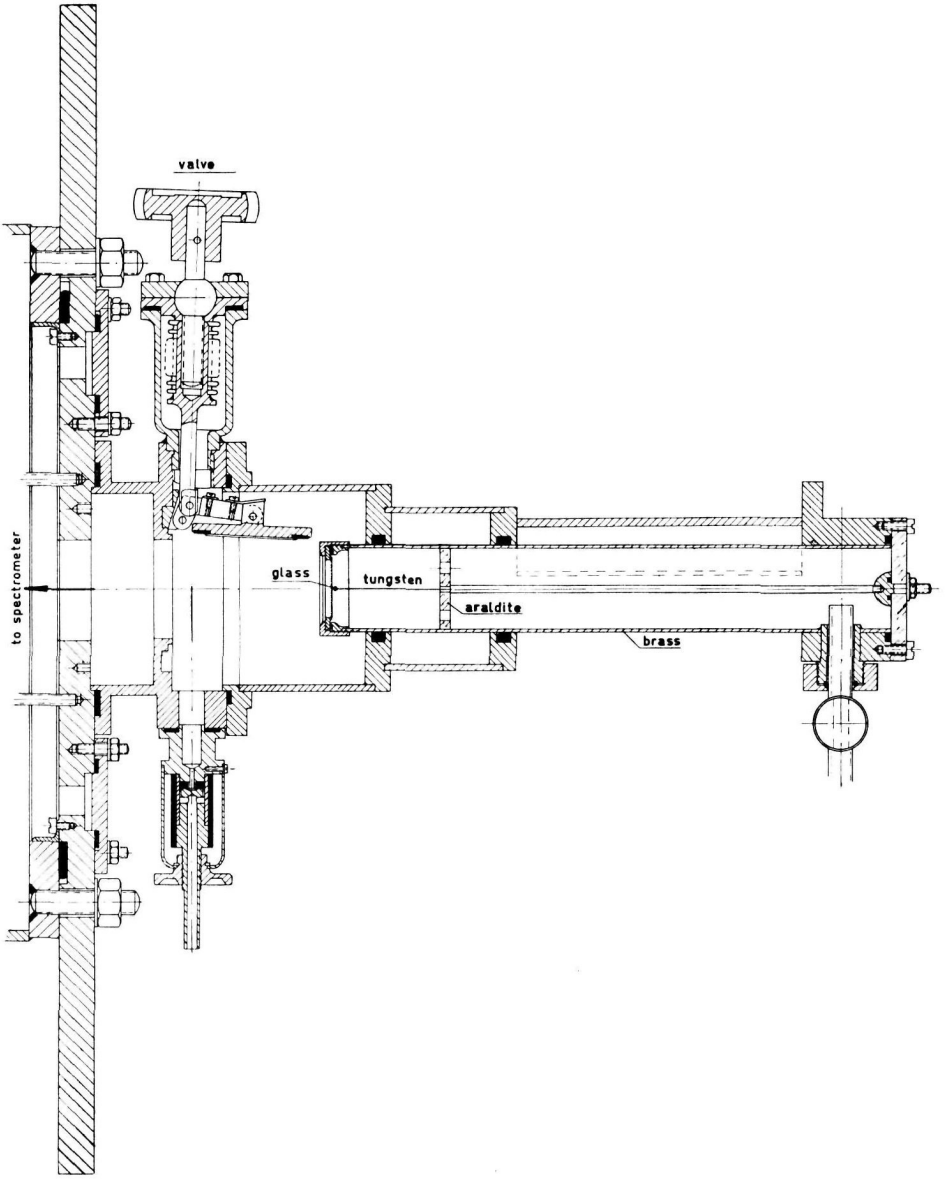

FIG. 1,7

Schematic drawing of the Geiger-Müller counter.

is independent of the electron energy, the anthracene scintillation counter can be replaced by a Geiger-Müller counter. G.M. counters are also more suitable for counting low energy electrons. Pulses originating from such electrons are comparable with the noise of the multiplier, giving either a large background or (if small pulses are cut off) reduced efficiency. This photomultiplier noise can be reduced by cooling the photomultiplier; another solution is to replace the anthracene counter by a G.M. counter provided with a thin window. A G.M. counter was therefore constructed. The arrangement is schematically shown in Fig. 1,7. The G.M. counter can be inserted in the spectrometer through a vacuum lock. The counter is filled with a mixture of 90% argon and 10% alcohol from a storage bottle.

This G.M. counter has not yet been used, since, in the experiments described in this thesis, the anthracene scintillation counter has certain advantages. It allows of a much higher counting rate than the G.M. counter. Furthermore, the rise time of the output pulses at the anode of the multiplier is of the order of 3×10^{-8} sec. (as compared with about 10^{-6} sec. in G.M. counters). This is especially important in making fast coincidence measurements. Moreover, the anthracene scintillation counter pulses can be selected according to pulse height, making it possible to reduce the background by using a differential discriminator.

In order to measure beta-gamma ray coincidences a gamma ray scintillation counter was constructed by HEYLIGERS (No 57). The scintillation counter was mounted behind the beta sample. A source holder was constructed in which a cylindrical NaI(Tl) crystal (dimensions $3/4'' \times 1''$) is placed near the source. The crystal is optically coupled to a Dumont 6292 photomultiplier by means of a perspex light guide in order to avoid placing the photomultiplier in a magnetic field.

The arrangement is schematically shown in Fig. 1,8. The light guide is mounted between small pieces of billiard cloth thus giving a small contact surface.

The shape of the light guide can be computed in such a way that the light emitted from the crystal undergoes successive internal total reflections until it is collected at the photocathode of the photomultiplier tube (Ge 55). The refractive index of perspex is 1.49 so that the critical angle α, with respect to air, is 42.15°. The dimensions of the instrument at hand forced us, however, to take a

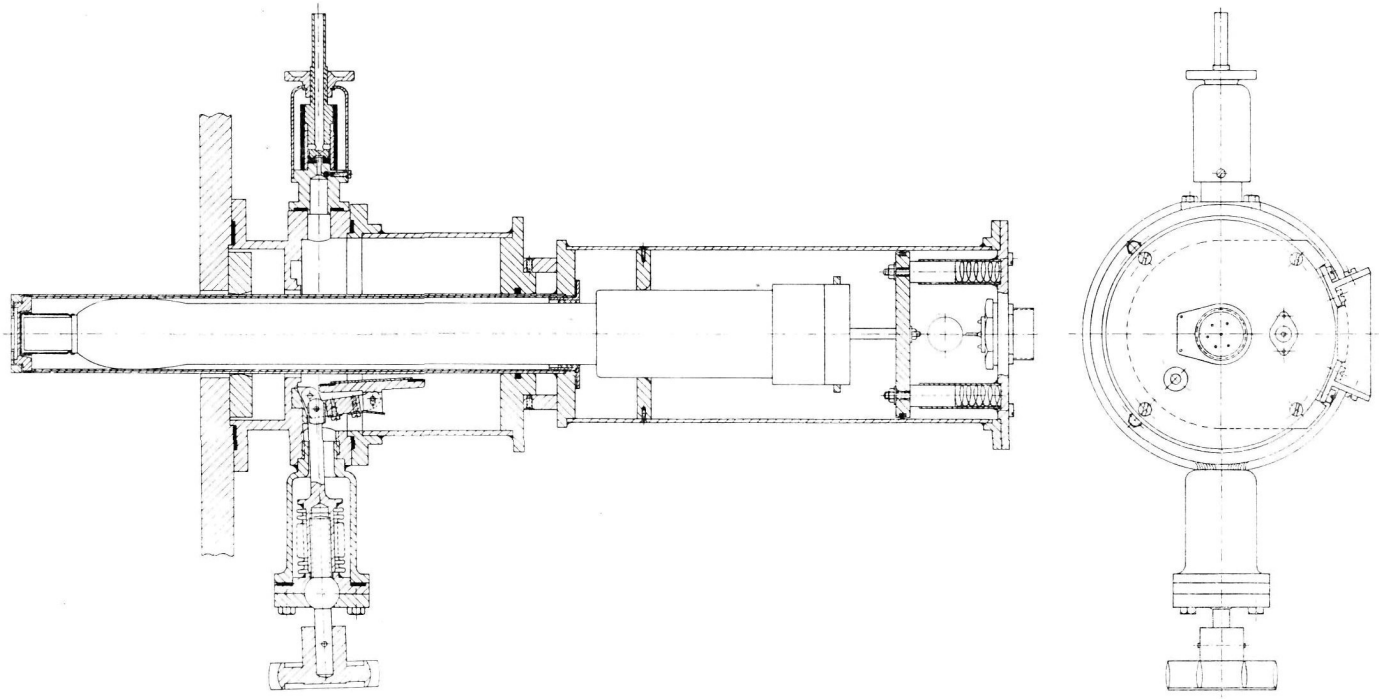

FIG. 1,8

Schematic drawing of the crystal arrangement in the beta-gamma ray coincidence equipment.

value for the minimum angle of reflection slightly lower (2°) than the total reflection angle. Moreover, in practice, the direction of that part of the light trapped in the light guide is changed by scattering in such a way as to be able to escape; another part of the light is absorbed within the light guide. Nevertheless the light collection using our 29.5 cm long light guide is only 42% less than without a light guide, a result which compares well with the loss of 40% found by GERHOLM (Ge 55), for a 22.5 cm long light guide.

The optical arrangement is mounted in an air-tight brass tube which can be inserted through the source vacuum lock of the magnetic beta ray spectrometer. The chamber containing the crystal is at atmospheric pressure. The brass tube is closed at the source side with 1 mm Dural, in order to avoid excessive absorption of gamma rays. The source is mounted on a ring which can be fixed on the source holder as shown in Fig. 1,8. The distance between source and crystal is 7.5 mm.

The influence of the magnetic stray field of the beta ray spectrometer on the amplification of the Dumont 6292 photomultiplier is tolerable. A measurement of this influence is shown in Fig. 1,9.

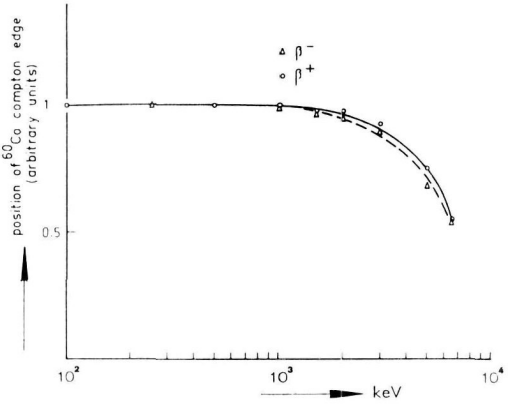

FIG. 1,9

The influence of the magnetic stray field on the amplification of the gamma ray scintillation spectrometer as a function of the energy of the focused electrons.

§ 7. THE STABILIZING CIRCUIT FOR THE MAGNET CURRENT

An electronic current regulator for the beta ray spectrometer has been built. The current necessary for the magnetic field is obtained from a 16 kW motor—d.c. generator with a maximum cur-

rent of 90 A. The way of stabilizing the current is rather like the one followed by VERSTER (Ve 51).

The momentum of the focused electrons is nearly proportional to the current through the magnet coils. This current can therefore conveniently be used as a measure for the momentum.

The magnet current is measured and stabilized by means of a compensator. A constant voltage supply (85A2) of 85 volts causes a constant current i of 1.2 mA through a standard resistance of 70 k Ω. This current is calibrated with a Philips GM 4569 standard cell, by compensating the E.M.F. of this cell with the voltage drop of i through a 1 k Ω resistance. The current i gives a voltage drop V_1 of 1200 mV (see Fig. 1,10) over the four step decade resistance R_1 with steps of 100, 10, 1 and 0.1 Ω.

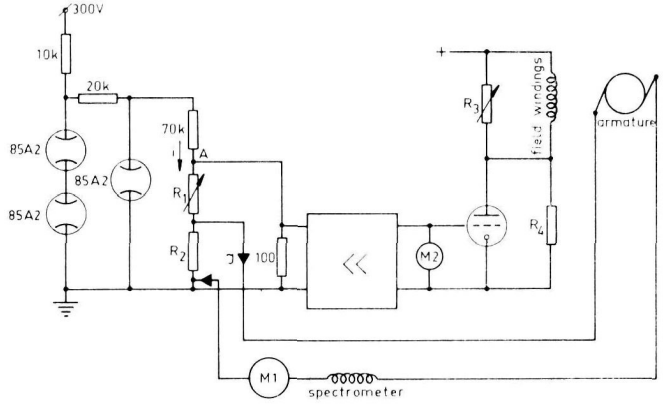

FIG. 1,10

Schematic circuit of the electronic current regulator.

The voltage drop V_2 of the magnet current I across the manganin resistance R_2 is compensated with the reference voltage V_1. The resistance R_2 can be switched to 0.19087, 0.048380 and 0.012568 Ω for current ranges of I: 1.5 — 6.25 A, 6.25 — 25 A, and 25 — 100 A. These resistors are cooled in oil.

When the voltage at point A in Fig. 1,10, $V_A = V_1 + V_2$, is kept zero, then

$$I = R_1 \frac{i}{R_2} \qquad (1.11)$$

R_1 is proportional to I since i is independent of the value of R_1 when $V_A = 0$ (thus i and R_2 being constant).

Point A is also grounded with a resistance of 100 Ω. As demonstrated below the output voltage V_A is nearly proportional to the relative variation $\triangle I/I$ (without this resistor, V_A would be proportional to $\triangle I$).

Let $V_A \neq 0$; then, $V_A = i_1 \times 100$, where i_1 is the current through the 100 Ω resistance. Thus,

$$i_1 = \triangle I \frac{R_2}{R_1 + 100} \approx \triangle I \frac{R_2}{R_1} = \frac{\triangle I}{I} i \qquad (1.12)$$

(since R_1 is chosen large compared with 100 Ω), and therefore,

$$V_A = \frac{\triangle I}{I} i \times 100 \qquad (1.13)$$

The voltage $V_A = 100$ μV is obtained when $\triangle I/I = 0.1\%$, according to the last formula.

The current stabilization is based on the following principle: The voltage V_A is amplified and changes the exciting current of the generator by means of four transmitting valves, PE 1/100, feeding about 15% of the maximum field current (4.5 A), until V_A is zero. The other part of the field current is shunted by two electric radiator elements, R_4.

A certain current setting of the spectrometer is now achieved in the following way: The decade resistance R_1 is set at the desired value. The magnet current I is then adjusted by regulating the exciting current with a variable field resistance R_3 and shunting the field windings (see Fig. 1,10) to approximately the correct value. Electronical stabilization will do the rest. Variations of about 10% in the magnet current can be adjusted by electronical stabilization.

The voltage V_A is amplified in the following way: The *D.C.* voltage is transformed by a Brown converter into an *A.C.* voltage. The Brown converter is operated by a 70 cycles *RC* oscillator with variable frequency regulation (EL 49). The block voltage obtained is amplified in an *A.C.* amplifier, and then rectified. Use was made of a selective network in the feed back loop, consisting of a double *T* or notch-filter, in order to obtain selective amplification. The resonant frequency of the filter and the frequency of the oscillator are both given by the expression $\nu = \frac{1}{2\pi RC}$. The frequency of the converter is matched to that of the filter ($\nu = 69$ cycles). The

polarity of the signal at the end of the amplifier is restored by means of contact 5 of the converter, grounding one half of every cycle. A double diode sets limits (6 V) to the positive and negative peaks of the cycle, making this apparatus insensitive to overloading.

The total amplification for the resonant frequency of the selective network is about 40,000 $\times$. However, a factor of 2 in the gain is lost when determining the polarity of the signal at the output. In the integrator circuit another factor of 2 is lost so that the amplification is reduced to 10,000 $\times$. A micro ammeter in the integrating circuit acts as a zero indicator. A voltage V_A of 100 μV corresponds to 5 μA in this meter, when the overall gain is 10,000 $\times$. A stability of $\triangle I/I = 0.1\%$ is then obtained. The correct adjustment of the *RC* time of the integrating circuit is important and provides a useful anti-hunt circuit. The *D.C.* signal coming from the integrating circuit is amplified by a factor of 10 by means of a *D.C.* amplifier and supplied to the four PE 1/100 transmitting valves, each of which gives a maximal anode current of 250 mA.

§ 8. The calibration of the beta ray spectrometer

The beta ray spectrometer was calibrated several times. The transmission of the spectrometer was found from beta-gamma ray coincidence measurements.

We shall consider the measurement of a sample emitting N electrons of the same momentum, $B\rho$, per unit of time. The top counting rate of the measured line divided by N will be called the *transmission* T (this quantity is smaller than the *solid angle* defined by α (see Fig. 1,1) due to the helical baffle and the ring focus baffle). Let the *resolution* R be the relative width of the line at half height, $R = \triangle B\rho/B\rho$. We shall assume that, as usual, the spectrum is plotted in the divided way (i.e. $N/B\rho$ is plotted against $B\rho$). Experimentally, it is found that the surface of the line is then equal to 1.25 $\times$ TRN. The beta spectrometer constant 1.25 $\times$ TR should be equal to the quantity $\Omega\beta$ defined in Chapter 3, § 3, which is essentially equal to the number of coincidences per measured gamma ray.

The beta ray spectrometer was adjusted in such a way that $\alpha_{max.} = 23°$ and $\alpha_{min.} = 13°$ giving a solid angle of 2.74% of 4π, except in the last measurement VI, mentioned in Table 1,I in which the limits were 23° and 17°. The coincidence was measured for two adjustments of the ring focus. The values of $\Omega\beta$ were found to be

$(5.5 \pm 0.1) \times 10^{-4}$ and $(1.95 \pm 0.01) \times 10^{-4}$, the widths of the ring focus being set at 20 mm and 8 mm, respectively. The resolutions $\triangle B\rho/B\rho$ of the spectrometer were, with these adjustments, $(3.2 \pm 0.1)\%$ and $(2.0 \pm 0.1)\%$, giving the following values for the transmission T: $(1.38 \pm 0.05)\%$ and $(0.78 \pm 0.04)\%$, respectively. The value of $T = 1.38\%$ is slightly lower than the maximum possible, being 80% of the subtended solid angle given above; this may be explained by some electrons still hitting other baffles. (This 80% arises from the fact that the helical baffle was mounted in the spectrometer, see § 5 of this chapter). In Fig. 1,11 the K

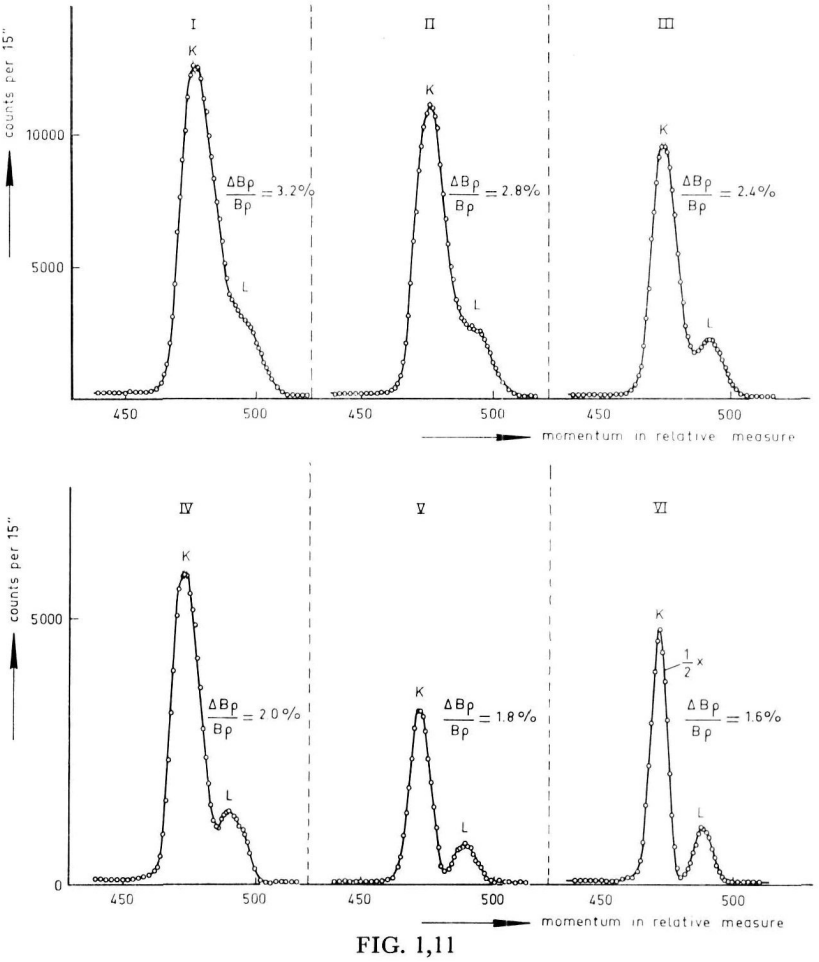

FIG. 1,11

The K and L conversion lines occurring in the decay of ^{137}Cs, shown for different adjustments of the spectrometer. (See also Table 1,I).

and L conversion lines from the decay of ^{137}Cs are shown for different adjustments of the beta ray spectrometer. The transmissions and resolutions following from these measurements are collected in Table 1,I.

TABLE 1,I

Calibration of the magnetic long lens beta ray spectrometer.

Spectrometer adjustment	Solid angle (in % of 4π)	Width of ring focus (in mm)	Resolution ($R = \triangle B\rho/B\rho$ in %)	Transmission T	
				from $\beta-\gamma$ coincidences (in %)	from Fig. 1,11 (in %)
I	2.74	20	3.2	1.38 ± 0.05	1.38
II	2.74	16	2.8		1.22
III	2.74	12	2.4		1.05
IV	2.74	8	2.0	0.78 ± 0.04	0.65
V	2.74	4	1.8		0.36
VI	1.62	4	1.6		0.26

TABLE 1,II

Energy calibration of the magnetic long lens beta ray spectrometer.

Source	Line	$B\rho$ (in gauss cm)	Energy (in keV)	Spectrometer range					
				I		II		III	
				R_1 (in Ω)	$B\rho/R_1$	R_1 (in Ω)	$B\rho/R_1$	R_1 (in Ω)	$B\rho/R_1$
Th B	E	1110	98.8	598.6	1.854				
Th B	F	1388.44	148.1	751.5	1.848				
Th C″	G	1596	189	864.9	1.845	220.6	7.235		
^{203}Hg	K_{279}	1618.1	193.6	864.5	1.872	223.5	7.240		
Th B	H	1697	210	916.5	1.852	233.3	7.274		
Th B	I	1753.91	222.2	947.3	1.851	241.8	7.254		
Th B	J	1811.11	234.6	982.0	1.844	249.8	7.250		
Th B	J_a	1824	237	987	1.848				
^{203}Hg	L_{279}	1942.8	264	1045.5	1.858	268.5	7.236		
^{203}Hg	M_{279}	1996	276	1074	1.858	276	7.232		
Th B	J_c	2027	283			279	7.265		
^{198}Au	K_{412}	2222.6	328.7			301.7	7.367		
^{198}Au	L_{412}	2503.6	397			340.4	7.355		
Th C″	L	2607.17	422.8			357.7	7.289		
Th C″	M	2891	495			397.1	7.280		
^{137}Cs	K_{661}	3381.28	624.2			464	7.287	123.2	27.45
^{137}Cs	L_{661}	3498	656			480.8	7.276		
^{32}P	end point	7203	1708			983.6	7.323	262.5	27.44

The energy calibration of the beta ray spectrometer was carried out using conversion lines and continuous beta spectra from the decays of ^{32}P, ^{137}Cs, ^{198}Au, ^{203}Hg and Th(B + C′ + C″). The results are given in Table 1,II which shows that the calibration constant is almost independent of the energy, thus confirming the fact that the iron has little influence on the calibration (compare § 3). The calibration constant drifted slowly about 2% in the course of four years; it was, therefore, checked before and after each measurement.

The negaton distribution in the decay of ^{32}P was measured in order to test whether the efficiency of the beta counter was sufficiently independent of the energy. The Kurie plots (Na 52) of two different measurements are shown in Fig. 1,12 a and b. The

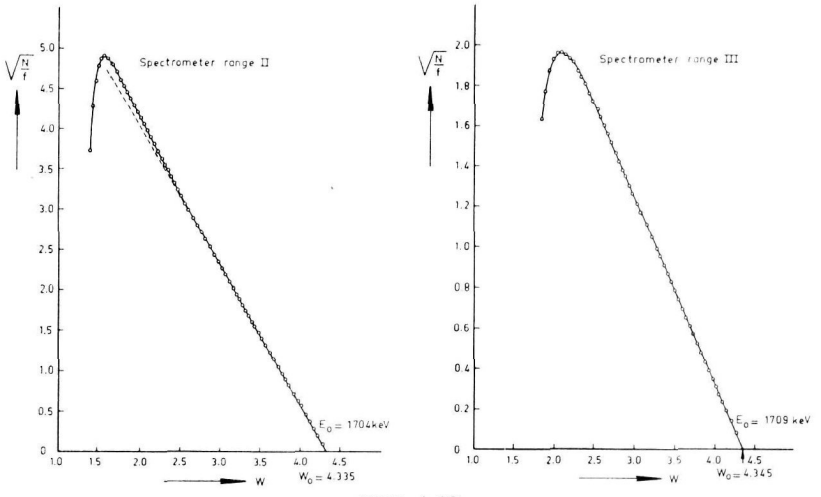

FIG. 1,12

Kurie plots of the negaton distribution of ^{32}P. The energy in units of m_0c^2 is indicated by W.

a: Spectrometer range II. b: Spectrometer range III.

straightness of these Kurie plots is checked by plotting the function $G = \frac{1}{W_0 - W}\sqrt{\frac{N}{f}}$ as a function of W (see Fig. 1,13); W being the energy, W_0 the end point energy of the negaton distribution, and f the Fermi function. The function G should be constant if the Kurie plot is straight. The results, presented in Fig. 1,13, show almost exclusively small variations in this function at the high energy limit, which may, however, at least be partly explained by

the fact that no correction was made for the finite resolution. The influence of scattered electrons on the shape of the Kurie plot is shown to be small, by comparing a normal run with one in which the beta source was turned upside down.

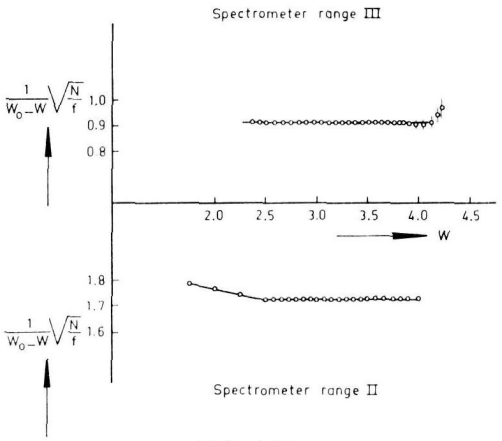

FIG. 1,13

The function $G = \frac{1}{W_0 - W}\sqrt{\frac{N}{f}}$, as obtained from the measurement depicted in Fig. 1,12, is plotted as a function of W.

In order to check the performance of the instrument some properties of known decay schemes were measured. The most convenient lines to use for calibration are the internal conversion lines from ^{137}Cs, since it has a relatively simple disintegration scheme (e.g. Si 55) and a relatively long half-life (33 years). It emits one gamma ray of 661.65 $\pm$ 0.15 keV. The measurement VI depicted in Fig. 1,11 yields a value of 4.55 $\pm$ 0.14 for the K/(L + M) ratio, in good agreement with GRAVES et al. (Gr 52), who obtained the value 4.64. Measurements of the decay of ^{203}Hg yield the following results: The end point of the continuous negaton distribution was found to be 219 $\pm$ 5 keV. The conversion coefficients of the 279 keV gamma ray transition were $\alpha_K = 0.185 \pm 0.025$ and $\alpha_L = 0.047 \pm 0.007$, the K/(L + M) ratio was 2.44 $\pm$ 0.10, and the L/M ratio, 3.8 $\pm$ 0.2. All these results are in agreement with earlier results, which are listed in the Nuclear Data Sheets (Nu 58).

§ 9. SOURCE TECHNIQUE AND CONVERTERS

In beta spectroscopy thin films are used as backings for sources, and the active material itself has to be prepared as a thin layer on

the backing foil, both in order to diminish the influence of absorption and back-scattering of the beta rays. Absorption decreases the energy of the beta particles and back-scattering increases the number of low energy beta rays, producing a distortion in the experimentally observed beta spectrum.

It is therefore advantageous when the source material has as high a specific activity as possible; it is preferable wherever possible to prepare the material carrier-free. An impression of the importance of thin sources and backings when studying the shape of beta spectra is shown by the investigation of Wu and Feldman (Wu 49).

The variation of the amount back-scattering with thickness and atomic weight of the back-scatterer for beta radiation was studied by Engelkemeir et al. (En 51). Backings should preferably be made from materials with low atomic numbers. The backings are, therefore, commonly made from organic compounds such as zapon, formvar, collodium and nylon. The sources described in this thesis were mostly deposited on zapon foils or formvar films. These materials are good insulators. The thin films were therefore rendered conductive by evaporating aluminium onto their backing; this prevents the sources charging themselves when emitting beta rays. The backings of aluminium have usually a resistance of a few megaohms.

Formvar films are made from a solution of 500 mg formvar (polyvinyl formal) in 100 cc dichlorethylene or chloroform. A glass plate, a little larger than the film desired, is vertically inserted in this solution. The glass plate is slowly drawn out of the solution and after drying put into water. The water then immediately penetrates between the formvar film and the glass. The film will float on the water surface and can be removed with a frame made, for instance of copper wire. The film is then dried under an infrared lamp. It is important for the glass plate to be clean. Not every glass plate is suitable for this kind of work; photographic glass plates are preferable. The films will release more quickly when they are breathed on before being put into the water. By careful treatment it is possible to obtain quite homogeneous films down to a thickness of about 300 Å.

Zapon films are produced by putting one or more drops of zapon lacquer (cellulose nitrate dissolved in amyl acetate or acetone) on a surface of distilled water. The drops are then immediately spread

out by surface tension forces into a thin film over the water surface. The film, after a few minutes drying, can be removed with a frame as described above.

The radio-active material is often dissolved in acid which attacks formvar films. These films are therefore covered with a polystyrene layer in the following way: The glass plate, after being drawn out of the formvar solution and dried, is dipped in a solution of 400 mg polystyrene in 100 cc benzene. After drying the complex foil is removed in the same way as described above.

Droplets of a solution containing the radio-active material are brought onto the foils by means of a pipet and subsequently dried under an infra-red lamp. Samples made in this way are not uniform as a rule, especially when extended sources are necessary; this can be improved by putting a drop of insulin diluted with water on the film spot before preparing the source, the excess insulin being removed with a pipet. The drop of radio-active material then spreads uniformly over this wetted area.

Aluminium foils of about 6 μ thickness are also useful as backing material. Such foils are advantageous when making sources by evaporating the radio-active material in vacuo onto them. This is somewhat wasteful of radio-active material, but if this material is plentiful, and a chemical compound suitable for this purpose can be found, a thin and uniform source can thus be prepared.

In this connection "radiators" may also be considered. Radiators are thin foils used for producing photo-electrons (external conversion) by a gamma ray source. The energies of the gamma rays can be determined from the energy of these photo-electrons. Elements of high atomic number are used as converters, since the photo-electric cross-section per unit mass increases approximately as Z^5 (Z = charge of the nucleus) (He 44).

The difficulties met with the external conversion are similar to those in internal conversion line measurements; the photo-electrons loose energy by absorption in the converter, and a continuum is present because of Compton electrons. The size of the source (which here means the converter) should be fairly large for intensity reasons. The basic features of the external conversion method have been considered by DEUTSCH et al. (De 44). Investigations have later been made for the purpose of increasing the accuracy, by studying the effects of electron straggling in the converter (see HORNYAK et al., Ho 49).

Lead radiators of 113 mg/cm² to about 34 mg/cm² were obtained by rolling a small lead plate to the desired thickness. Thinner lead radiators may be obtained by evaporating lead on a foil of aluminium.

Uranium converters have been made in a way similar to that described by GLOVER and BORELL (Gl 55). Drops of a 5% uranyl nitrate solution in ethyl alcohol with 1% zapon lacquer are brought onto an aluminium foil or plate by means of a brush. The strokes with the brush must all be in the same direction. The painted foil is heated for about 15 min. at 500°C to convert the nitrate into the oxide. After cooling, the plate is wiped off with a piece of soft cloth to remove any oxide particles which do not adhere to the plate. This must be done very carefully in order not to damage the foil or the coating. The following coat is painted in a direction perpendicular to the first coating. This procedure is repeated until the layer is of the desired thickness. The mean thickness of the uranium converter, obtained in this way, is determined by weighing. Three radiators having thicknesses of 4 mg/cm², 2 mg/cm² and 1 mg/cm², respectively, were made in this way.

As an example, the high energy external conversion electrons produced by the 986 keV and 1314 keV gamma rays occurring in the decay of ^{48}V, are shown in Fig. 1,14. The lead radiator used

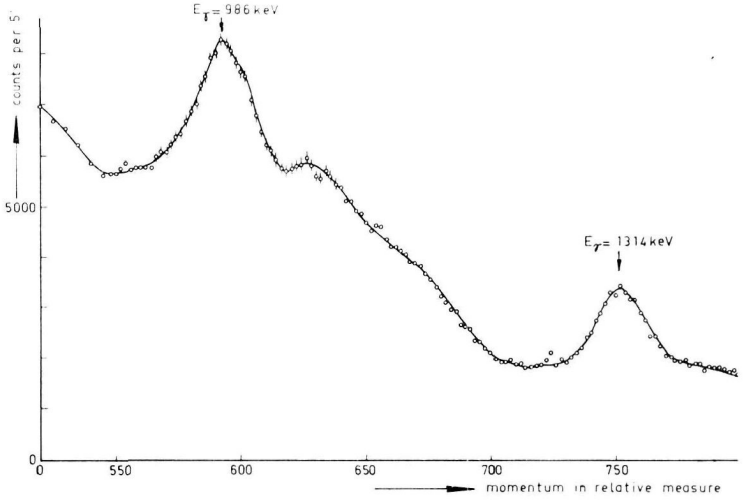

FIG. 1,14

High energy region of the external conversion spectrum of ^{48}V, recorded in the beta spectrometer by means of a lead converter (34 mg/cm²).

in this measurement had a thickness of 34 mg/cm². Part of the gamma ray spectrum recorded with a 113 mg/cm² thick lead converter is shown in Fig. 1,15. The measurements depicted in this figure show the influence of using radiators with different diameters (4 mm and 20 mm respectively).

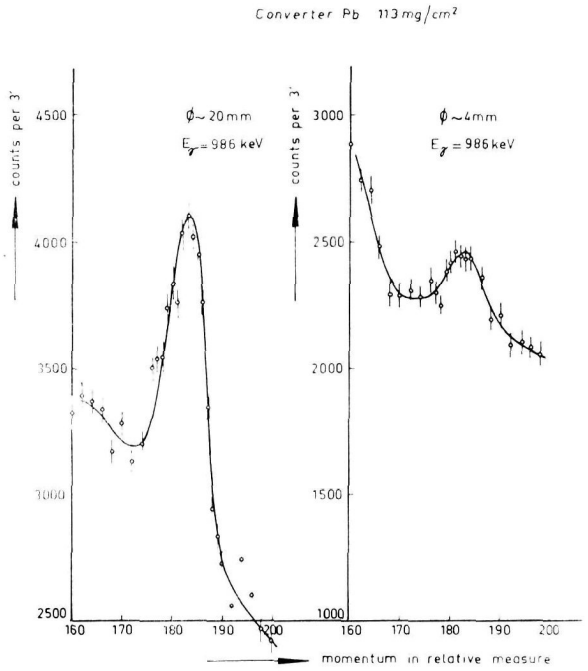

FIG. 1,15

The photo-electrons produced by the 986 keV gamma ray transition (in ^{48}V) in a lead converter (113 mg/cm²). These measurements show the influence of using radiators with different diameters.

§ 10. Other equipment

Apart from the beta ray spectrometer, other instruments such as scintillation spectrometers, proportional counters and coincidence spectrometers, are frequently used in the experiments.

The scintillation counter and its equipment is extensively described by Van Nooijen (No 58), and will only briefly be mentioned here. Use was made of cylindrical NaI(Tl) crystals (dimensions: $1'' \times 1^1/_2''$) in the standard Harshaw mounting, Dumont 6292 photomultipliers, linear pulse amplifiers and single channel pulse height analyzers. The spectrometer was calibrated for energy and

intensity measurements using sources emitting at least two gamma rays of known energy and intensity, (^{22}Na, ^{24}Na, ^{88}Y, ^{137}Cs, ^{203}Hg). The dependence of the detection efficiency of the crystal on the distance between source and crystal was taken into account (Ri 55).

The proportional counter was designed and calibrated by HAGEDOORN (Ha 58), who gives a detailed description of the counter. The ratio of electron capture to positon emission, ε/β^+, has been determined for several nuclei with this proportional counter, used in a coincidence arrangement with a scintillation spectrometer. The proportional counter was filled with krypton or xenon. The pulses from the scintillation counter were delayed in order to take into account the delay in the proportional counter. The resolving time of the coincidence circuit was 2.5×10^{-6} sec. The source was mounted in the proportional counter in such a way that the solid angle was nearly 2π. The number of coincidences between positons and X-rays measured in the proportional counter and gamma rays detected in the scintillation spectrometer can then be represented by the following formula:

$$\frac{N_c}{N_\gamma} = \frac{1}{2}\beta^+ + \frac{1}{2}(1 - \beta^+)\frac{\varepsilon_K}{\varepsilon}\omega_K A \qquad (1.14)$$

where N_c is the number of coincidences, N_γ the number of gamma quanta counted by the scintillation counter, β^+ the percentage of positon emission, $\varepsilon_K/\varepsilon$ the ratio of K capture to total electron capture, A the efficiency of the proportional counter for K X-rays and ω_K the fluorescent yield of the K shell. The proportional counter was calibrated by means of beta-gamma ray coincidence measurements from the decay of ^{198}Au (see Chapter 3).

Gamma-gamma coincidences and angular correlations were measured by means of two single channel NaI(Tl) scintillation spectrometers in a fast-slow coincidence arrangement with a resolving time of 3×10^{-8} sec. For a detailed description of this arrangement, reference is made to VAN NOOIJEN (No 58).

Beta-gamma coincidence measurements were also made in the beta ray spectrometer. The gamma ray scintillation spectrometer used for these experiments is described in § 6 of this chapter. This set up was used in a slow coincidence arrangement with a resolving time of about 6×10^{-7} sec. The arrangement was calibrated by measuring beta-gamma ray coincidences in the decay of ^{198}Au (see Chapter 3).

CHAPTER 2

BETA DECAY THEORY

§ 1. Spectrum shape

The beta decay is pictured as a change of the state of a nucleon together with the emission of a beta particle and a neutrino. The theory of beta radio-activity has been constructed in analogy with the theory of electromagnetic radiation. The beta interaction is, however, considerably more complicated than the electromagnetic one, firstly, since two particles are emitted instead of one, and, secondly, since the interaction Hamiltonian is unknown. The beta decay theory that was first developed by Fermi (Fe 34) and later by Konopinski and Uhlenbeck (Ko 41) and by Greuling (Gr 42) (see also Si 55, for instance). The modern beta decay theory is based on the neutrino hypothesis advanced by Pauli, and on the Dirac equations for leptons and nucleons, and assumes the interaction Hamiltonian to be a linear combination of the relativistic invariants *S*, *V*, *T*, *A* and *P*. Each of the last symbols represents the scalar product of combinations of nucleon and lepton wave functions which, considered separately, have the transformation properties of scalars, vectors, tensors, axial vectors and pseudoscalars in the four dimensional (Minkowski) space.

The theory provides a general classification of the beta transitions in terms of degrees of forbiddenness: beta transitions can be allowed, first forbidden, second forbidden, and so on (see below). The number of beta particles with energy W in an interval dW emitted per second in a single n^{th} forbidden transition is:

$$N_{\pm}(W)dW = (g^2/2\pi^3)\,\eta W\, q^2\, F_o\,(\mp Z, A, W)\, S_n/\,(n!)\, dW \quad (2.1)$$

in which g is the Fermi coupling constant (analogous to e in the electromagnetic case), W_o the energy release (in units of m_oc^2) involved in the nuclear transition, η the momentum of the electron and q ($=W_o - W$) the neutrino momentum in units of m_oc, F_o the Fermi function, and S_n the shape factor for n^{th} forbidden transitions.

The upper sign in equation (2.1) refers to positon, the lower to negaton emission.

Equation (2.1) is written in this way since in allowed transitions ($n = 0$) the shape factor is, in a good approximation,

$$S_o = 1 \mp 2b/W \qquad (2.2)$$

the so-called Fierz term. The constant b is zero if only scalar and tensor, or only vector and axial vector interactions are present. The spectrum has the "statistical shape" $\sim \eta^2 q^2$ for small nuclear charges, modified by F_o for the Coulomb effect for higher Z. Experimentally it is found that also for first forbidden transitions, the shape factor is nearly constant (except for unique first forbidden transitions mentioned below). In general, S_n will depend upon the energy, the interaction constants and the nuclear matrix elements. In allowed spectra the shape factor is uniquely determined if $b = 0$: from equation (2.1) and (2.2) it then follows that:

$$[N_{\pm}(W)/F_o(\mp Z, A, W,)\ \eta\ W]^{1/2} = Kq = K\ (W_o - W) \quad (2.3)$$

in which K is independent of the energy W. A plot of the function at the left-hand side of equation (2.3) versus the energy (a *Kurie plot*) is therefore linear. This plot is very useful in analysing complex beta spectra. In non-unique first forbidden spectra the shape factor is in most cases only slightly dependent on W. The Kurie plot will therefore yield, in good approximation, a straight line.

In unique n^{th} forbidden transitions [$\triangle J = n + 1$, parity change $(-1)^n$] all matrix elements are zero except one. The shape is unique unless a Fierz term is present. S_n is then strongly energy dependent and becomes

$$\text{in 1st forbidden spectra: } (\triangle J = 2, \text{ yes})\ S_1 \sim \eta^2 + q^2$$

$$\text{in 2nd forbidden spectra: } (\triangle J = 3, \text{ no})\ S_2 \sim \eta^4 + \frac{10}{3}\ \eta^2 q^2 + q^4.$$

§ 2. Transition probabilities

The total transition probabilities for beta emission are obtained by integration of formula (2.1). The function $f = \int_1^{W_o} \eta q^2 F_o W dW$ therefore becomes important. This quantity f times the half-life t is called the reduced or comparative half-life; it is a good measure

for the degree of forbiddenness. Values of $\log ft$ can be determined most easily from nomograms (Mo 51).

The total transition probability for electron capture from the X shell (X = K, L_{II}, M_I etc.) is:

$$N_x = (g^2/2\pi^3)\, q^2_x\, S_{n(x)} \tag{2.4}$$

The momentum of the neutrino in this process is $q = W_o - W_x$, where W_x is the electron binding energy in the X shell. In allowed transitions is:

$$S_o \sim (1 + 2b/W_x) \tag{2.5}$$

The Fierz term parameter b is identical with that defined in equation (2.2). A ft value can also be defined for electron capture (see reference Mo 51).

TABLE 2,I

Classification of the beta transitions.

Order of forbiddenness	Change in J	Change in parity	$\log ft$
Allowed	0, 1	no	5 ± 1
(Super allowed)	0	no	3.5 ± 0.5
(1-forbidden)	1	no	may be > 6
1st forbidden	0, 1	yes	7 ± 1
Unique 1st forbidden ..	2	yes	$\log f_1 t = 8.5 \pm 0.5$
2nd forbidden	2, 3	no	~ 13
3rd forbidden	3, 4	yes	~ 18

Empirically, it is found that the $\log ft$ values can be divided into the groups given in Table 2,I. The shape factor in unique first forbidden transitions is $S_1 \sim \frac{1}{12}(\eta^2 + q^2)$. Averaging over the spectrum gives $\overline{S_1} \sim \frac{1}{24}(W_o^2 - 1)$, and $f_1 t$ is, therefore, a better measure for the reduced half-life than ft, if f_1 is defined as $\frac{1}{24}(W_o^2 - 1)$f. [An even better definition for f_1 is given by Davidson Jr (Da 51)].

§ 3. Interactions

The beta interactions S, V, T and A occurring in allowed transitions may be further classified as follows:

(a) By the nuclear spin selection rules.

(a1) The Fermi selection rules are characteristic for S and V interactions. They require no spin change and no parity change in the nuclear transition.

(a2) The Gamow-Teller selection rules, for T and A interactions, require a spin change of one unit ($|\triangle J| = 1$) and no parity change.

(b) By the directional correlation between electron and neutrino. The correlation function is

$$W(\vartheta) \sim 1 + a(v/c)\cos\vartheta \qquad (2.6)$$

if $b = 0$ (b being the Fierz term parameter). The electron-neutrino correlation measurements are relied upon to distinguish between the scalar and vector forms of the Fermi coupling (F) and between the tensor and axial vector forms of Gamow-Teller coupling (GT). In V and T interactions, a is positive, which means that the electrons and the neutrinos are preferably emitted in the same direction. In S and A interactions, the reverse situation applies.

Recently, it has been found useful to introduce two kinds of neutrinos characterized by their *helicity* (Le 57): The helicity of a neutrino is defined as $+1$ (right-handed), if the spin and momentum are parallel (in a right-handed co-ordinate system), and as -1, if the spin and momentum are anti-parallel (left-handed). Neutrinos of opposite helicity will be denoted by ν_R and ν_L respectively. The corresponding anti-neutrinos $\bar{\nu}_R$ and $\bar{\nu}_L$ have opposite helicities with regard to ν_R and ν_L.

Due to the angular correlations between electron and neutrinos described above, the electrons emitted together with neutrinos of a well-defined helicity will also be polarized in the direction of their motion. It can be derived that the relative helicities of a negaton and an anti-neutrino (or of a positon and a neutrino) emitted in a beta decay process are:

(b1) The same in S and T interactions

(b2) Different in V and A interactions.

These classifications, (a) and (b), are summarized in Table 2,II.

TABLE 2,II

Classification of the beta decay interactions occurring in allowed transitions.

Selection rules	Change in J $\lvert\triangle J\rvert$	Change in parity	Same helicity (ν and β^+)	Opposite helicity (ν and β^+)
Fermi (F)	0	no	S	V
Gamow-Teller (GT)	1	no	T	A

We now introduce the parameters C_x^y ($x = S, V, T, A, P$ and $y = R, L$) being a measure of the relative strength of the forms of the different interactions in which right- and left-handed neutrinos are emitted. This gives us in allowed transitions a total of eight parameters: C_i^R and C_i^L (i stands for S, V, T and A); thus for example, C_S^R describes a right-handed neutrino together with a right-handed positon etc. (in accordance with Table 2,II).

If parity were conserved in beta decay, the emitted electron would not be longitudinally polarized. Wu et al. (Wu 57) discovered, however, that parity is not conserved in beta transitions, and slightly later Frauenfelder et al. (Fr 57) were the first to observe the longitudinal electron polarization; many other laboratories have confirmed this result.

The general expression for the beta ray polarization in allowed transitions is:

$$P_{\beta^\pm} = \mp \frac{v}{c} \frac{\{|C_S^L|^2 - |C_S^R|^2 - |C_V^L|^2 + |C_V^R|^2\}|M_F|^2 + \{|C_T^L|^2 - |C_T^R|^2 - |C_A^L|^2 + |C_A^R|^2\}|M_{GT}|^2}{\{|C_S^L|^2 + |C_S^R|^2 + |C_V^L|^2 + |C_V^R|^2\}|M_F|^2 + \{|C_T^L|^2 + |C_T^R|^2 + |C_A^L|^2 + |C_A^R|^2\}|M_{GT}|^2} \quad (2.7)$$

in which M_F and M_{GT} are the nuclear matrix elements involved in F and GT coupling respectively. The electron polarizations measured so far are almost equal to $\pm \frac{v}{c}$ with an accuracy of about 10%. Thus, negatons are polarized left-handed (—v/c), positons, right-handed (+v/c). This experimental result is in agreement with the following combination:

$$C_S^L = C_T^L = C_V^R = C_A^R = 0 \quad (2.8)$$

§ 4. The Fierz term parameter and ε/β^+ branching ratios in allowed transitions

The Fierz term parameter b as defined in equation (2.2) has the following form:

$$b = \gamma \frac{\mathrm{Re}\,\{C_S^{R*}\,C_V^R + C_S^{L*}\,C_V^L\}|M_F|^2 + \mathrm{Re}\,\{C_T^{R*}\,C_A^R + C_T^{L*}\,C_A^L\}|M_{GT}|^2}{\{|C_S^R|^2+|C_S^L|^2+|C_V^R|^2+|C_V^L|^2\}|M_F|^2 + \{|C_T^R|^2+|C_T^L|^2+|C_A^R|^2+|C_A^L|^2\}|M_{GT}|^2} \quad (2.9)$$

in which $\gamma = \sqrt{1-(\alpha Z)^2} \approx 1$, α being the fine structure constant.

In fact, the modification (2.8) automatically cancels any Fierz interference terms, no matter what values C_S, C_V, C_T, C_A are found to have. The accuracy of the polarization experiments, however, still allows considerable errors in the determination of the Fierz term so that one can only conclude that $b = 0.0 \pm 0.2$. Measurements of the shape of allowed and unique forbidden spectra show that $|b|$ was smaller than 0.15 (Ma 52), and an analysis of reduced half-lives of Fermi transitions gave a similar limit (Sh 56).

The best evidence that the Fierz term parameter is small or even zero is obtained from measurement of the ratio of K capture to positon emission in the same transitions. This ratio can be written:

$$\varepsilon_K/\beta^+ = (\varepsilon_K/\beta^+)_o \times \frac{1 + 2b\,W_K^{-1}}{1 - 2b\,\overline{W^{-1}}} \quad (2.10)$$

$\overline{W^{-1}}$ is the average value of W^{-1} over the continuous beta spectrum. According to § 2, the ratio $(\varepsilon_K/\beta^+)_o$ does not depend on b. Evidently, the ratio ε_K/β^+ is very sensitive to the actual value of b.

Values of $(\varepsilon_K/\beta^+)_o$ have been calculated by Zweifel (Zw 57) for certain values of Z. Values $\{(\varepsilon_K/\beta^+)_o\ (W_o - 1)^4\ Z^{-4}\ (W_o + 1)^{-2}\}$ show much less variation as a function of Z and W_o than $(\varepsilon_K/\beta^+)_o$. Therefore, this combination is given as a function of Z in Fig. 2,1. This figure can be used to obtain accurate interpolated values of $(\varepsilon_K/\beta^+)_o$. A rapid estimate of $(\varepsilon_K/\beta^+)_o$ can be obtained from Fig. 2,2 which has been constructed using the interpolation method explained above.

The Fierz term parameter b can be derived from experimental values for ε_K/β^+ by the following relation which can easily be derived from formula (2.10):

$$b = \frac{1}{2}\,\frac{\varepsilon_K/\beta^+ - (\varepsilon_K/\beta^+)_o}{(\varepsilon_K/\beta^+)_o + (\varepsilon_K/\beta^+)\,\overline{W^{-1}}} \quad (2.11)$$

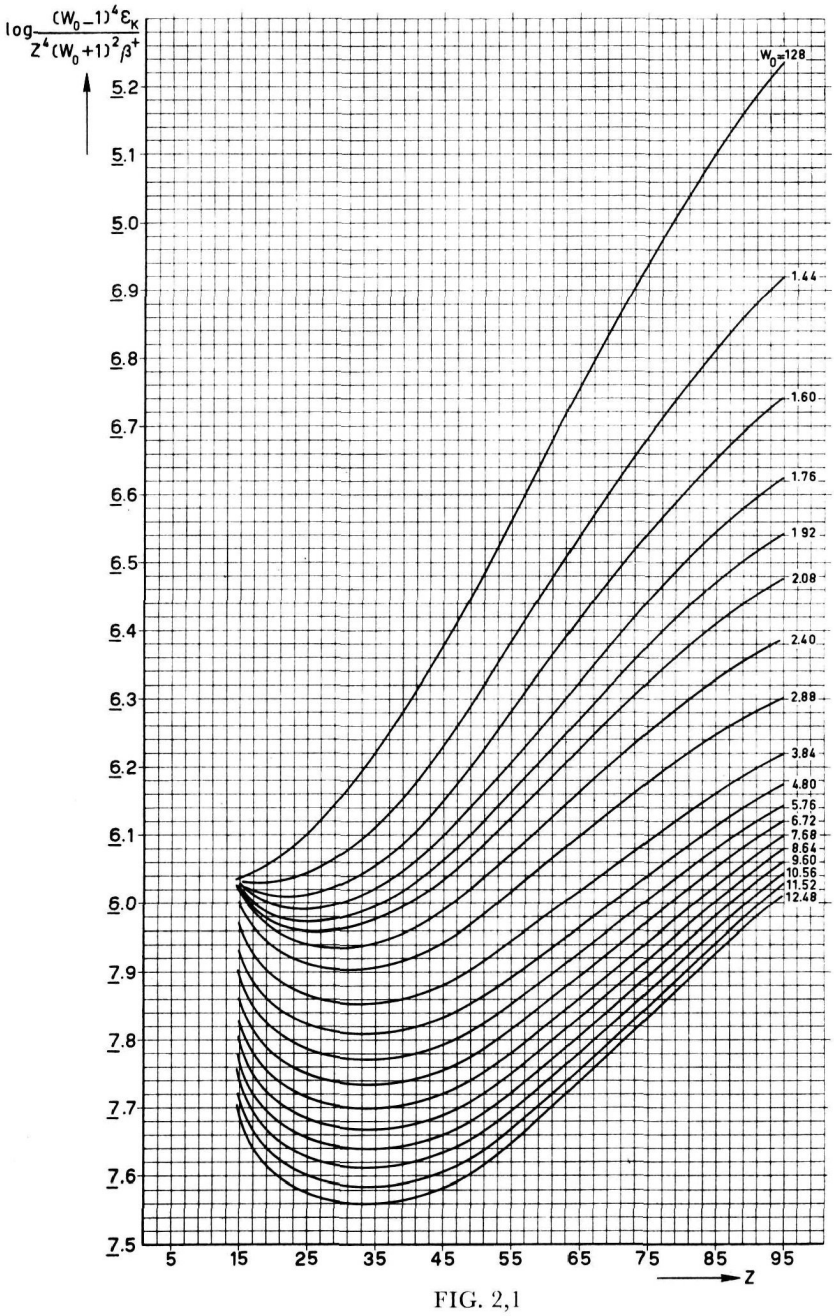

FIG. 2,1

$\{(\varepsilon_K/\beta^+)_o\ (W_o - 1)^4\ Z^{-4}\ (W_o + 1)^{-2}\}$ as a function of Z (i.e. charge of the radio-active daughter nucleus) for the indicated values of W_o.

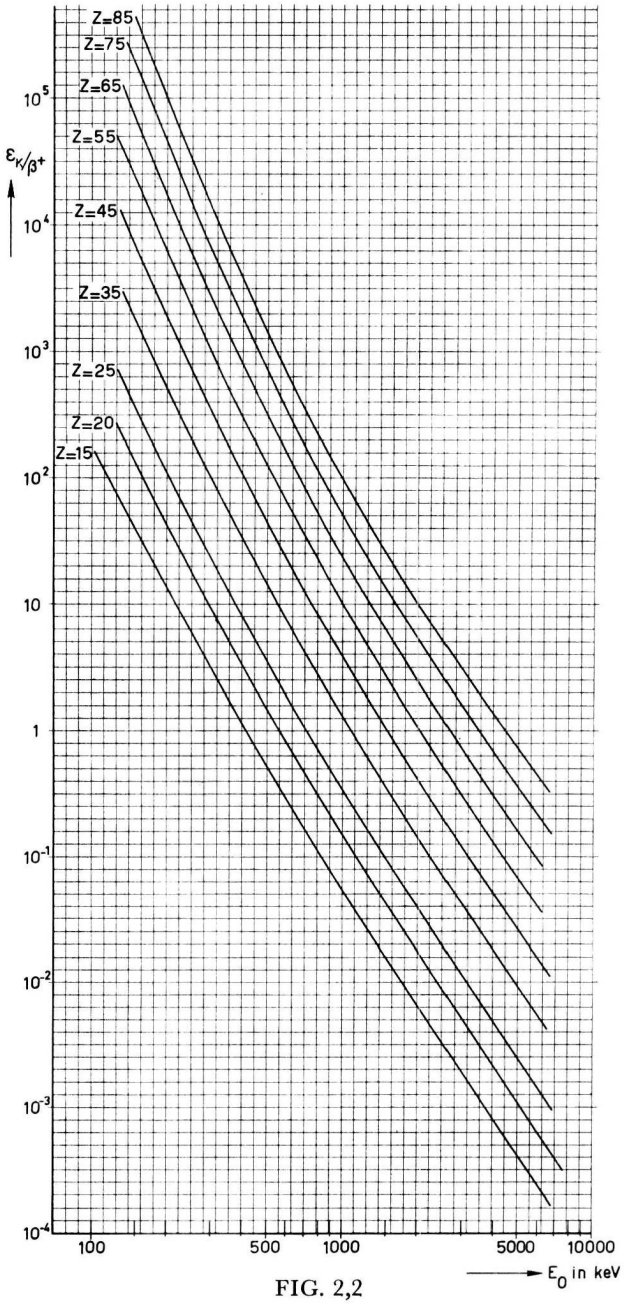

FIG. 2,2

The $(\varepsilon_K/\beta^+)_o$ branching ratios as a function of W_o with Z (charge of daughter nucleus) as a parameter. These values are obtained from the plots in Fig. 2,1.

The result of such measurements, described in Chapter 6, showed the Fierz term parameter to be very small.

For the sake of completeness it should be mentioned that the recent experiments by GOLDHABER et al. (Go 58) indicate that $C_V^L \approx -C_A^L$, and that all other coefficients are zero.

§ 5. ε_K/β^+ BRANCHING RATIOS IN 1ST FORBIDDEN BETA TRANSITIONS

In principle, the Fierz term parameter for T and A interaction can also be determined by measuring K capture to positon emission ratios in unique first forbidden transitions. A measurement on ^{126}I (see Chapter 6) again yields a parameter $|b|$ which is approximately equal to zero. Assuming $|b| = 0$ the electron capture to positon emission ratio for unique first forbidden transitions ($\triangle J = 2$, yes) is:

$$\varepsilon_K/\beta^+ = (\varepsilon_K/\beta^+)_o \times [q_K^2 / \overline{(\eta^2 + q^2)}] \approx (\varepsilon_K/\beta^+)_o \times \frac{2(W_o + 1)}{W_o - 1} \tag{2.12}$$

In first forbidden transitions with spin change of one unit ($|\triangle J| = 1$) this ratio (in the event that only V and A interactions are present, and $C_V^R = C_A^R = 0$) becomes approximately:

$$\frac{\varepsilon_K/\beta^+}{(\varepsilon_K/\beta^+)_o} = \left[\frac{v_{1a} + v_1 + a_1}{v_{1a} + v_1 - a_1}\right]^2 \tag{2.13}$$

The quantities v and a are combinations of interaction constants and matrix elements:

$$v_1 = C_V^L \int i\underline{r} \; ; \; a_1 = C_A^L \int \underline{\sigma} \times \underline{r} \; ; \; v_{1a} = \xi^{-1} \, C_V^L \int \underline{\alpha} \, ,$$

in the notation used by KONOPINSKI (Ko 41); $\xi = \alpha\hbar Z/2m_ocR$ in which Z and R are the charge and radius of the daughter nuclei and α is the fine structure constant. These quantities v and a have the same order of magnitude. Theoretically, it is to be expected that v_{1a} and a_1 are approximately equal. Then the ε_K/β^+ ratios for first forbidden transitions will be approximately equal to those for allowed transitions. A small deviation from $v_{1a} = a_1$, however, introduces a large variation in the ε_K/β^+ ratio.

In first forbidden transitions with spin change $|\triangle J| = 0$, the electron capture to positon emission ratio becomes equal to the allowed ratio using the same approximations as used in equation (2.13). A few measurements of these ratios in first forbidden transitions are discussed in Chapter 6.

CHAPTER 3

SOME MEASUREMENTS ON THE RADIO-ACTIVE DECAY OF ^{52}Mn

§ 1. Introduction

^{52}Mn decays to ^{52}Cr by electron capture and positon emission with a half-life of 5.6 days (Bu 54, Ba 55, Ka 56, Ru 56). The β^+ spectrum has been reported as simple; the end point was found to be 582 $\pm$ 15 keV (Pe 46). Three gamma rays have been observed with the following energies: γ_1: 0.73 MeV; γ_2: 0.94 MeV; γ_3: 1.45 MeV (Pe 46, Ke 54). The total conversion coefficients have been reported to be $(3.0 \pm 0.3) \times 10^{-4}$, $(1.8 \pm 0.2) \times 10^{-4}$, and $(7.2 \pm 0.7) \times 10^{-5}$ respectively, showing that all the three gamma rays are E2 transitions (Ke 54). The angular correlation measurements (Sl 55) for all gamma pairs and experiments on oriented nuclei (Hu 56) support the level scheme shown in Fig. 3,1. The spin of the ^{52}Mn ground state is 6^+ (B 58).

The excited states of ^{52}Cr have been studied by Mazari et al. (Ma 57) through the ^{55}Mn (p, α) ^{52}Cr reaction and by an investigation of inelastic proton scattering from chromium. Excited states in ^{52}Cr have been found at 1433 $\pm$ 5 keV, 2368 $\pm$ 5 keV, 2648 $\pm$ 8 keV, 2767 $\pm$ 8 keV, 2965 $\pm$ 8 keV, and 3161 $\pm$ 8 keV.

The reported gamma rays of 0.94 and 1.45 MeV in the decay of ^{52}Mn agree well with these energies. The gamma energy measurement of Peacock and Deutsch (Pe 46), giving a value of 734 $\pm$ 15 keV for the lowest energy gamma ray, places the 6^+ level at 3102 $\pm$ 16 keV, a value which does not agree with any of the excitation energies of the levels reported by Mazari et al.

Another value for the energy of this state can be found by using the decay data of the isomeric 21 min. level in ^{52}Mn, which decays by a 2631 $\pm$ 15 keV positon transition (Ar 56) to the 1433 keV state in ^{52}Cr or, alternatively by a 392 $\pm$ 8 keV gamma ray (Os 47) to the ^{52}Mn ground state. Together with energy of the positon spectrum from this ground state reported above, the energy of the

6^+ level is found to be 3090 ± 25 keV in agreement with the value mentioned above.

The capture-positon branching ratio has been determined by Good et al. (Go 46) and Sehr (Se 54) who found values for ε/β^+ of 1.86 ± 0.17 and 2.01 ± 0.22, respectively.

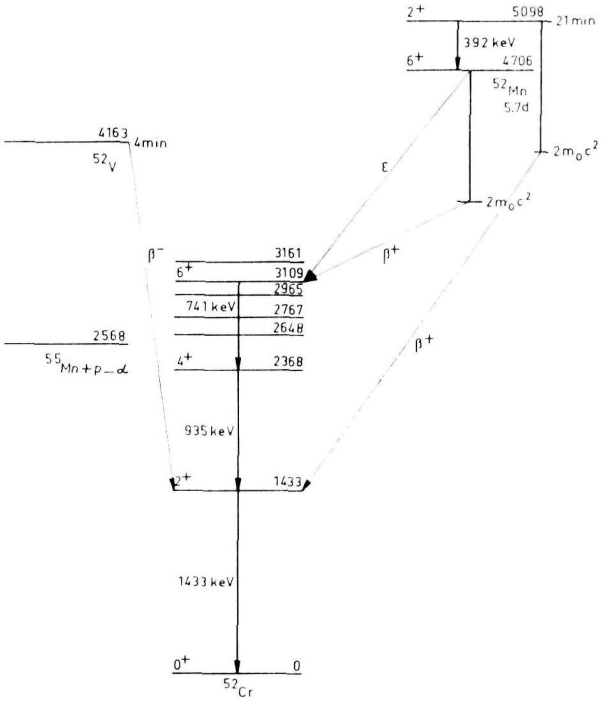

FIG. 3,1

Decay scheme of ^{52}Mn, incorporating the present and previous results.

The present investigation has been undertaken in order to obtain a more accurate value of the capture-positon branching ratio and to establish that the 6^+ level was different from any of the states mentioned by Mazari et al.

§ 2. Measurements with the proportional counter

Carrier-free sources were prepared in the I.K.O. synchro-cyclotron in Amsterdam by the reaction ^{52}Cr (d, 2n) ^{52}Mn. The radioactive material was separated chemically and converted into the chloride.

The electron capture to positon emission ratio was determined by means of beta-gamma ray coincidence measurements. The gamma rays were recorded in a NaI(Tl) gamma ray spectrometer; the beta rays in a proportional counter, filled with xenon. The proportional counter is described in Chapter 1.

The proportional counter, subtending a solid angle of nearly 2π, registered the positons and the K X-rays. Its efficiency for the ^{52}Mn gamma rays was found to be less than 0.2%. The scintillation

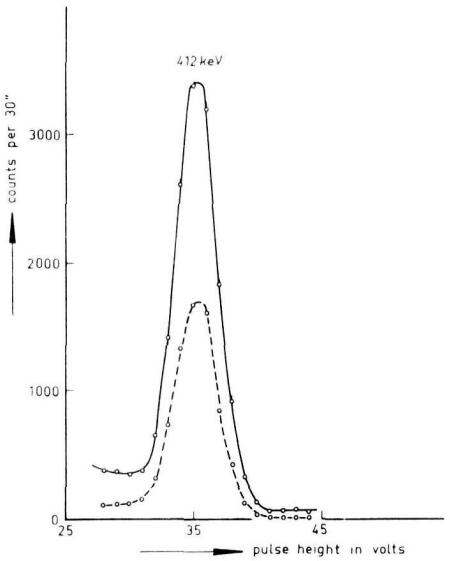

FIG. 3,2

Single and coincidence spectra from the decay of ^{198}Au.
The dotted curve is the coincidence spectrum.

spectrometer recorded the gamma ray photopeaks. The arrangement was calibrated by a measurement on ^{198}Au, which decays by negaton emission. The single and coincidence spectra from the decay of ^{198}Au are shown in Fig. 3,2. The gamma rays were measured in coincidence with all pulses corresponding to energies larger than 1 keV as recorded in the proportional counter. This cut-off necessitated only a small correction to the electron counting rate. The ratio of true to accidental coincidences was at least 20 : 1 in all measurements.

The three gamma rays of ^{52}Mn were measured in the same way as those of ^{198}Au. Fig. 3,3 shows the single and coincidence spectra

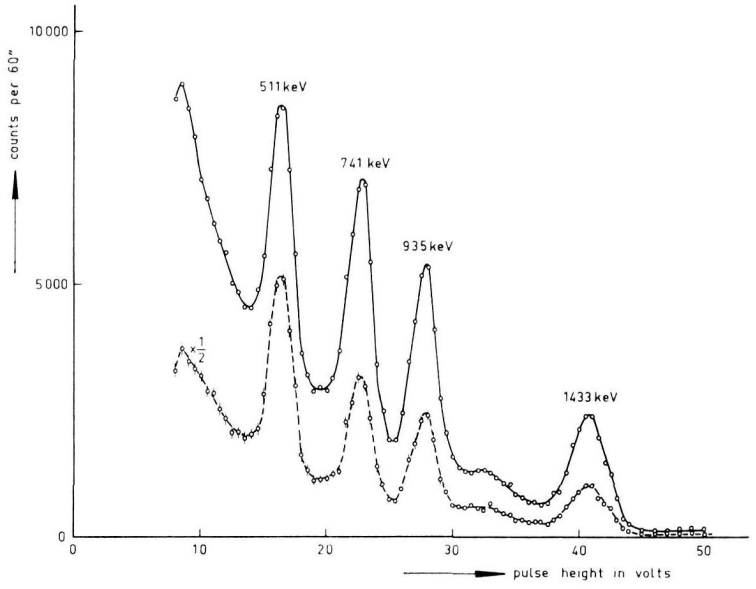

FIG. 3,3

Single and coincidence spectra from the decay of ^{52}Mn. The $\beta - \gamma$ coincidences are measured as a function of the pulse height in the scintillation counter. The drawn curve is the single, and the dotted one the coincidence spectrum.

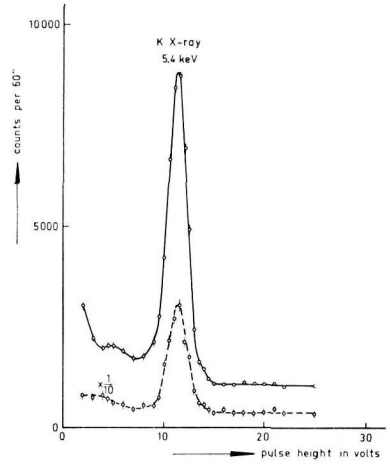

FIG. 3,4

Single and coincidence spectra from the decay of ^{52}Mn. The 5.4 keV K X-ray peak and positons in the proportional counter are measured in coincidence with the 1.43 MeV gamma ray photopeak, recorded in a NaI(Tl) scintillation counter. The drawn curve is the single spectrum, the dotted one the coincidence spectrum.

in the scintillation counter; the proportional counter accepted both positons with energies larger than 1 keV and K X-rays. Corrections for coincidences with these X-rays were made using the result of measurements of the spectra in the proportional counter in coincidence with each of the three gamma ray photopeaks in the scintillation counter. A plot of one of these measurements is shown in Fig. 3,4. It was found that $(8.4 \pm 0.6)\%$ of the coincidences were due to X-rays. The percentage, k, of positon emission in the decay of ^{52}Mn was found to be $(33.8 \pm 0.8)\%$, giving a value for ε/β^+ of 1.97 ± 0.07.

The fluorescent yield in chromium is determined from the single spectrum depicted in Fig. 3,4, which gives the ratio of emitted K X-rays to positons (Ha 58). Corrections due to internal conversion of the gamma rays occurring in the decay of ^{52}Mn are negligible. The result is $\omega_K = 0.219 \pm 0.012$ in chromium.

§ 3. Beta ray measurements in a long lens beta spectrometer

The long lens β ray spectrometer and its auxiliary equipment is described in Chapter 1.

The positon spectrum of ^{52}Mn was measured in the spectrometer, using a source of about 4 mm diameter, deposited on a thin formvar film which was rendered conductive by evaporating aluminium onto the backing. The Kurie plot of the positon distribution is shown in Fig. 3,5. The end point of the positon spectrum was found to be 575 ± 4 keV. This value was obtained from the results of several runs.

The percentage positon emission was determined with the $\beta - \gamma$ ray coincidence method, using here the magnetic lens beta spectrometer for detection of the positons. By mounting a NaI(Tl) scintillation counter behind the sample in the beta spectrometer, $\beta - \gamma$ coincidences could be achieved. For a description of the arrangement, reference is made to Chapter 1.

The percentage, k, of positon emission, in the decay of ^{52}Mn was determined in the following way. The positons were counted in the spectrometer which, in order to reduce the influence of scattered positons, was set to receive β rays of higher momentum, than that relating to the maximum intensity of the positon spectrum. The gamma ray scintillation counter was set to receive the photopeak of the 1.43 keV gamma rays and part of its Compton continuum.

In the case of ^{52}Mn, the ratio of beta-gamma ray coincidences to single gamma counts is then:

$$(N\beta\gamma/N\gamma)_{Mn} = \Omega\beta \; k \; f_{Mn}(\eta) \qquad (3.1)$$

in which $N\beta\gamma$ represents the coincidences, $f_{Mn}(\eta)$ the momentum distribution of the beta rays, η the electron momentum in units

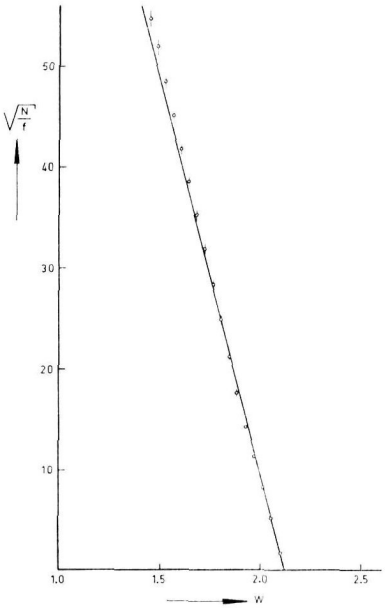

FIG. 3,5

Kurie plot of the positon distribution of ^{52}Mn. A helical baffle was used for separating positons and conversion electrons. The energy of the β rays in units of m_oc^2 is indicated by W.

m_oc, and $\Omega\beta$ is a beta spectrometer constant involving the resolution and solid angle of the instrument.

The value of $\Omega\beta$ was determined experimentally by measuring $\beta - \gamma$ coincidences between the 965 ± 5 keV negaton distribution and the 412 keV gamma rays in ^{198}Au (Po 56). This gives:

$$(N\beta\gamma/N\gamma)_{Au} = 0.989 \times \Omega\beta \; f_{Au}(\eta) \qquad (3.2)$$

The factor 0.989 arises from the fact that only 98.9% of the 412 keV γ rays is preceded by the 965 keV negaton group (the other part

being preceded by a lower energy negaton branch). The value of k can be calculated from (3.1) and (3.2):

$$k = [N\beta\gamma/N\gamma f(\eta)]_{Mn} \times [N\gamma f(\eta)/N\beta\gamma]_{Au} \times 0.989 \qquad (3.3)$$

The measurements, corrected for background, counting losses in the scalers and chance coincidences give a value for k of 0.33 ± 0.01, from which a value for ε/β^+ of 2.03 ± 0.09 is found. In all measurements the ratio of true to chance coincidences was at least 5 : 1.

Measurement of the energy of γ_1 using internal conversion electrons yielded a value for $E(\gamma_1)$ of 741 ± 5 keV, in good agreement with the value of 734 ± 15 keV found by PEACOCK and DEUTSCH (Pe 46). The total conversion coefficient of this gamma ray was found to be $\alpha = (2.9 \pm 0.3) \times 10^{-4}$ in agreement with earlier measurements (Ke 54).

§ 4. DISCUSSION AND CONCLUSIONS

The values of 1.97 ± 0.07 and 2.03 ± 0.09 for the ratio of electron capture to positon emission in the decay of ^{52}Mn obtained in § 2 and § 3 are in good agreement.

These two independent measurements give an average value for ε/β^+ of 1.99 ± 0.06, in agreement with the theoretical value of 2.03 ± 0.06 (accepting a maximum positon energy of 575 ± 4 keV). The theoretical value was derived from K/β^+ ratios as computed by ZWEIFEL (Zw 57) together with an L_I/K capture ratio of 0.087 (Ro 49) and a value of 0.08 for the ratio of capture in higher shells to that in the L shells (Wa 58) (see also Chapter 2). Limits to the magnitude of the Fierz term parameter b, may be derived from comparison of the theoretical and experimental results given above, as pointed out in Chapter 2:

$$b = -0.006 \pm 0.012$$

The energy measurement for γ_1 of $(741 \pm 5$ keV) yields a value of 3109 ± 7 keV for the excitation energy of the 6^+ state (see Fig. 3,1). Measurement of the end point of the positon spectrum reported above, in combination with the data from the isomeric state in ^{52}Mn, gives a value of 3097 ± 18 keV. These two values agree excellently, with each other and with earlier data.

MAZARI et al., however, have reported that no excited state could be observed at 3109 ± 7 keV in the charged-particle reactions

$^{55}Mn(p,\alpha)^{52}Cr$ and $^{52}Cr(p,p')^{52}Cr$. According to these authors, all the alpha groups of the first reactions studied in these experiments were of low intensity, and a weak group associated with a level at 3109 keV might easily have been overlooked. (Moreover, no alpha ray group corresponding to the 3161 keV state, known from $^{52}Cr(p,p')^{52}Cr$ reactions, was observed). The same authors have reported that a proton peak associated with the 3109 keV level in inelastic proton scattering with an intensity greater than 3% of the one corresponding to the 3161 keV level, would have been detected.

A difference in intensity of the transitions to the 3109 keV and 3161 keV levels might, however, be caused by the first level having a higher spin than the latter. Since the spin of the 3109 keV level is 6^+, either the incident or the scattered proton, in processes exciting this level, must have an angular momentum of at least three units. The average distance to the centre of the nucleus is then more than twice the nuclear radius. This process may therefore be considerably more difficult than exciting a level with a spin of, say, 4 units.

Conversely, it would be convenient to conclude, on the basis of the foregoing considerations, that the spins of the 2648, 2767, 2965 and 3161 keV states, reported by MAZARI et al., are less than 5. This would explain why these states are not excited in the ground state decay of the 5.7d ^{52}Mn isotope. Some of them might be excited in the decays of 4 min. ^{52}V and 21 min. $^{52}Mn^*$, which probably both have spins 2^+ (Wa 55). However, transitions to these states could have relative intensities of less than about 5% only if the log *ft* values are equal to those of the allowed transitions to the 1433 keV level. This may easily explain why such transitions, even assuming them to be present, have not yet been observed.

The measured value for ω_K of 0.219 ± 0.012 for the fluorescent yield in chromium (see § 2) agrees well with the theoretical value of 0.22 (Bu 52). The semi-empirical formulae as given by BURHOP (Bu 55) and by LABERRIGUE-FROLOW and RADVANYI (La 56) predict values for ω_K of 0.25 and 0.24 respectively. No earlier measurements of the fluorescent yield in chromium are known.

CHAPTER 4

THE RADIO-ACTIVE DECAY OF ^{57}Ni

§ 1. Introduction

The nuclide ^{57}Ni decays to ^{57}Co by electron capture and by positon emission in about equal intensities (Ma 49, Fr 50), with a half-life of 36 hours (Li 38, Ma 49, Fr 50). The positon spectrum has been reported as simple and the Kurie plot as straight (Fr 50, Ca 51); the end point, as measured by a magnetic lens spectrometer, has been reported as 845 $\pm$ 10 keV (Fr 50) and as 835 $\pm$ 10 keV (Ca 51). Three gamma rays have been observed in the decay with energies of 128, 1375, and 1914 keV, as measured in a magnetic lens spectrometer by observing the photo-electrons produced in a uranium converter (Ca 51). The ground state of ^{57}Co has a spin 7/2 as measured by paramagnetic resonance (Ba 53). A tentative ^{57}Co level scheme was put forward with levels at 1375, 1503, and 1914 keV, of which at least the first and third are fed directly from ^{57}Ni (Ca 51).

The present investigation was undertaken in order to put the decay scheme on a sounder basis by means of measurements of the gamma ray scintillation spectrum and by gamma-gamma coincidence and angular correlation measurements. A renewed investigation of the positon spectrum appeared desirable, as it seemed improbable that the β^+ spectrum would be simple. It also appeared worth while to make $\beta - \gamma$ coincidence measurements in order to determine the branching ratios of the electron capture to positon emission.

§ 2. Scintillation spectrum and gamma-gamma coincidence measurements

Some ^{57}Ni sources were prepared by bombarding natural nickel with 28 MeV deuterons in the I.K.O. synchro-cyclotron in Amsterdam. They were separated chemically and converted into the oxide. Carrier-free sources were prepared by bombarding natural

iron with alpha particles in the same cyclotron. These sources were purified chemically and converted into the chloride.

The scintillation spectrometer and its calibration are described in Chapter 1. The carrier-free sources were deposited on thin zapon films in order to avoid absorption of the 128 keV gamma rays

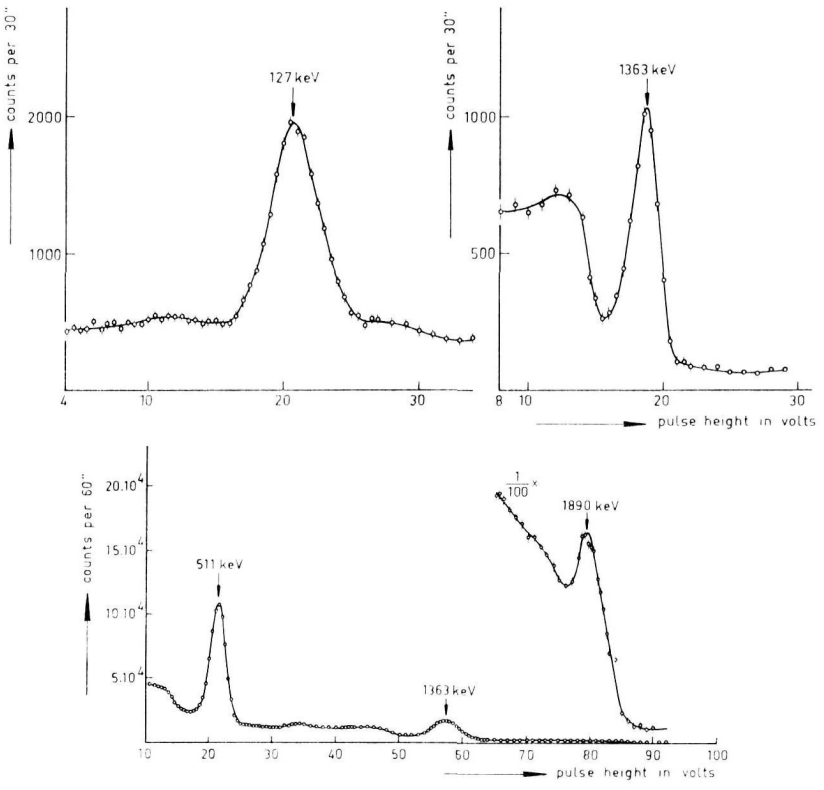

FIG. 4,1a and b

Scintillation spectra of ^{57}Ni.

a: Low energy region. b: High energy region.

in the source. The gamma ray spectra are shown in Fig. 4,1a and b. Three gamma rays were found with the following energies γ_1: 127 $\pm$ 3 keV, annihilation radiation 511 keV, γ_2: 1363 $\pm$ 6 keV and γ_3: 1890 $\pm$ 20 keV. For the energy measurement of γ_2 repeated calibrations were performed with ^{22}Na and ^{60}Co sources.

The decay scheme proposed by CANADA and MITCHELL (Ca 51) indicated the possible existence of 400 keV and 530 keV gamma

rays. So far these gamma rays had not been observed because of the presence of the intense annihilation radiation. In order to investigate this point the annihilation peak was reduced by a factor of about 10 by using a thin nickel source (< 1 mg/cm^2) deposited on a formvar film. Since most positons will have left the

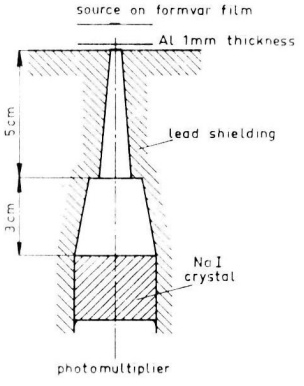

FIG. 4,2

Arrangement for the reduction of recorded annihilation radiation.

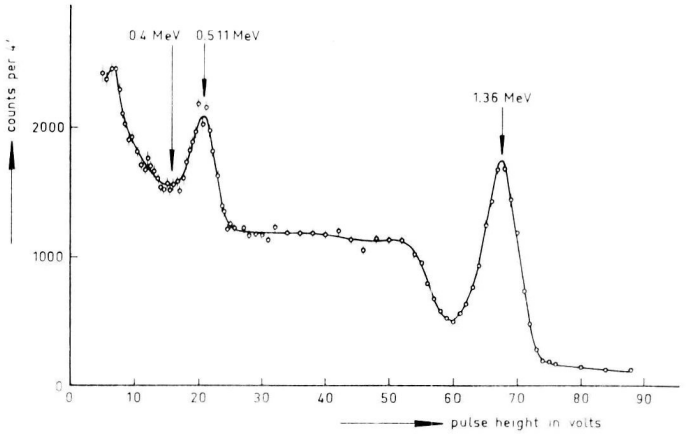

FIG. 4,3

Scintillation spectrum with reduced annihilation peak.
No 400 keV gamma ray is observed.

source before annihilating, the number of annihilation quanta reaching the crystal can be reduced considerably by proper shielding. For further details of the arrangement see Fig. 4,2. The result of one of these measurements is shown in Fig. 4,3. The intensity of

a possible 400 keV gamma ray is, according to this measurement, certainly less than 2% of the intensity of the 1363 keV gamma ray. A more restrictive upper limit for this intensity is given in § 3.

The ratio ε/β^+ has been measured by comparing the intensity ratio of annihilation radiation and the 1363 keV and 1277 keV gamma rays in the decays of ^{57}Ni and ^{22}Na, respectively. The source was mounted between two plates of aluminium, thick enough to stop all positons. The total electron capture to positon emission ratio in ^{57}Ni is found to be $\varepsilon/\beta^+ = 1.13 \pm 0.10$ on the assumption that the 1363 keV gamma rays occur in $(86 \pm 1)\%$ of the ^{57}Ni transitions.

A complete list of the observed gamma rays and their number per decay is given in Table 4,I, it being assumed that the 1890 keV

TABLE 4,I

Energies and intensities of ^{57}Ni gamma rays as computed from the scintillation spectrum.

Eγ *) in keV	γ ray intensities in % per decay
127.2 ± 0.5	14 ± 1
511 (e^+, e^-)	94 ± 5
1364 ± 6	86
1889 ± 13	14 ± 1

*) Average values of the results obtained from the γ and β ray measurements.

together with the 1363 keV gamma rays occur in 100% of the ^{57}Ni transitions. The intensity of γ_3 has been corrected for sum pulses of γ_2 and annihilation radiation.

For the $\gamma - \gamma$ coincidence measurements two single-channel NaI(Tl) scintillation spectrometers were used in a slow coincidence arrangement with a resolving time of 2.5×10^{-7} sec. (see Chapter 1). First it was investigated which gamma rays were in coincidence with the annihilation radiation. One channel was adjusted to detect the annihilation radiation, while the spectrum was scanned with the other channel. From these measurements it may be concluded that γ_1, γ_2 and γ_3 are all in coincidence with the annihilation radiation. Similarly, it was shown that γ_1 is in coincidence with γ_2, while γ_3 is not (see Fig. 4,4). Neither are γ_2 and γ_3

coincident. These measurements therefore confirm the decay scheme discussed in the introduction.

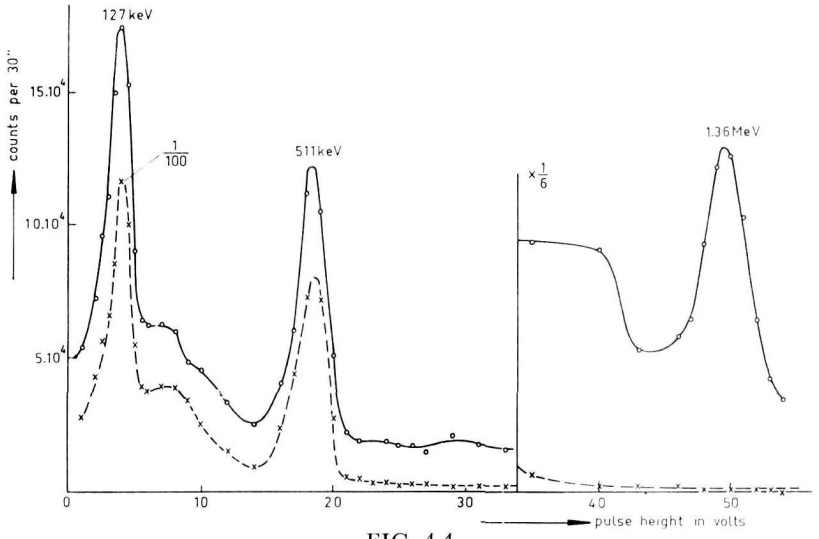

FIG. 4,4

Spectrum of gamma rays coincident with γ_2 ($E\gamma = 1364$ keV).

§ 3. Measurements with the proportional counter

The proportional counter (see Chapter 1) filled with xenon was used to determine the percentage positon emission to the three excited levels in ^{57}Co separately. The proportional counter, subtending a solid angle of nearly 2π, registered the positons and the K X-rays. The proportional counter was calibrated with ^{198}Au and the measurements were performed in the same way as described in Chapter 3. The ratio of true to accidental coincidences was, in all measurements, at least 20 : 1.

The three gamma rays were measured in coincidence with all pulses larger than 1 keV recorded with the proportional counter. Thus, coincidences between K X-rays and gamma rays are included in our results which are shown in Fig. 4,5a and b. In order to correct for this effect, coincidences were measured as a function of the pulse height in the proportional counter. This measurement was made in the same way as described in Chapter 3, § 2. Special care was taken to prevent sum pulses from the 1363 keV gamma rays and annihilation radiation from falsifying the coincidence measurements with the 1889 keV line. Coincidences due to conversion

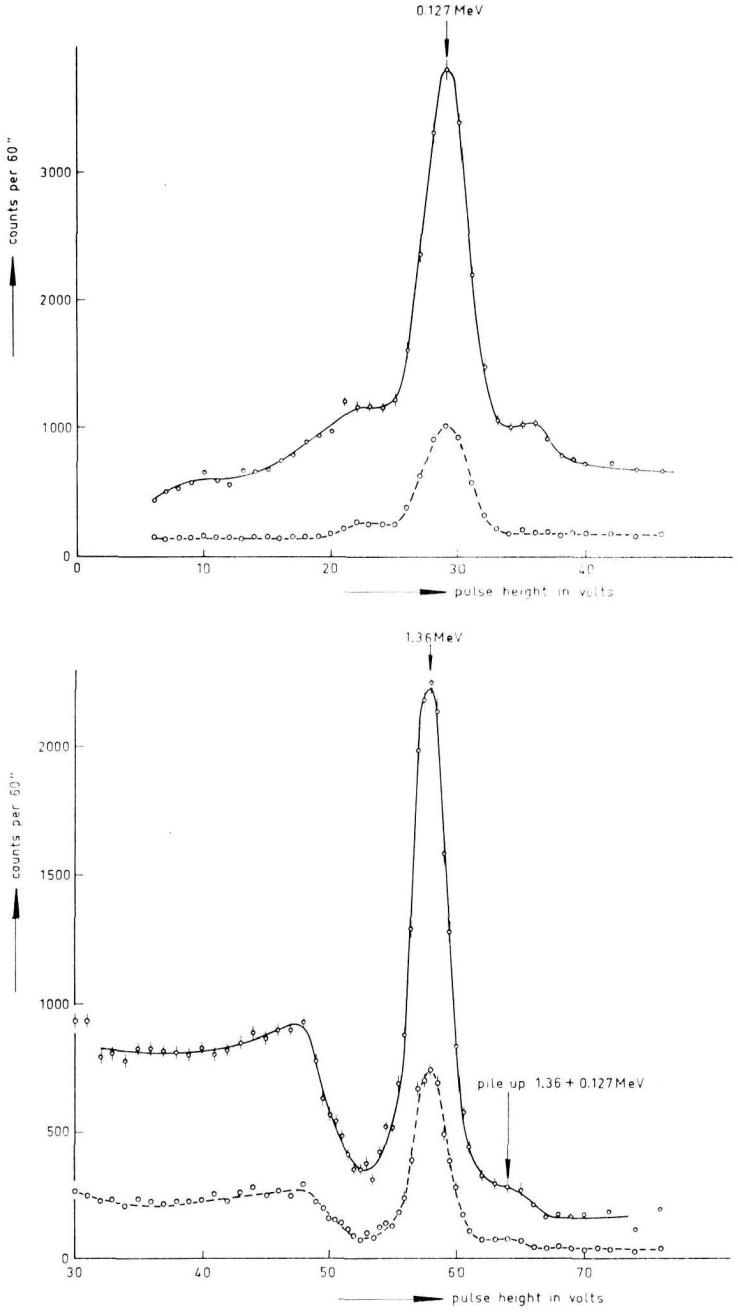

FIG. 4,5a and b

Single and β — γ coincidence spectra from the decay of ^{57}Ni. The unbroken curve is the single and the dotted curve the coincidence spectrum. Coincidences with the 1889 keV γ ray have only been measured with an integral discriminator.

electrons and gamma rays from the 127 keV γ transition with the 1364 keV gamma rays were taken into account. The results are presented in Table 4,II.

TABLE 4,II

Percentage of the gamma rays coincident with positon emission.

Eγ in keV	$\beta^+/(\varepsilon + \beta^+)$ in %
127.2 ± 0.5	41 ± 1
1364 ± 6	53 ± 1
1889 ± 13	6 ± 2

Special observations were made for the 400 keV gamma ray, which could not be detected in the measurements reported in § 2, and for a possible 520 keV transition between the levels 1.89 MeV and 1.36 MeV. The scintillation spectrum in the region between 300 keV and 800 keV was measured in coincidence with the K X-rays registered by the proportional counter. The result is shown in Fig. 4,6. The dotted peak at 400 keV shows the size of

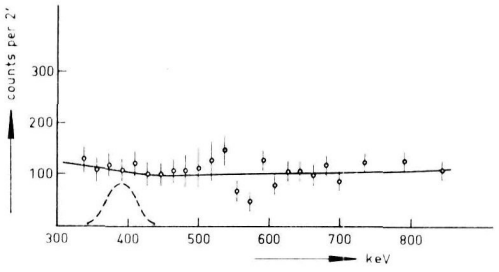

FIG. 4,6

Scintillation spectrum in the region between 300 keV and 800 keV as measured in coincidence with the K X-rays registered by the proportional counter. This spectrum is the difference between a measurement with (K + β^+) rays registered in the proportional counter and one with β^+ rays only; the irregularities at ~ 500 keV are probably due to a slight shift in the scintillation spectrum between the two measurements. The dotted peak at 400 keV shows the size of a line of 1% intensity.

a line of 1% intensity. The upper limits for the intensity of the 400 keV and 520 keV gamma rays as derived from these measurements are 0.5 and 1% respectively.

The percentage positon emission and electron capture in the transitions to the three ^{57}Co levels can be calculated from Table 4,II in conjunction with the gamma ray intensities given in Table 4,I. These data are shown in Table 4,III.

TABLE 4,III

Branching of electron capture and positon emission as measured with the proportional counter.

E_x in MeV	Total branching in % computed from Table 4,I	β^+ branching in %	ε branching in %
1.89	14 ± 1	0.86 ± 0.34	13.2 ± 1.0
1.49	14 ± 1	5.7 ± 0.4	8.3 ± 0.6
1.36	72 ± 1	39.8 ± 1.1	32.2 ± 0.9

The ratio of electron capture to positon emission, according to the results given in Table 4,II, is $(\varepsilon/\beta^+)_{\text{total}} = 1.15 \pm 0.04$. A value of $(\varepsilon/\beta^+)_{\text{total}} = 1.13 \pm 0.15$ follows from the K X-rays to positons in the single spectrum in the proportional counter in conjunction with the value $\omega_K = 0.31 \pm 0.01$ (Ha 58). Both results are in good agreement with the value 1.13 ± 0.10 discussed in § 2.

§ 4. Beta ray measurements

The long lens β ray spectrometer and its accessories are described in Chapter 1. The source (carrier-free), with a diameter of about 4 mm, was deposited on a thin formvar film, which was made conductive by evaporating aluminium on the backing. A helical baffle for separating conversion electrons from positons was used in some of the measurements.

The Kurie plot (Na 52) of the positon distribution is shown in Fig. 4,7. The positon spectrum appears to be complex and contains three β^+ components. Analysis of the Kurie plot of the positons gives the following end points for the two high energy β^+ branches: 849 ± 10 keV and 712 ± 15 keV; the intensity ratio is then 7.6 ± 0.8. This value agrees with the ratio 7.0 ± 0.5 calculated from the results given in Table 4,III. Measurements on the low energy branch (350 keV) are not reliable due to scattering on the helical baffle.

In earlier measurements for which no helical baffle was used, the end points were observed at 854 $\pm$ 9 keV, 720 $\pm$ 30 keV, and 350 $\pm$ 50 keV in agreement with the above measurements. The relative intensity of the 350 keV positon distribution was then

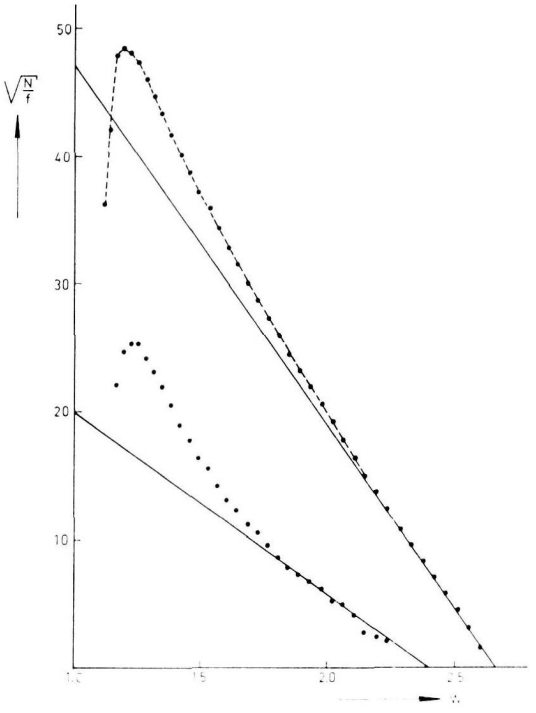

FIG. 4,7

Kurie plot of the positon distribution of ^{57}Ni, using a helical baffle for separating positons and negatons. The total energy of the positons in units of m_0c^2 is indicated by W.

estimated as (2 $\pm$ 1)%. The intensity ratio of the two high energy β^+ branches was found to be 4 $\pm$ 2; this result is probably much less reliable.

The percentage positon emission in the transition to the 1364 keV level in ^{57}Co was also determined by means of β — γ ray coincidence measurements using the beta spectrometer. The experimental method is described in Chapter 3, § 3. The percentage positon emission was found to be (56.7 $\pm$ 2.7) % of the disintegrations to this level, in agreement with the value (55.3 $\pm$ 1.5)% calculated from the results shown in Table 4,III.

TABLE 4,IV

Average values for positon emission and electron capture intensities in the different branches as calculated from both sets of experiments (§ 3 and § 4), (computed by a least squares analysis).

E_x in keV	β^+ branching in % per decay	ε/β^+ experimental values	$(\varepsilon/\beta^+)_o$ theoretical values obtained from references (Zw 57, Ro 49 and Wa 58)
1889 ± 13	0.86 ± 0.34	18 ± 6	24 ± 6.5
1491 ± 6	5.6 ± 0.4	1.438 ± 0.059	1.485 ± 0.040
1364 ± 6	39.9 ± 1.0	0.805 ± 0.040	0.860 ± 0.020
Total	46.4 ± 1.1	1.15 ± 0.04	

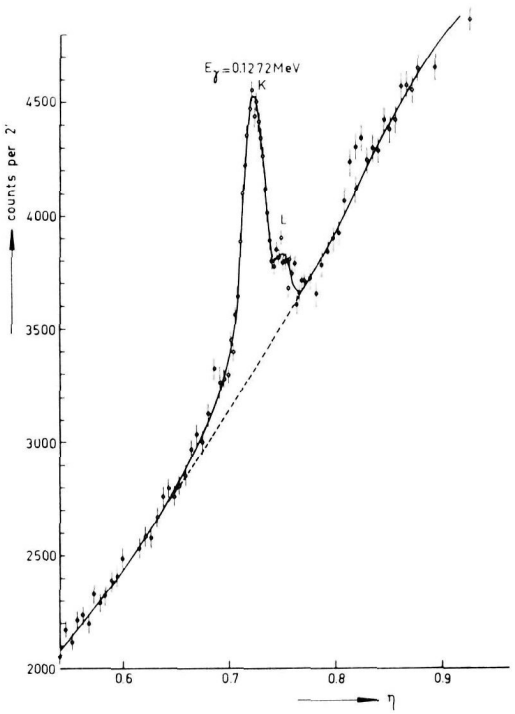

FIG. 4,8

Conversion electrons of γ_1 measured in the long lens beta ray spectrometer. The momentum of the electrons in units of m_oc is indicated by η.

Average values for positon emission and electron capture intensities in different branches, as calculated from both sets of experiments, are given in Table 4,IV (see also § 6).

The K conversion line of the 127 keV γ ray is clearly shown in Fig. 4,8. The energy of the γ_1 transition computed from the K line was $E(\gamma_1) = 127.2 \pm 0.5$ keV. The L conversion line was only partially resolved; the K/L ratio was 9 ± 4. The ratio of the number conversion electrons of γ_1 to the number positons in the 849 keV spectrum was:

$$(N_{e^-})_{total} / N\beta^+(849\ keV) = (7.68 \pm 0.77) \times 10^{-3}.$$

The experimental total conversion coefficient follows from this result and from the total ε/β^+ ratio, discussed in § 3: $\alpha_{total} = 0.023 \pm 0.003$.

External conversion measurements were made with a lead converter (41 mg/cm^2). The energies of the two high energetic gamma rays were found to be 1367 ± 15 keV and 1888 ± 18 keV. The effect of multiple scattering has been taken into account (Si 55). These values are in satisfactory agreement with the results of CANADA and MITCHELL (Ca 51), who found 1375 keV and 1914 keV respectively, and with the values of 1363 ± 6 keV and 1890 ± 20 keV found in § 2.

§ 5. ANGULAR CORRELATION MEASUREMENTS

The angular correlation between the 127 keV and 1363 keV gamma rays has been measured utilizing the equipment mentioned

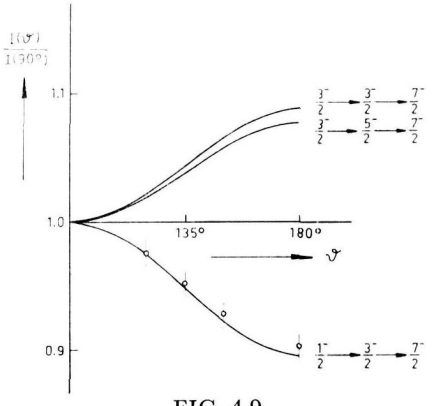

FIG. 4,9

Angular correlation for the $\gamma_1 - \gamma_2$ cascade. The drawn curves represent the theoretical possibilities assuming pure gamma transitions.

in Chapter 1. The ratio of true to chance coincidences was about 10 : 1.

The results of two runs, corrected for half-life, finite solid angle, source size (Wa 50) and coincidences between Compton pulses of the annihilation radiation and 1364 keV gamma rays, were:

$$W(\vartheta) = 1 - (0.096 \pm 0.009) \cos^2\vartheta \text{ and}$$
$$W(\vartheta) = 1 - (0.107 \pm 0.010) \cos^2\vartheta$$

This result was found from the experimental data by a least squares analysis (Ro 53).

The measured correlation is plotted in Fig. 4,9. The drawn curves represent the theoretical possibilities assuming pure gamma transitions.

§ 6. Discussion and conclusions

A decay scheme of ^{57}Ni, incorporating present and previous results, is given in Fig. 4,10.

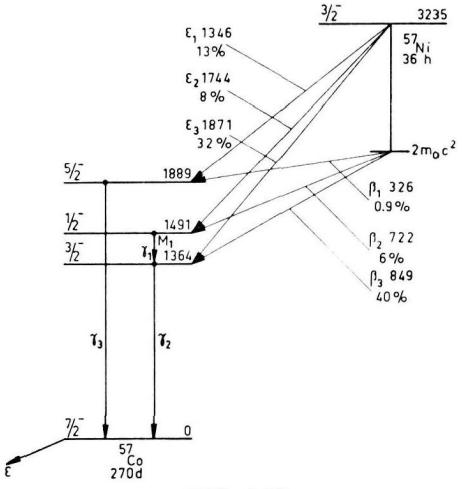

FIG. 4,10

Decay scheme of ^{57}Ni. All decay and excitation energies are given in keV.

From the energy measurements of the gamma rays the following average values can be computed: $E(\gamma_1) = 127.2 \pm 0.5$ keV, $E(\gamma_2) = 1364 \pm 6$ keV, and $E(\gamma_3) = 1889 \pm 13$ keV. The total decay energy of ^{57}Ni being the sum of the average values of the energy of γ_2 and the end point of the 849 keV positon branch, is $Q = 3235 \pm 9$ keV.

The shell model predicts J = 3/2 and odd parity for the ground state of ^{57}Ni in analogy with the fact that the 29th proton as well as the 29th neutron are also bound in a $p_{3/2}$ orbit in other nuclei (^{63}Cu, ^{65}Cu, ^{53}Cr). The ground state in ^{57}Co is $7/2^-$ (Ba 53). The β^+ transitions are all allowed, the log *ft* values of the 850 keV, 720 keV, and 350 keV transitions being 5.2, 5.8, and 5.3. The spins of all three ^{57}Co levels are therefore restricted to J = $1/2^-$, $3/2^-$ or $5/2^-$.

A spin J = $5/2^-$ for the 1491 keV level is improbable, since a transition to the ^{57}Co ground state could not be observed. If such a transition exists, its relative intensity must be smaller than 0.3%.

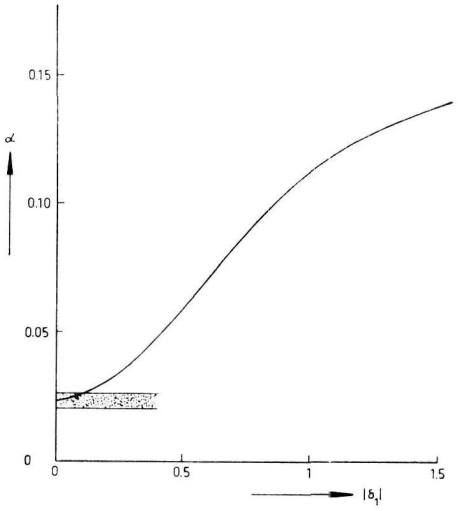

FIG. 4,11

Total conversion coefficient of γ_1 as a function of the amplitude mixing ratio $|\delta_1|$. The experimental value is indicated as a shaded area.

A spin 1/2 for the 1364 keV level can be ruled out, because the angular correlation between γ_1 and γ_2 is not isotropic. A spin 3/2 for the 1491 keV level is improbable, since then the intensity ratio of a transition between the 1491 keV level and the ground state and the 127 keV gamma ray would be at least about 500, according to the Weisskopf estimate (Si 55), whereas the experimental value is < 0.02. The same reasoning for a spin 5/2 gives an even larger discrepancy.

The experimental conversion measurement of the 127 keV gamma ray indicates it to be mainly a Ml transition, with no more than

1.5% E2 admixture (see Fig. 4,11 and Table 4,V; a combination E1 + M2 is not possible since all levels have odd parity). The spin difference between the 1491 keV and 1364 keV levels cannot therefore be larger than 1. A combination of the above reasonings indicates spins 1/2 and 3/2 for these two levels.

TABLE 4,V

Values of the K/L ratio and total conversion coefficient for γ_1.

Character		K/L ratio	Total conversion coefficient
Computed from Rose's tables (Ro pr)	M1	11.7	0.0233
	E1	11.6	0.021
	E2	9.6	0.204
Experimental value		9 ± 4	0.023 ± 0.003

One argument against a spin assignment 3/2 for the 1491 keV state follows from intensity considerations as mentioned above, another argument follows from the measured angular correlation between γ_1 and γ_2. In Fig. 4,12 the anisotropy coefficient A_2 is plotted as a function of the amplitude mixing ratio δ_1, assuming that γ_2 is a pure quadrupole transition, for the cases 1/2 — 3/2 and 3/2 — 3/2. The limit on $|\delta_1|$ following from the experimental

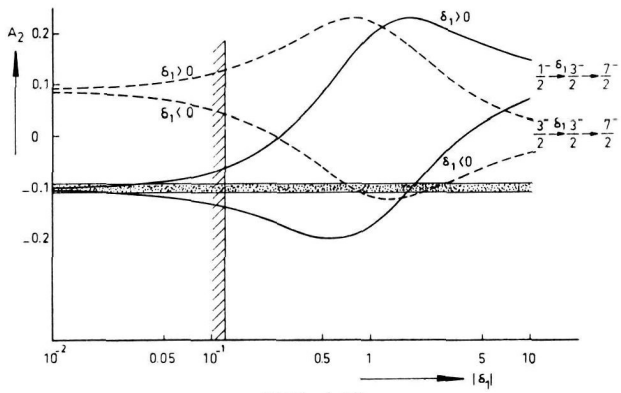

FIG. 4,12

Theoretical curves of the anisotropy coefficient A_2 versus the amplitude mixing ratio δ_1 for different spin values at the 1.49 and 1.36 MeV levels assuming that γ_2 is a pure quadrupole transition. The experimental value is indicated as a shaded area, the upper limit on $|\delta_1|$ found from the experimental conversion coefficient of γ_1 has also been indicated.

value of the conversion coefficient discussed above has also been indicated. Only a spin combination 1/2 and 3/2 agrees with these data; in agreement with above reasoning. The E2/M1 amplitude mixing ratio in γ_1 is $|\delta_1| = 0.002 \pm 0.030$. As follows from this result, the angular correlation is in perfect agreement with a 1/2 (M1) 3/2 (E2) 7/2 sequence, as is shown in Fig. 4,9.

On the basis of angular correlations alone, spins 3/2 and 5/2 for the 1491 keV and 1364 keV levels cannot be excluded. Fig. 4,13

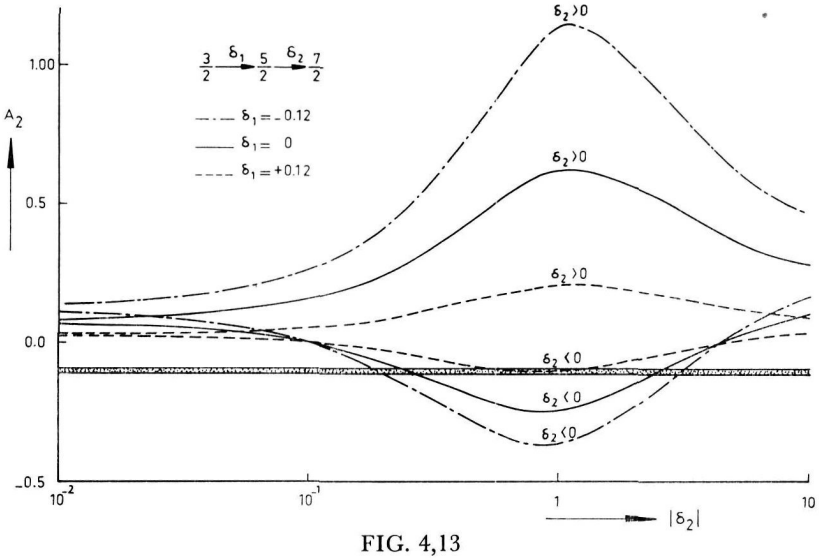

FIG. 4,13

Theoretical curves of the anisotropy coefficient A_2 versus the amplitude mixing ratio δ_2 with δ_1 as a parameter for a spin 3/2 of the 1491 keV and a spin 5/2 of the 1364 keV level. The experimental value is indicated as a shaded area.

shows the anisotropy coefficient A_2 as a function of the amplitude mixing ratio δ_2 (γ_2) for $\delta_1 = 0$ and for the extreme values $\delta_1 = \pm 0.12$ allowed by the experimental conversion coefficient of the 127 keV gamma ray. Nevertheless, reasonable agreement with our values can only be obtained if at least one of the two gamma rays contains a considerable admixture of E2 transitions, which is not very probable (the Weisskopf estimate for δ_2 is 0.055).

Considering these arguments, it appears very probable that the 1491 keV and 1364 keV levels have spins $1/2^-$ and $3/2^-$ respectively, and that the 127 keV and 1364 keV gamma rays are nearly pure M1 and E2 transitions.

The spin of the third level in ^{57}Co is also restricted to $J = 1/2^-$, $3/2^-$ or $5/2^-$, since the β^+ transition to this level is allowed. A spin $J = 1/2^-$ can be ruled out at once because of the presence of the 1889 keV gamma transition to the ground state and the absence of 400 keV and 520 keV gamma rays. The intensity as obtained from the Weisskopf estimate (Si 55) gives the following results (see Table 4,VI):

TABLE 4,VI

Spin 1889 keV level	Intensity ratio $\frac{400 \text{ keV}}{1889 \text{ keV}}$	Intensity ratio $\frac{500 \text{ keV}}{1889 \text{ keV}}$
$3/2^-$	0.83	1.8
$5/2^-$	1.1×10^{-6}	1.2×10^{-2}

The measured intensities of the 400 keV and 520 keV gamma rays were actually smaller than 0.5% and 1% respectively, giving intensity ratios less than 0.036 and 0.072, which tends to exclude the spin $J = 3/2^-$. Therefore a spin assignment $J = 5/2^-$ for the 1889 keV level is proposed.

From these data the following spins and parities can be assigned to the three levels in ^{57}Co: $E_x = 1364 \pm 6$ keV ($J = 3/2^-$), $E_x = 1491 \pm 6$ keV ($J = 1/2^-$) and $E_x = 1889 \pm 13$ keV ($J = 5/2^-$).

The measurements of the ratio of the total electron capture rate to the total positon emission rate, as discussed in § 3, give the values 1.13 ± 0.15, 1.13 ± 0.10, and 1.15 ± 0.04, which are in good agreement with the result 1.1 ± 0.1 obtained by FRIEDLANDER et al. (Fr 50).

The individual ε/β^+ ratios for transitions to the three ^{57}Co levels are given in Table 4,IV. The last column of this table presents the theoretical values derived from K/β^+ ratios computed by ZWEIFEL (Zw 57) in conjunction with an L_I/K capture ratio of 0.093 obtained by ROSE and JACKSON (Ro 49) and a value of 0.090 for the ratio of capture in higher shells to that in the L shells (Wa 58). The experimental data given in Table 4,IV are averages of the results discussed in § 1, 2, 3 and 4. The average values of the positon spectra, used to calculate the theoretical ε/β^+ ratios, have been computed as 849 ± 6 keV, 722 ± 6 keV, and 326 ± 20 keV from the gamma and beta ray measurements described in § 1 — 4.

The experimental ε/β^+ ratios may be used to set limits to the Fierz term parameter described in Chapter 2. The following values for b can be derived from our results for the transitions to the three levels in ^{57}Co: $b = -0.020 \pm 0.017$, $b = -0.008 \pm 0.015$, and $b = -0.080 \pm 0.110$. These values will be compared with other results in Chapter 6.

CHAPTER 5

ON THE RADIO-ACTIVE DECAY OF ^{86}Y

§ 1. Introduction

The isotope ^{86}Y decays by positon emission and electron capture in about equal intensities, with a half-life of 14.6 hours (Cas 51, Hy 51). The positon spectrum consists of two main groups of 1.80 and about 1.19 MeV energy; the spectrum of the latter component is reported to have a shape characteristic of a $\triangle J = 2$, yes transition, as measured with an anthracene scintillation counter (Cas 51, Hy 51). Four gamma rays have been observed with energies of 0.18, 0.635, 1.08 and 1.93 MeV, as measured in a NaI(Tl) scintillation spectrometer. Each gamma ray transition has been reported to be in coincidence with all others and with annihilation radiation; no cross-over gamma ray has been observed (Hy 54).

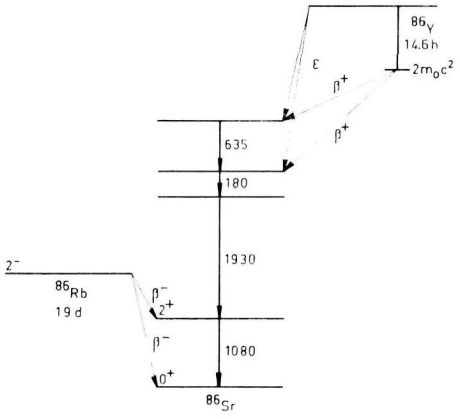

FIG. 5,1

Decay scheme of ^{86}Y, as proposed by Hyde et al. (Hy 54).

The positon spectrum showed no difference in shape when recorded in coincidence with the 1.9 MeV gamma ray, hence all positons are in coincidence with the 1.9 MeV gamma rays. Strontium

X-rays were identified in ^{86}Y by pulse height analysis of pulses produced in a proportional counter, but no quantitative intensity measurements were made. The X-rays have been reported to be in coincidence with the gamma rays. A minimum value of about 6 MeV for the decay energy has been found by registering coincidences from gamma summation spectra in two large sodium iodide crystals (Hy 54).

The position of a 1.08 MeV level in the decay scheme proposed by HYDE et al. (Hy 54) (see Fig. 5,1) has been derived from the decay of ^{86}Rb; it is the only gamma ray occurring in its decay. Polarization-direction correlation of beta and gamma rays in ^{86}Rb show that the 1.08 MeV level has a spin assignment of 2^+ and that the 1.08 MeV gamma ray is an E2 transition.

When considering the level energies of neighbouring isotopes with the same or nearly the same number of protons or neutrons, such as given in Table 5,I, one would expect a 2^+ level at about

TABLE 5,I

Excitation energies of lowest states in even-even isotopes with $Z \approx 38$ and $N \approx 48$.

Spin assignment of level	Isotopes (excitation energies in MeV)					
	$^{80}_{34}Se_{46}$	$^{80}_{36}Kr_{44}$	$^{82}_{34}Se_{48}$	$^{82}_{36}Kr_{46}$	$^{84}_{36}Kr_{48}$	$^{88}_{38}Sr_{50}$
2^+	0.65	0.62	0.88	0.77	0.88	1.85
2^+				1.45	1.91	
3^-				) (1.60 ?	2.7 ?	2.76
4^+				( ) 2.07		

1 MeV and another identical level at about 2 MeV. This second 2^+ level might be expected to be populated in the decay of ^{86}Y; this has not, however, been found in the above measurements. In addition, the plots of the scintillation spectra reported by HYDE et al. (Hy 54) suggest that the four gamma rays have different intensities, thus implying that more gamma rays, hitherto unobserved, must occur. Moreover, from the large decay energy of ^{86}Y, it may be expected that ^{86}Y decays in a more complicated way than is assumed in Fig. 5,1.

The present investigation was undertaken in order to check the

above-mentioned assumptions and to obtain a more accurate value for the decay energy.

§ 2. Beta ray measurements

For a description of the long lens beta ray spectrometer, reference is made to Chapter 1. The sources (carrier-free) were prepared by the reaction ^{86}Sr (d, 2n)^{86}Y in the I.K.O. synchro-cyclotron in Amsterdam. Targets of natural strontium oxide, as well as oxide enriched with ^{86}Sr, were used. The sources were purified chemically and converted into the chloride.

A helical baffle (see Chapter 1, § 5) was used for separating the conversion electrons from the positons. An analysis of the Kurie plot of the positon distribution is shown in Fig. 5,2. The positon spectrum appears to be complex and yields seven β^+ components.

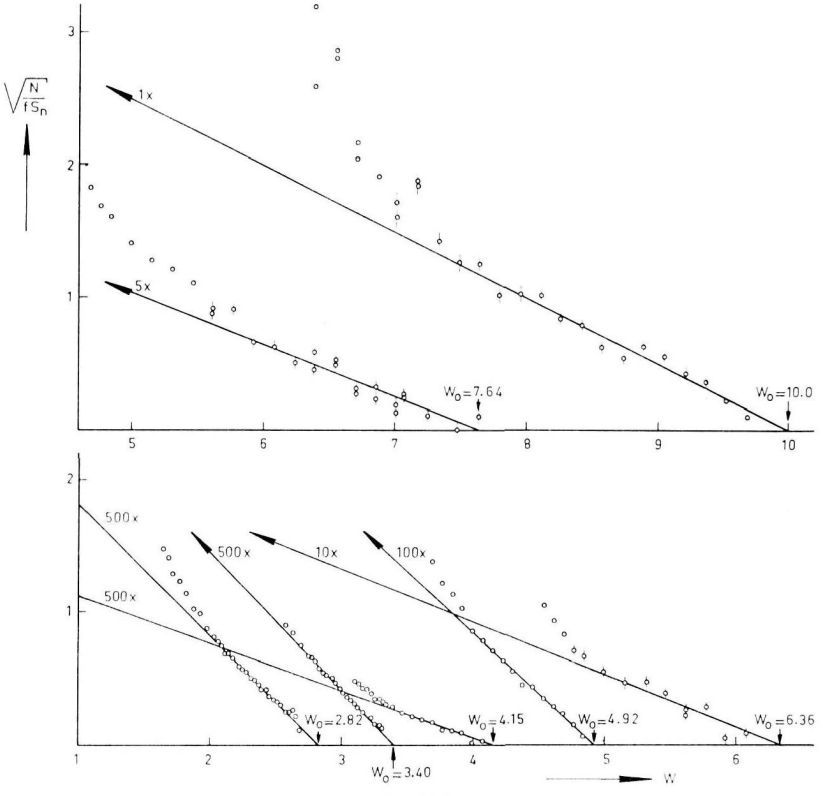

FIG. 5,2

Analysis of the Kurie plot of the positon distribution in the decay of ^{86}Y.

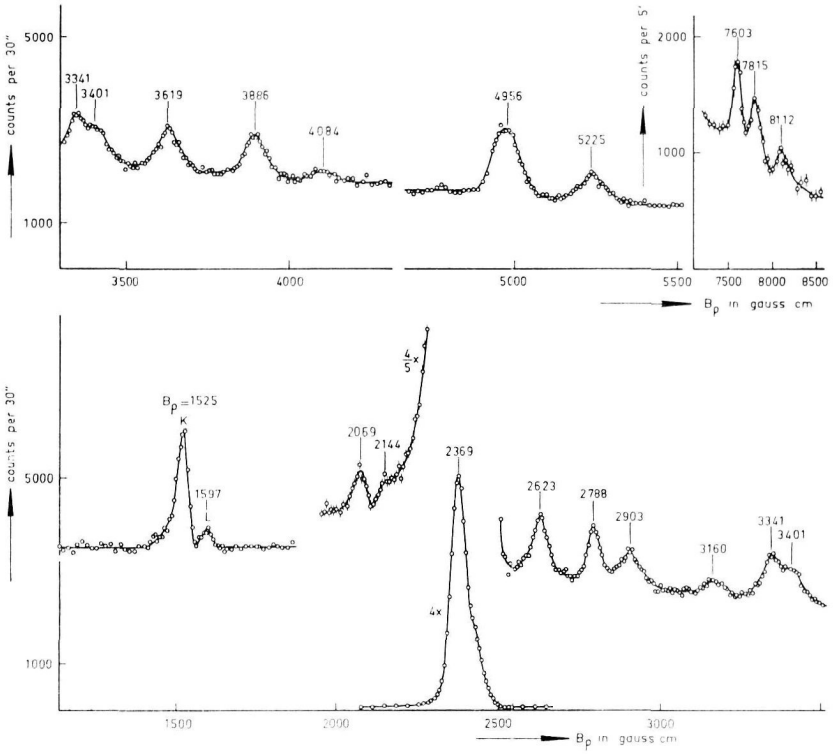

FIG. 5,3

Internal conversion spectrum from the decay of ^{86}Y, recorded in a long lens beta ray spectrometer.

TABLE 5,II

End points of the positon spectra E_o in keV	Relative intensities of the positon spectra in %	Assumed spectrum shape	Comparative half-lives	
			log ft	log f_1t *)
4600 ± 60	0.88	$\Delta J = 2$, yes	10.6	11.3
3370 ± 30	1.9	$\Delta J = 2$, yes	9.4	9.8
2760 ± 200	2.1	$\Delta J = 2$, yes	9.1	9.3
2005 ± 8	13.2	Allowed	7.6	
1610 ± 90	18.8	Allowed	7.1	
1226 ± 6	49.1	Allowed	6.1	
930 ± 12	14.0	Allowed	6.2	

*) See DAVIDSON (Da 51).

TABLE 5,III

Internal conversion peaks in the decay of ^{86}Y.

Bp in gauss cm of the electrons	Relative intensity	Assignment (energies in keV)	Bp in gauss cm of the electrons	Relative intensity	Assignment (energies in keV)
1525	333	191 K			
1597	42	191 L	3619	79	704 K
2065	41	309 K	3886	57	770 K
2156	7.5	329 K	4084	9.7	832 K
2623	98	443 K	4956	100	1076 K
2903	66	514 K	5225	33	1153 K
3160	34	581 K	7603	0.86	1841 K
3341	61	630 K	7815	1.50	1903 K
3401	47	646 K	8112	1.94	1990 K

The end points and relative intensities of these beta transitions are shown in Table 5,II. The comparative half-lives in the last two columns of Table 5,II were computed on the assumption that the total intensity of the positon emission is about 46% of the ^{86}Y disintegrations (see § 4 of this chapter).

The internal conversion spectrum was recorded and its decay was followed in order to determine which of the lines occurred in the decay of ^{86}Y. A typical run of the conversion line spectrum is shown in Fig. 5,3. At least 16 gamma rays have been observed in these measurements; their energies and the relative intensities of the internal conversion peaks are given in Table 5,III. The $K/(L + M)$ ratio of the conversion electrons from the 191 keV gamma ray was 7.9 ± 0.4. The results given in the Tables 5,II and III must be considered as preliminary results with the exception of those pertaining to the proper subject of our investigation.

§ 3. The scintillation spectrum and gamma-gamma coincidence measurements

The scintillation spectrometer and its calibration are described in Chapter 1. Since the scintillation spectrum of ^{86}Y could be expected to be complex (see § 2), use was also made of a 100 channel pulse height analyzer at the I.K.O. laboratory in Amsterdam. The scintillation spectra as recorded with a NaI(Tl) scintillation spectrometer is shown in Fig. 5,4.

Strong contamination of ^{87}Y in the sample hampered the detection of weak gamma ray transitions in the low energy region. The internal conversion spectrum showed that three of the four gamma rays reported by HYDE et al. consisted of at least two transitions. The energy systematics of nuclear levels discussed in § 1, suggests that the 1153 keV gamma ray found above occurs between the

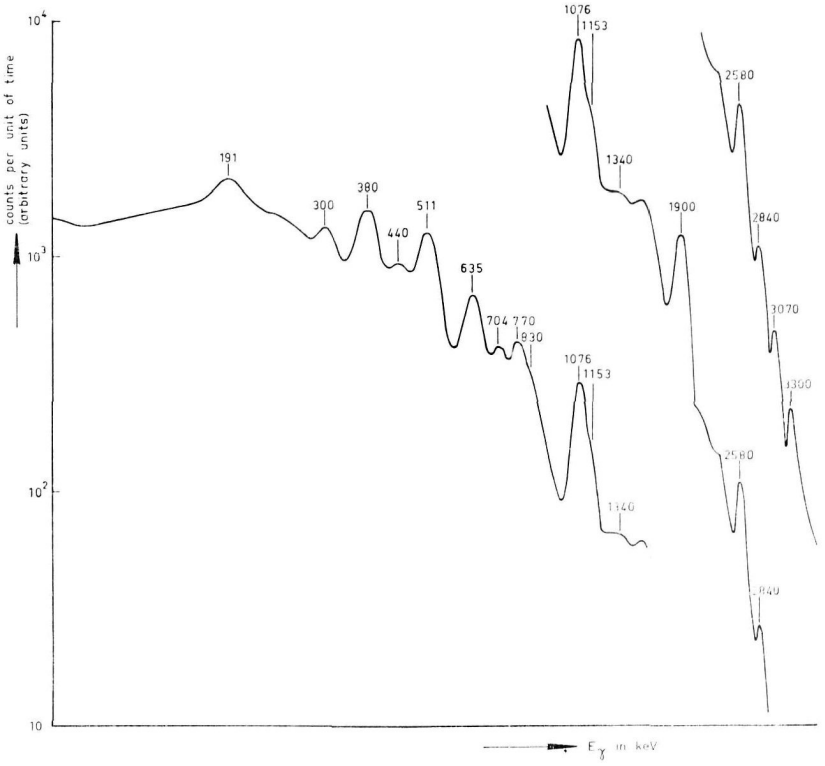

FIG. 5,4

The scintillation spectra from the decay of ^{86}Y.

two 2^+ levels. In order to check this assumption gamma-gamma coincidence measurements were made. Spectra were recorded in coincidence with photopeaks at 1076 keV and 1153 keV, and with the region with energies higher than 1400 keV. The result of these measurements are shown in Fig. 5,5.

The preliminary results from the scintillation and coincidence measurements are summarized in Table 5,IV, and include gamma

rays at about 385 keV (?), 1350 keV, 2580 keV, 2840 keV, 3070 keV and 3300 keV (?) which have not yet been observed in conversion line measurements.

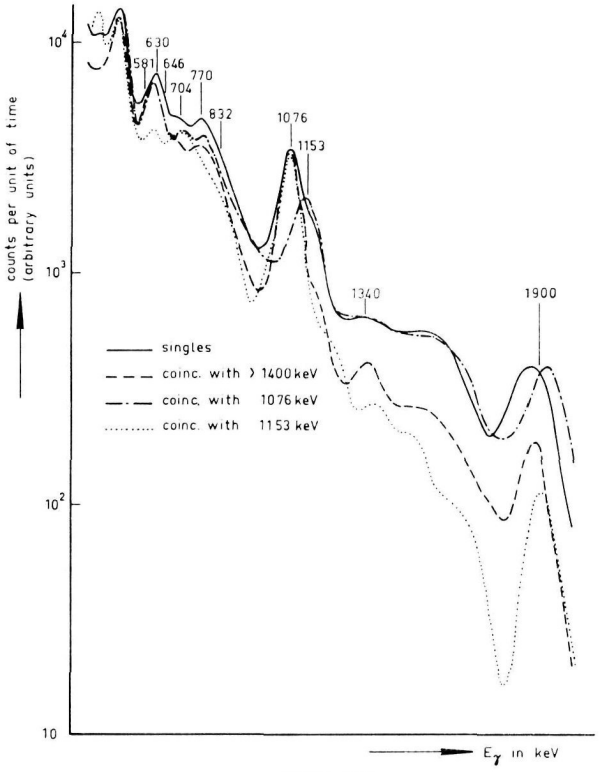

FIG. 5,5

The gamma ray spectra in coincidence with the gamma ray photopeaks at 1076 keV, 1153 keV and the region of energies larger than 1400 keV.

§ 4. Measurements with a proportional counter

Beta-gamma ray coincidence measurements have been performed with the proportional counter and a NaI(Tl) scintillation spectrometer in the same way as described in Chapter 3, § 2. The results of these measurements are shown in the last column of Table 5,IV; a typical run of this measurement is shown in Fig. 5,6.

The fluorescent yield in strontium was determined in the same way as described in Chapter 2, § 2 yielding a value of $\omega_k = 0.64 \pm 0.03$, in good agreement with the semi-empirical value of 0.653 (Wa 58).

TABLE 5,IV

Results from the gamma ray scintillation spectra and coincidence measurements.

Gamma ray	E_γ in keV	Estimated rel. intens. in %	In coincidence with	$\beta^+/(\varepsilon+\beta^+)$ in % (from § 4)
γ_1	191 *)	7 ± 2		41 ± 5
γ_2	309 *)			
γ_3	329 *)			
γ_4	385 ?			
γ_5	443 *)		not $>$ 1400, (γ_{14} ?)	
γ_6	514 *)			
γ_7	581 *)			
γ_8	630 *)	40 ± 3	$>$ 1400, γ_{13}	20 ± 2
γ_9	646 *)		($>$ 1400), (γ_{13})	
γ_{10}	704 *)	15 ± 2	γ_{14}	20 ± 10
γ_{11}	770 *)	14 ± 2	(γ_{14}), γ_{13}	
γ_{12}	832 *)		(γ_{14} ?)	
γ_{13}	1076 *)	100	γ_{18}, (γ_{17}), γ_{14}, (γ_{13}), γ_{11}, (γ_9), γ_8	43 ± 2
γ_{14}	1153 *)	39 ± 6	γ_{17}, (γ_{15} ?), γ_{13}, (γ_{12} ?), (γ_{11}), γ_{10}, (γ_5 ?)	43 ± 4
γ_{15}	1350	~ 5	$>$ 1400, (γ_{14} ?)	
γ_{16}	1841 *)	49 ± 5	γ_{17}	46 ± 4
γ_{17}	1903 *)		γ_{16}, γ_{18}, γ_{14}, (γ_{13})	
γ_{18}	1990 *)		γ_{17}, γ_{13}	
γ_{19}	2580	5 ± 2		
γ_{20}	2840	0.8		
γ_{21}	3070	0.4		
γ_{22}	3300 ?	0.7		
region	$>$ 1400		γ_{17}, γ_{15}, (γ_{14}), γ_{13}, (γ_9), γ_8, not γ_5	

*) Energy from conversion line measurements see Table 5,III.

§ 5. Conclusions

The coincidence measurements represented in Fig. 5,5 show that the 1076 keV line is coincident with practically all other lines (the slight difference between the coincident spectrum and the single spectrum at the high energy end may be explained by a slight shift in amplification due to the high counting rates in the single spectra).

The spectrum coincident with the 1153 keV line shows relatively much less coincidences with the 1900 keV line group; this indicates that the 1153 keV transition is parallel to two of the three gamma rays in this group. Energy sum relations ($1153 + 832 \approx 1990$; $1153 + 704 \approx 1841$, whereas $1903 - 1153 = 750$ agrees somewhat less well with other known gamma ray energies) indicate that the

1841 and 1990 keV gamma rays may be the parallel gamma rays; the third gamma ray would explain the remaining coincidences. Fig. 5,5 shows that coincidences are also present between gamma rays in the 1900 keV group, indicating that the 1903 keV line

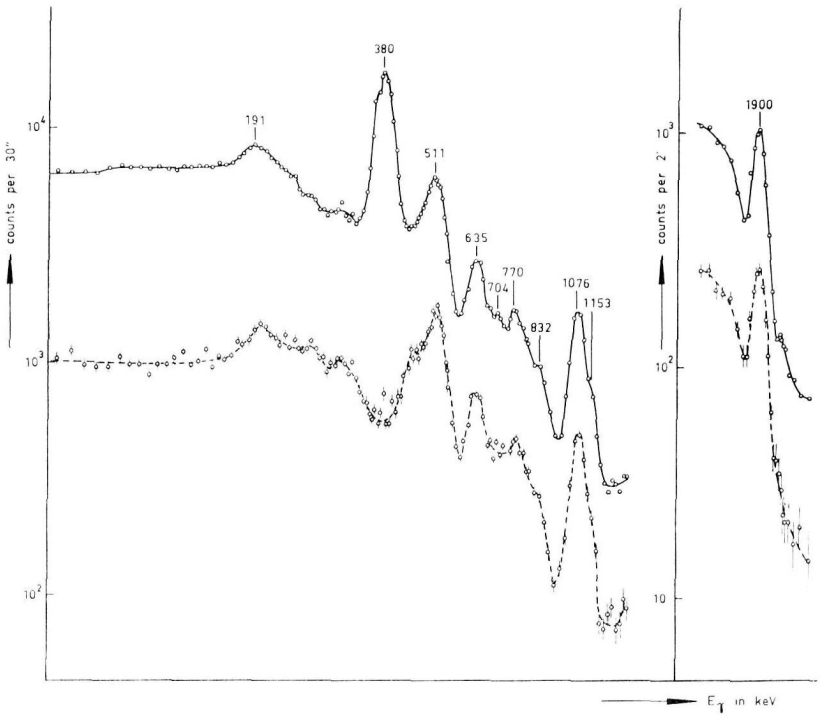

FIG. 5,6

Single and coincidence spectra from the decay of ^{86}Y. Beta-gamma coincidences were recorded, using the proportional counter in coincidence with a gamma ray scintillation spectrometer. The dotted curve is the coincidence spectrum.

preceeds either the 1841, or the 1990 keV line (or perhaps both). In total, these results provide the partial decay scheme given in Fig. 5,7.

The measurement of the positon spectrum strongly indicates that the three most energetic branches are $\triangle J = 2$, yes transitions. The value of $\log f_1 t$ are somewhat high compared with the average value 8.5; this may, however, be explained by the poor overlap of the wave functions which near the closed shells ($N = 50$, $Z = 38$) are unusually pure. (A similar deviation occurs in ^{84}Rb, where the

value for $\log f_i t$ of the ground state transition is 9.20). Explanation as second forbidden transitions would require about 1000 times higher comparative half-lives.

As reported in § 1 of this chapter, the ground state and the first excited state in ^{86}Sr have spin assignments of 0^+ and 2^+, as is usual for even-even nuclides. The conclusion inevitably drawn, therefore, is that the ground state of ^{86}Y has a spin assignment of 4^-, in agreement with the strong Nordheim coupling rule (No 50). The three most energetic positon branches should then all decay to 2^+ levels.

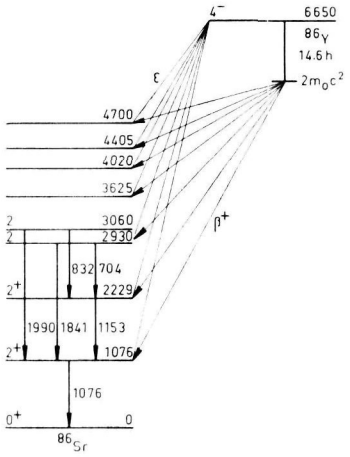

FIG. 5,7

Partial decay scheme of ^{86}Y, as deduced from the measurements mentioned in § 2, 3 and 4.

The third branch may be complex and feed the 2930 keV and 3060 keV levels. Both levels would be expected to have spin assignments 2, if the spins were lower, high intensity transitions to the ground state would be present; if they were higher, the positon transitions feeding these levels would be rather more intense. At least one of these levels should have a positive parity for evident reasons.

The decay energy of ^{86}Y, as computed from the three most energetic positon branches in conjunction with the energies of respective levels, becomes 6700 $\pm$ 60 keV, 6620 $\pm$ 30 keV and 6770 $\pm$ 200 keV, if the last branch is assumed to feed the 2930 and 3060 keV levels in about equal amounts. As an average value for the ^{86}Y decay energy Q, 6650 $\pm$ 30 keV is proposed.

According to the analysis in ^{86}Sr of the positon spectra in Table 5,II, other levels should be present at 3625 $\pm$ 35, 4020 $\pm$ 90, 4405 $\pm$ 35 and 4700 $\pm$ 40 keV. The data collected so far do not allow the construction of a complete disintegration scheme consistent with the reported gamma ray and beta ray energies and intensities.

CHAPTER 6

ELECTRON CAPTURE TO POSITON EMISSION BRANCHING RATIOS

§ 1. Introduction

The uncertainties in the experimental values of electron capture to positon emission branching ratios are mostly of the order of 10% or larger. Exceptions are the measurements, by Sherr and Miller (Sh 54), Drever et al. (Dr 56), and Scobie and Lewis (Sc 57), of ^{22}Na, ^{18}F and ^{11}C respectively. These measurements show excellent agreement with theory, when it is assumed that no Fierz term is present. In this thesis precise measurements have been extended to cover other nuclei. Comparison of the experimentally obtained material with theory, sets limits to the Fierz term. According to Brysk and Rose (Br 55), electron capture to positon emission branching ratios in non-unique first forbidden transitions should not differ much from those in allowed transitions. Below, a description is given of measurements designed to test this assumption.

The ε/β^+ branching ratios have been measured by means of beta-gamma ray coincidence measurements. The gamma rays were recorded in a NaI(Tl) scintillation spectrometer; the beta rays, in either a long lens beta ray spectrometer or a proportional counter. For details of the arrangements reference is made to Chapters 1 and 3.

Both the beta ray spectrometer and the proportional counter were calibrated by beta-gamma ray coincidence measurements relating to the decay of ^{198}Au (see Chapter 3). The ratio of true to accidental coincidences was larger than 4 : 1 for the beta ray spectrometer measurements, and at least 20 : 1 in all measurements using the proportional counter.

The following isotopes were investigated: ^{22}Na, ^{44}Sc, ^{48}V, ^{52}Mn, ^{58}Co, ^{57}Ni and ^{84}Rb. Carrier-free sources were used, deposited on formvar films rendered conductive by evaporating aluminium onto

the backing. All sources were prepared in the I.K.O. synchro-cyclotron in Amsterdam.

The experimental values of electron capture to positon emission ratios ε/β^+ had to be compared with theoretical ratios derived from ε_K/β^+ ratios (Zw 57), L_I/K capture ratios (Ro 49) and ratios of capture in higher shells to that in the L shell (Wa 58) (see Chapters 2 and 3).

§ 2. ^{22}Na

A review of measurements relating to this nuclide has recently been given by ENDT and BRAAMS (En 57). The decay scheme of ^{22}Na is shown in Fig. 6,1. The end point of the continuous positon

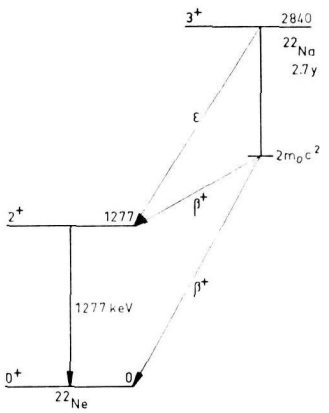

FIG. 6,1

Decay scheme of ^{22}Na.

branch feeding the 1277 keV level in ^{22}Ne has been reported to be 540 $\pm$ 5 keV (Ma 50) and 542 $\pm$ 5 keV (Wr 53). The ratio of electron capture to positon emission in the decay of ^{22}Na has been measured earlier by several investigators. The most accurate values obtained from these measurements are given in Table 6,II (see § 9 of this chapter).

In earlier experiments (Ha 57), measurements of ^{22}Na were used for the calibration of the experimental arrangement of the proportional counter. Subsequently, however, careful calibration was carried out with the aid of beta-gamma ray coincidences from the known decay of ^{198}Au (see Chapter 3). Accurate comparison of the ^{198}Au with the ^{22}Na measurements in the proportional counter

gave a value for $\beta^+/(\varepsilon + \beta^+)$ of 90.2 $\pm$ 0.6%, this value being the percentage positon emission occurring in the decay to the 1277 keV level in ^{22}Ne. This result yields a ratio for ε/β^+ of 0.109 $\pm$ 0.008. A typical run of the single and coincidence spectra from the decay of ^{22}Na is shown in Fig. 6,2.

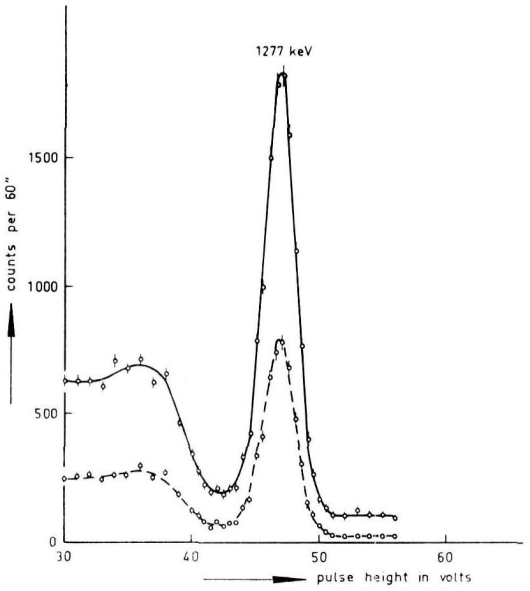

FIG. 6,2

Single and coincidence spectra from the decay of ^{22}Na.
The dotted curve is the coincidence spectrum.

The experimental value is in excellent agreement with the values found by SHERR and MILLER (Sh 54), KREGER (Kr 54), ALLEN et al. (Al 55) (see Table 6,II), and with the theoretical ratio of 0.1135 $\pm$ 0.0020 as computed by SHERR and MILLER.

§ 3. ^{44}Sc

The 3.9 h ^{44}Sc isotope was produced by the reaction ^{41}K (α, n) ^{44}Sc. The sources were rendered carrier-free by chemical separation and converted into the chloride.

The decay scheme of ^{44}Sc is shown in Fig. 6,3. The spin of the ^{44}Sc ground state is 2^+ (Bo 58). The value for the end point of the positon spectrum has been reported by BRUNER and LANGER (Br 50) and by BLUE and BLEULER (Bl 55), as 1463 $\pm$ 5 keV, and

1471 $\pm$ 5 keV, respectively. The electron capture to positon emission branching ratio has also been investigated by these authors. They found the values $\sim$ 0.02 (Br 50), and 0.073 $\pm$ 0.017 (Bl 55), respectively, for the ε/β^+ ratio of the transitions to the 1159 keV level in ^{44}Ca.

Measurements using the proportional counter yielded an ε/β^+ ratio of 0.023 $\pm$ 0.019, this value being computed from the measured value for $\beta^+/(\varepsilon + \beta^+)$ of 97.8 $\pm$ 1.8%. This value for ε/β^+ must be compared with the above-mentioned experimental values

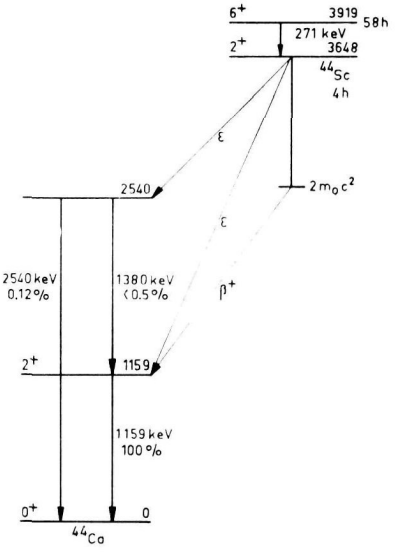

FIG. 6,3

Decay scheme of ^{44}Sc.

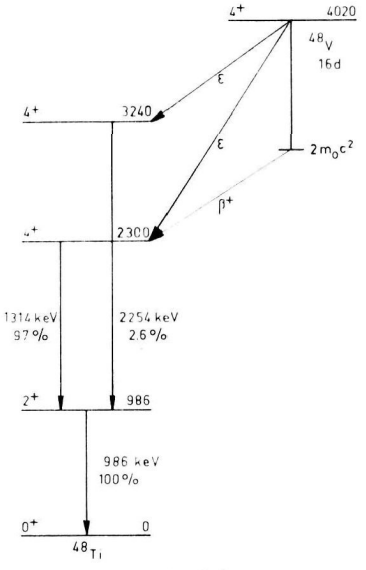

FIG. 6,4

Decay scheme of ^{48}V.

and with the theoretical value for ε/β^+ of 0.049 $\pm$ 0.001, calculated for the average value of the end point of the positon distribution, 1467 $\pm$ 3 keV.

§ 4. ^{48}V

The decay of the nuclide ^{48}V (half-life 16 days) was recently investigated in this laboratory (No 58, Ha 57). The decay scheme is given in Fig. 6,4. It is important for the interpretation of our measurements that no transitions are present between the two 4^+ levels. Such transitions were reported by Casson et al. (Ca 53) as

a result of triple coincidence measurements; repetition of these experiments by VAN NOOIJEN et al. (N 58), however, indicated a much lower intensity for this possible gamma ray transition. The spin of the ^{48}V ground state is 4^+ (Bo 58). The end point for the positon spectrum was found to be 698 $\pm$ 4 keV (No 58), whereas other authors have reported 693 $\pm$ 6 keV (Ki 55), 692 $\pm$ 5 keV (Ma 53) and 690 $\pm$ 10 keV (Ro 52). Earlier experimental values, obtained by various authors, for the ε/β^+ ratio are presented in Table 6,II.

Carrier-free ^{48}V sources were prepared by bombarding natural titanium with 28 MeV deuterons in the I.K.O. synchro-cyclotron in Amsterdam. They were purified chemically and converted into the chloride.

Two independent measurements of the ratio of electron capture to positon emission to the 2300 keV (4^+) level in ^{48}Ti were made with the beta ray spectrometer and with the proportional counter; the values for $\beta^+/(\varepsilon + \beta^+)$ so obtained were 55.6 $\pm$ 0.8% and 56.0 $\pm$ 0.6%, respectively. From these ratios, values for ε/β^+ (electron capture to positon emission branching ratio) of 0.75 $\pm$ 0.03 and 0.74 $\pm$ 0.02, respectively, were computed. Taking 695 $\pm$ 3 keV as the average value for the end point of the positon distribution a theoretical value for $(\varepsilon/\beta^+)_0$ of 0.765 $\pm$ 0.014 could be derived.

§ 5. ^{52}Mn

The investigation into the decay of the ^{52}Mn isotope is described in Chapter 3 of this thesis. The percentage positon emission in this decay was measured, using both the beta ray spectrometer and the proportional counter. For further details of the measurements, reference is made to Chapter 3 and to Table 6,II of this chapter.

§ 6. ^{58}Co

The 72 d ^{58}Co isotope was prepared by bombarding natural manganese with 14 MeV alpha particles. The sources were separated chemically and converted into the chloride.

Fig. 6,5 shows the decay scheme of ^{58}Co as given by FRAUENFELDER et al. (Fr 56). The spin of the ^{58}Co ground state is 2^+ (Bo 58). The end point of the positon distribution has been reported as 472 $\pm$ 6 keV (Ch 52) and 485 $\pm$ 10 keV (Co 55). Meas-

urements of the ε/β^+ ratio have been made by Good et al. (Go 46) and Cook and Tomnovec (Co 56); both publications report a value for ε/β^+ of 5.9 ± 0.2, corrected for the presence of the transition between the two 2^+ levels, the ε/β^+ ratio for the transition to the 805 keV level then becomes 5.8 ± 0.2.

The percentage positon emission was measured by means of beta-gamma ray coincidences using the proportional counter. From

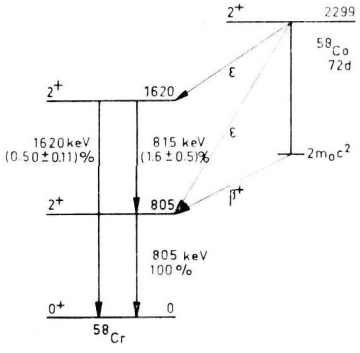

FIG. 6,5

Decay scheme of ^{58}Co.

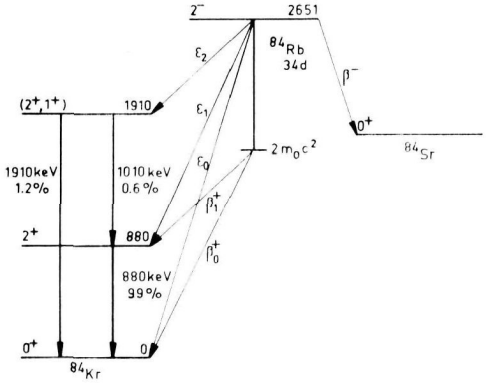

FIG. 6,6

Decay scheme of ^{84}Rb.

this measurement a value for $\beta^+/(\varepsilon + \beta^+)$ of 14.77 ± 0.30 was found, giving an electron capture to positon emission branching ratio ε/β^+ of 5.67 ± 0.14 for the transition to the 805 keV level, which is in good agreement with earlier results (see also Table 6,II), and with the theoretical value of 5.56 ± 0.26.

§ 7. ^{57}Ni

The radio-active decay of ^{57}Ni is described in detail in Chapter 4 of this thesis. The values for electron capture to positon emission branching ratios are shown in Table 6,II.

§ 8. ^{84}Rb

The nucleus ^{84}Rb decays with a half-life of 33 days (We 55) by positon emission and electron capture to ^{84}Kr and by negaton emission to the ground state of ^{84}Sr. The decay scheme as given by Welker and Perlman (We 55) and by Johnson and O'Kelly (Jo 57) is shown in Fig. 6,6. The spin of the ^{84}Rb ground state has

been measured and found to be 2 (Ho 56). The positon distribution has been reported to be complex and to contain two branches. The end point of the most energetic beta ray branch, which has a $\Delta J = 2$, yes shape, has been measured and found to be: 1629 $\pm$ 5 keV (Hu 52), 1700 $\pm$ 70 keV (We 55) and 1656 keV (Be 58); the relative intensity of this branch is 40% (Hu 52) and 49.5 $\pm$ 2.6% (We 55) of all positons. Three gamma rays have been observed

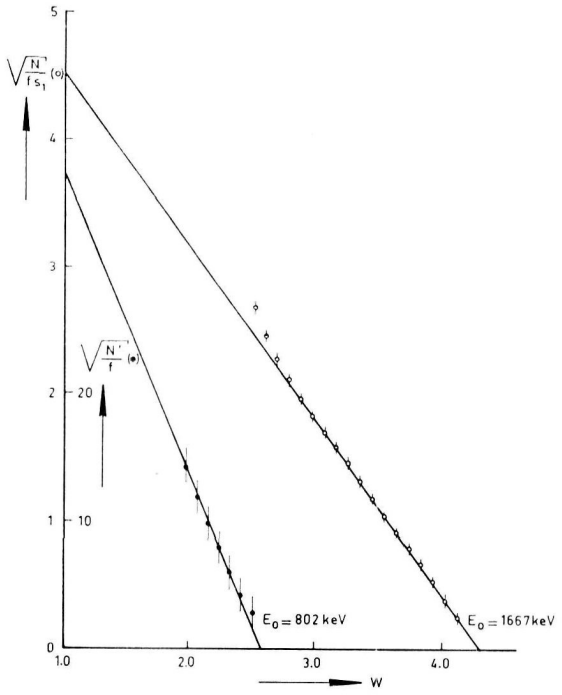

FIG. 6,7

Analysis of the Kurie plot of the positon distribution in the decay of ^{84}Rb.

with the following energies and relative intensities γ_1: 0.88 MeV (100), γ_2: 1.01 MeV (0.6 $\pm$ 0.2) and γ_3: 1.91 MeV (1.2 $\pm$ 0.2), these being average values of the results reported by (We 55) and (Jo 57). The first excited level in ^{84}Kr is reported to have an energy of 880 $\pm$ 5 keV (Pi 57, Te 56). Coincidence measurements between the annihilation radiation and γ_1 yielded a value for $\beta^+/(\varepsilon + \beta^+)$ of 15.0 $\pm$ 1.1% (We 55). The percentage K capture preceding the 880 keV transition is reported to be 71 $\pm$ 3% of the total K capture (We 55).

The sources used in the measurements described below, were obtained by the reaction ^{86}Sr (d, α) ^{84}Rb, using natural strontium as well as targets enriched with ^{86}Sr. The sources were purified chemically and converted into the nitrate.

The positon distribution from a ^{84}Rb source prepared from an enriched target was measured in the long lens beta ray spectrometer provided with the helical baffle. An analysis of the Kurie plot is shown in Fig. 6,7; the most energetic branch has been plotted using the shape factor for a unique first forbidden transition. This

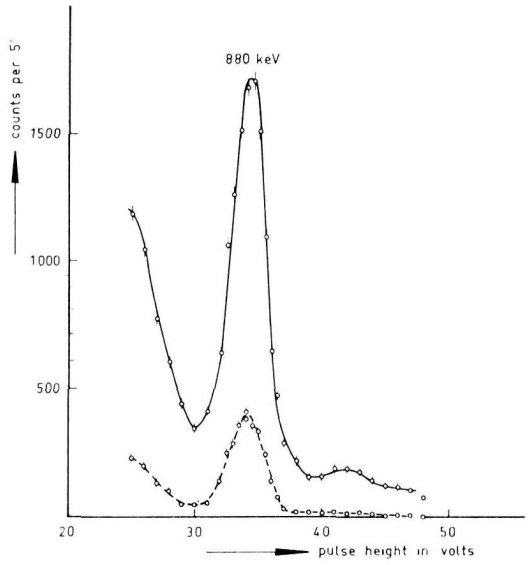

FIG. 6,8

Single and coincidence spectra from the decay of ^{84}Rb. The dotted line is the coincidence spectrum. The radio-active source was obtained from an enriched ^{86}Sr target.

measurement yielded the following end points and relative intensities: 1667 $\pm$ 11 keV (0.44 $\pm$ 0.04) and 802 $\pm$ 25 keV (0.56 $\pm$ 0.04).

Coincidences between the positons in the proportional counter and the gamma ray spectrum in a NaI(Tl) scintillation spectrometer were performed in the usual way; a value for $\beta^+/(\varepsilon + \beta^+)$ of 14.80 $\pm$ 0.26% was found for the percentage positons coincident with the 880 keV gamma rays. This result was the average of several measurements using sources produced from natural, as well

as enriched, ^{86}Sr targets. A typical run of the single and coincidence spectra from the decay of ^{84}Rb is shown in Fig. 6,8.

The electron capture to positon emission branching ratio for the ground state transition in ^{84}Rb can be computed from the similar ratio in the transition to the 880 keV state, the ratio of the intensities of the two positon branches and the ratio of the capture transitions. The ratio $\beta_o^+/(\beta_o^+ + \beta_1^+)$ can be determined most accurately by comparing coincidences between the 880 keV gamma rays in the scintillation counter and the positons in the proportional counter from the decay of ^{84}Rb, with the coincidences between the 880 keV gamma rays and the negatons in the decay of ^{46}Sc:

$$(^{46}Sc): \frac{N_c}{N_\beta} = \Omega_\gamma \tag{6.1}$$

$$(^{84}Rb): \frac{N_c}{N_\beta} = \frac{\beta_1^+}{\beta_o^+ + \beta_1^+} \Omega_\gamma \tag{6.2}$$

The ratio of the electron capture transitions can be determined by measuring coincidences with K X-rays counted in the proportional counter:

$$\frac{N_c}{N_K} = \frac{\varepsilon_1 + 0.33\varepsilon_2}{\varepsilon_0 + \varepsilon_1 + \varepsilon_2} \Omega_\gamma \tag{6.3}$$

A sequence of alternating measurements on ^{84}Rb and ^{46}Sc were performed in order to verify that the geometry of the coincidence arrangement was reproducible. The results of these measurements were $\beta_1^+/(\beta_o^+ + \beta_1^+) = 52.5 \pm 2.4\%$ and $(\varepsilon_1 + 0.33\varepsilon_2)/(\varepsilon_1 + \varepsilon_2 + \varepsilon_3) = 82.3 \pm 3.1\%$.

The present and previous results of the measurements of the different quantities from the ^{84}Rb decay are given in Table 6,I. The last column of this table gives the accepted mean values.

The ε/β^+ ratio of the transition to the 880 keV level derived from above measurements is: $\varepsilon_1/\beta_1^+ = 5.72 \pm 0.12$. This is in close agreement with the value 5.6 ± 0.5 found by WELKER and PERLMAN (We 55). The theoretical value for allowed transitions, derived from the curves given in Chapter 3 of this thesis, was found to be 3.6 ± 0.2 (using an end point energy of 787 ± 12 keV).

The ε/β^+ ratio of the ground state transition can be obtained from the measured quantities by the following equation (see Table 6,I):

$$\varepsilon_o/\beta_o^+ = \left\{(\varepsilon'_1/\beta_1^+) \times (\beta_1^+/\beta_o^+) \times \left(\frac{1}{\varepsilon'_1/\Sigma\varepsilon} - 1\right) \times \left(\frac{1}{1 + 0.67\ \varepsilon_2/\varepsilon_o}\right)\right\} \tag{6.4}$$

in which $\varepsilon_2/\varepsilon_o$ is approximately equal to 0.1. The equation (6.4) yields a value for ε_o/β_o^+ of 1.25 ± 0.28, when, apart from our values, the mean value of 0.515 ± 0.018 for β_1^+ is used. Using the same method, WELKER and PERLMAN found a value of 2.2 ± 0.4 for this ratio. The theoretical ratio for an allowed transition is 0.312 ± 0.009, and that for a unique first forbidden transition, 1.01 ± 0.03 (see Chapter 2, § 5). The experimental value obtained from our measurements shows agreement with theory, contrary to the results of WELKER and PERLMAN.

§ 9. Discussion and conclusions

The electron capture to positon emission ratios of all measurements of allowed beta transitions are shown in Table 6,II; earlier precise measurements have also been included. The theoretical electron capture to positon emission branching ratios are derived, as described, from the curves in Fig. 2,1 and the data mentioned in § 1 of this chapter.

The experimental values for the allowed transitions are all in close agreement with theoretical predictions. Limits to the Fierz term parameter b, mentioned in Chapter 2, are obtained by comparing our results with the theoretical ratios, using formula (2.11). In the last column of Table 6,II the Fierz term parameter b has been calculated separately for each of our measurements. The mean value found for b is -0.007 ± 0.005. The error in this result does not include a possible systematic error due to the calibration of the coincidence arrangement. Such a systematic error could be caused by the intensity of the back-scattered electrons being different for isotopes with different maximum positon energies (Se 51). This error is about 0.005. In order to allow for various other small experimental errors which may occur, inaccuracies in the theoretical values obtained by the interpolation procedure, and the approximations used by ZWEIFEL in computing the latter values, the following value for b is proposed as a result of our experiments:

$$b = -0.007 \pm 0.010$$

Most transitions investigated in this work occur without spin

TABLE 6,I

Energies and intensities of transitions in the decay of ^{84}Rb.

Measured quantity	Reference					Accepted mean value
	(Hu 52)	(We 55)	(Jo 57)	Others	This thesis	
β_1^+ (keV)	820 ± 50	810 ± 50			802 ± 25	1667 — 880 = 787 ± 12
β_0^+ (keV)	1629 ± 5	1700 ± 70		1656 (Be 58)	1667 ± 11	1667 ± 11
E_x (keV)				880 ± 5 (Pi 57, Te 56)		
γ_1 (rel. int.)		100	100			100
γ_2 ('')		< 0.45	0.66			0.6 ± 0.2
γ_3 ('')		1.35 ± 0.1	1.11			1.2 ± 0.2
$\beta_1^+/(\beta_0^+ + \beta_1^+)$	0.60	0.505 ± 0.026			0.56 ± 0.04 *) 0.525 ± 0.024 **)	0.515 ± 0.018
β_1^+/γ_1		15.0 ± 1.1 %			14.80 ± 0.26%	14.80 ± 0.26%
$\varepsilon'_1/\Sigma\varepsilon$		71 ± 3%			82 ± 3%	82 ± 3%

*) From Kurie plots.

**) From coincidence measurements in which ^{84}Rb is compared with ^{46}Sc.

change. Nevertheless, there are reasons (Bo 58) for believing that even these transitions are due almost entirely to Gamow-Teller interactions (Fermi transitions being forbidden by isotopic spin selection rules). Our results therefore prove that

$$\frac{\mathrm{Re}\ (C_T^{R*} C_A^R + C_T^{L*} C_A^L)}{|C_T^R|^2 + |C_T^L|^2 + |C_A^R|^2 + |C_A^L|^2} = -0.007 \pm 0.010 \quad (6.5)$$

Unique first forbidden transitions have been measured in the case of three isotopes, viz.: ^{84}Rb, ^{122}Sb and ^{126}I. The most accurate of the measurements of these isotopes are shown in Table 6,III. The measurements relating to ^{84}Rb are described in § 8 of this chapter. Other measurements of the K/β^+ ratio of the unique first forbidden transition in ^{126}I have been made by MARTY et al. (M 53) and PERLMAN and WELKER (Pe 54) who found K/β^+ to be 12.5^{+7}_{-3} and 21 ± 8, respectively. GLAUBMAN (Gla 55) has reported a measurement yielding a K/β^+ value of 300 ± 130 for the transition in ^{122}Sb.

The experiments and theory agree within the uncertainties. The mean value of the Fierz term parameter b, as derived from these measurements (see the last column of Table 6,III), is:

$$b = 0.02 \pm 0.03$$

On non-unique first forbidden beta transitions little information is available; accurate measurements are available only for $2^- \rightarrow 2^+$ transitions in ^{74}As, ^{84}Rb and ^{126}I. The observed and calculated K capture to positon emission ratios for these non-unique first forbidden transitions are shown in Table 6,IV. For measurements of the decay of ^{84}Rb, reference is made to § 8 of this chapter. Other investigations into the K/β^+ ratio in ^{126}I have been carried out by MARTY et al. (M 53) and KOERTS et al. (Ko 55), who found this ratio to be larger than 75 and equal to 95 ± 10 respectively. The value, in Table 6,IV, reported by HARMER and PERLMAN, is a tentative, hitherto unpublished value, which has been chosen in preference to earlier values, because it is a result of a direct measurement.

The experimental values for $2^- \rightarrow 2^+$ non-unique first forbidden transitions are 20% to 60% higher than the theoretical values for allowed transitions (see Chapter 2, § 4). PERLMAN et al. (Pe 58) try to explain these differences by assuming that the K/β^+ ratio in the part of the transitions in which the spin change $|\Delta J|$ is 0 or 1, is nearly equal to that for allowed transitions, but that, in all

TABLE 6,II

Electron capture to positon emission ratios for allowed beta transitions.

Nuclide	End point of the positon spectrum		Experimental results					Theoretical value $(\varepsilon/\beta^+)_o$	Fierz term parameter (this thesis) b in $^o/_{oo}$
			This thesis		Earlier results				
	Average value in keV	Reference	P_{β^+} in %	ε/β^+	P_{β^+} in %	ε/β^+	Reference		
^{11}C	968 ± 8	Wo 54	—	—	99.83 ± 0.03	0.0020 ± 0.0003	Sc 57	0.0021	—
^{18}F	649 ± 9	Ru 51	—	—	96.9 ± 0.2	0.032 ± 0.002	Dr 56	0.0310	—
^{22}Na	541 ± 4	Ma 50 Wr 53	*) 90.2 ± 0.6	0.109 ± 0.008	89.0 ± 1.0 89.1 ± 0.8 90.1 ± 0.5	0.124 ± 0.012 0.122 ± 0.010 0.110 ± 0.006	Kr 54 Al 55 Sh 54	0.1135 ± 0.002	−12 ± 22
^{44}Sc	1467 ± 3	Br 50 Bl 55	*) 97.8 ± 1.8	0.023 ± 0.019	93.2 ± 1.5	0.073 ± 0.017	Bl 55	0.049 ± 0.001	(−220 ± 160)
^{48}V	695 ± 3	Ro 52 Ma 53 Ki 55 No 57	*) 56.0 ± 0.6 **) 55.6 ± 0.8	0.74 ± 0.02 0.75 ± 0.03	56 ± 3 58 ± 4 57 ± 3 60 ± 4	0.79 ± 0.10 0.72 ± 0.11 0.76 ± 0.09 0.67 ± 0.11	No 57 Go 46 Bo 55 St 53	0.765 ± 0.014	−10 ± 10 −6 ± 13
^{52}Mn	575 ± 4	this thesis	*) 33.8 ± 0.8 **) 33.0 ± 1.0	1.97 ± 0.07 2.03 ± 0.09	35 ± 2 33 ± 2	1.86 ± 0.17 2.01 ± 0.22	Go 46 Se 54	2.03 ± 0.06	−9 ± 13 0 ± 16
^{58}Co	472 ± 6	Ch 52	*) 14.77 ± 0.30	5.67 ± 0.14	14.48 ± 0.44 14.48 ± 0.44	5.8 ± 0.2 5.8 ± 0.2	Go 46 Co 56	5.56 ± 0.26	+6 ± 16
^{57}Ni	324 ± 16	this thesis	*) 6 ± 2	18 ± 6	—	—	—	24 ± 6.5	(−80 ± 110)
	722 ± 6		*) 41.0 ± 1.0	1.438 ± 0.059	—	—	—	1.477 ± 0.040	−8 ± 15
	849 ± 6		*)**) 55.4 ± 1.2	0.805 ± 0.040	—	—	—	0.858 ± 0.020	−20 ± 17

*) Proportional counter.

**) Beta spectrometer.

TABLE 6,III

K capture to positon emission ratios in unique first forbidden ($2^- \rightarrow 0^+$) transitions.

Nucleus	End point of the positon spectrum E_o in keV (ref.)	K/β^+ experimental values (ref.)	Theoretical values of K/β^+ ratios for: Allowed transitions $(K/\beta^+)_o$	Theoretical values of K/β^+ ratios for: Unique first forbidden transitions $\frac{2(W_o+1)}{W_o-1}(K/\beta^+)_o$	Fierz term parameter b in $^o/_{oo}$
^{84}Rb	1667 ± 11 (this thesis)	1.12 ± 0.25 (this thesis)	0.280 ± 0.008	0.91 ± 0.02	98 ± 100
^{122}Sb	565 ± 25 (Pe 58)	300 ± 50 (Pe 58)	49	$275 \begin{smallmatrix}+70\\-55\end{smallmatrix}$	26 ± 80
^{126}I	1110 ± 20 (Ko 55)	20.2 ± 2.0 (Ko 55)	5.13	19.7 ± 0.8	8 ± 35

TABLE 6,IV

K capture to positon emission ratios in non-unique first forbidden ($2^- - 2^+$) transitions.

Nucleus	End point of the positon spectrum E_o in keV (ref.)	K/β^+ experimental values (ref.)	Theoretical values of K/β^+ ratios for: Allowed transitions $(K/\beta^+)_o$	Theoretical values of K/β^+ ratios for: Unique first forbidden transitions $\frac{2(W_o+1)}{W_o-1}(K/\beta^+)_o$	Ratio of the values from $\frac{\text{column 3}}{\text{column 4}}$
^{74}As	920 (Jo 51)	1.5 (Jo 51)	1.16	4.9	1.3
^{84}Rb	787 ± 12 (this thesis)	5.12 ± 0.11 (this thesis) 5.1 ± 0.4 (We 55)	3.23 ± 0.21	14.8 ± 2.4	1.58 ± 0.11
^{126}I	460 ± 15 (Ko 55)	148 (Har 58)	125 ± 7	$810 \begin{smallmatrix}+500\\-260\end{smallmatrix}$	1.2 ± 0.2

three cases in question, an appreciable part occurs with a spin change $|\triangle J|$ of 2. This explanation, however, demands somewhat higher intensities for the ($|\triangle J| = 2$)-part in these transitions than is compatible with the known reduced half-lives of unique first forbidden ($\triangle |J| = 2$) transitions. The above results therefore tend to indicate that in non-unique first forbidden transitions small deviations from $v_{1a} = a_1$ occur (see Chapter 2, § 5).

SURVEY OF THIS THESIS

In Chapter 1 of this thesis the experimental equipment is described. The construction, calibration and resolution of the long lens magnetic beta ray spectrometer are discussed. Details are given of the construction of the beta ray spectrometer and a helical baffle, a gamma ray scintillation spectrometer with a light guide, and a Geiger-Müller counter connected to the spectrometer. Other instruments used in the experiments, such as the gamma ray scintillation counter, the gamma-gamma ray angular correlation spectrometer, and the proportional counter are only briefly discussed.

Important aspects of theory, which are investigated in the experimental parts of this thesis (especially in Chapter 6), are discussed in Chapter 2.

Chapter 3 describes experiments concerning the radio-active decay of ^{52}Mn. The original purpose of this investigation was to measure the electron capture to positon emission ratio. The publication by MAZARI et al. (Ma 57), reporting excited states of ^{52}Cr as found in ^{55}Mn (p, α) ^{52}Cr reactions and inelastic proton scattering from chromium, however, led to further measurements in order to ascertain that the highest level excited in the decay of ^{52}Mn was different from any of the levels found by MAZARI et al.

Investigations into the decays of ^{57}Ni and ^{86}Y are discussed in Chapters 4 and 5. Gamma ray intensities, energies, coincidences, angular correlations, internal conversions, beta-gamma ray coincidences and beta ray measurements were carried out in order to determine the sequence, energies and spins of levels in ^{57}Co and ^{86}Sr respectively.

A description of an investigation on electron capture to positon emission branching ratios is given in Chapter 6. Beta-gamma ray coincidences have been measured with proportional counters, scintillation spectrometers and a beta ray spectrometer. Measurements carried out for allowed transitions on the decays of ^{22}Na, ^{44}Sc, ^{48}V, ^{52}Mn, ^{58}Co, and ^{57}Ni, and for first forbidden transitions on ^{84}Rb, are discussed.

SAMENVATTING

De gebruikte instrumenten worden behandeld in hoofdstuk 1. Dit gaat in op de constructie, ijking en het oplossend vermogen van de langelens-bêtaspectrometer. Details worden gegeven van de spectrometer en van een diafragma, dat nodig is om de schroeflijnvormige banen der positonen en negatonen te kunnen onderscheiden. Eveneens worden details gegeven van een scintillatieteller, voorzien van een lichtgeleider, en van een Geiger-Müller-teller. Andere instrumenten, die in de experimenten zijn gebruikt, zoals de NaI(Tl)-scintillatieteller, de richtingscorrelatie-opstelling en de proportionele telbuis, worden slechts in het kort beschreven.

Belangrijke aspecten der bêtatheorie, onderzocht als beschreven in het experimentele gedeelte van dit proefschrift (vooral in hoofdstuk 6), worden behandeld in hoofdstuk 2.

Hoofdstuk 3 vermeldt experimenten betreffende het radioactieve verval van ^{52}Mn. De oorspronkelijke bedoeling van dit onderzoek was de meting van de verhouding tussen elektronenvangst en positonenemissie. De publikatie van MAZARI e.a. (Ma 57) was aanleiding tot een verdergaand onderzoek, waaruit bleek dat de hoogste aangeslagen toestand in het verval van ^{52}Mn niet overeenkwam met een der niveaus, door MAZARI e.a. gevonden.

Onderzoekingen aan de desintegraties van ^{57}Ni en ^{86}Y worden beschreven in hoofdstukken 4 en 5. De verrichte metingen betreffen: intensiteiten, energieën en interne conversie van gammastralen, coïncidenties en correlaties tussen de richtingen van gammastralen, coïncidenties tussen gammastralen en positonen, intensiteiten en eindpunten van bêta-overgangen. Uit deze metingen zijn energieën en spins van niveaus in ^{57}Co en ^{86}Sr afgeleid.

Een onderzoek naar verhoudingen tussen elektronenvangst en positonenemissie wordt beschreven in hoofdstuk 6. Coïncidenties tussen gammastralen en positonen zijn gemeten met proportionele tellers, scintillatie-spectrometers en een bêtaspectrometer. Metingen in het geval van toegestane bêta-overgangen zijn verricht aan de desintegraties van de volgende isotopen: ^{22}Na, ^{44}Sc, ^{48}V, ^{52}Mn, ^{58}Co en ^{57}Ni, en in het geval van eenmaal verboden bêta-overgangen aan de desintegratie van ^{84}Rb.

REFERENCES

Al 55 ALLEN, R. A., BURCHAM, W. E., CHACKETT, K. F., MUNDAY, G. L., and REASBECK, P.; Proc. Phys. Soc. **68A** (1955) 681.

Ar 56 ARBMAN, E., and SVARTHOLM, N.; Ark. Fys. **10** (1956) 1.

B 58 BOEHM, F.; Phys. Rev. **109** (1958) 1019.

Ba 53 BAKER, J. M., BLEANEY, B., BOWERS, K. D., SHAW, P. F. D., and TRENAM, R. S.; Proc. Phys. Soc. **66A** (1953) 305.

Ba 55 BACKHOFEN, E. W., and HERBER, R. H.; Phys. Rev. **97** (1955) 743.

Be 34 BERKEY, D. K.; Phys. Rev. **45** (1934) 437.

Be 58 BENCZER, N., and WU, C. S.; see (Pe 58).

Bl 55 BLUE, J. W., and BLEULER, E.; Phys. Rev. **100** (1955) 1324.

Bo 55 BOCK, R., Max Planck Inst., Heidelberg; see (Wa 55).

Bo 58 BOEHM, F., and WAPSTRA, A. H.; Phys. Rev. **109** (1958) 456.

Br 50 BRUNER, J. A., and LANGER, L. M.; Phys. Rev. **79** (1950) 606.

Br 55 BRYSK, H., and ROSE, M. E.; ORNL 1830 report, Oak Ridge National Laboratory.

Bu 26 BUSCH, H.; Ann. Phys. **81** (1926) 974; Arch. Elektro. **18** (1927) 583.

Bu 52 BURHOP, E. H. S.; "The Auger Effect", Cambridge University Press (1952).

Bu 54 BURGUS, W. H., COWAN, G. A., HADLEY, J. W., HESS, W., SHULL, T., STEVENSON, M. L., and YORK, H. F.; Phys. Rev. **95** (1954) 750.

Bu 55 BURHOP, E. H. S.; J. Phys. Rad. **16** (1955) 625.

Ca 51 CANADA, R., and MITCHELL, A. C. G.; Phys. Rev. **83** (1951) 955.

Ca 53 CASSON, H., GOODMAN, L. S., and KROHN, V. E.; Phys. Rev. **92** (1953) 1517.

Cas 51 CASTNER, S. V.; University of California Unclassified Report UCRL-1099, (January 1951) (unpublished).

Ch 52 CHENG, L. S., DICK, J. L., KURBATOV, J. D.; Phys. Rev. **88** (1952) 887.

Co 55 Cork, J. M., Brice, M. K., and Smid, L. C.; Phys. Rev. **99** (1955) 703.
Co 56 Cook, C. S., and Tomnovec, F. M.; Phys. Rev. **104** (1956) 1407.

Da 51 Davidson Jr., J. P.; Phys. Rev. **82** (1951) 48.
De 44 Deutsch, M., Elliott, L. G., and Evans, R. D.; Rev. Sci. Inst. **15** (1944) 178.
Dr 56 Drever, R. W. P., Moljk, A., and Scobie, J.; Phil. Mag. **1** (1956) 942.

El 49 Elmore, W. C., and Sands, M.; "Electronics", McGraw-Hill Book Co., Inc. 1949.
En 51 Engelkemeir, D. W., Seiler, J. A., Steinberg, E. P., Winsberg, L., and Novey, T. B., paper 5 in Radiochemical Studies: The Fission Products; C. D. Coryell, N. Sugarman Editors, NNES, Div. IV, Vol. 9, McGraw-Hill Book Co., Inc. 1951.
En 57 Endt, P. M., and Braams, C. M.; Rev. Mod. Phys. **29** (1957) 683.

Fe 34 Fermi, E.; Z. Phys. **88** (1934) 161.
Fr 50 Friedlander, G., Perlman, M. L., Alburger, D., and Sunyar, A. W.; Phys. Rev. **80** (1950) 30.
Fr 56 Frauenfelder, H., Levine, N., Rossi, A., and Singer, S.; Phys. Rev. **103** (1956) 352.
Fr 57 Frauenfelder, H., Bobone, R., Von Goeler, E., Levine, N., Lewis, H. R., Peacock, R. N., Rossi, A., and De Pasquali, G.; Phys. Rev. **106** (1957) 386.

Ge 55 Gerholm, T. R.; Rev. Sci. Instr. **26** (1955) 1071.
Ge 56 Gerholm, T. R.; Handb. d. Phys. Bd. XXXIII, p. 609.
Gl 55 Glover, K. M., and Borrell, P.; J. Nuclear Energy **1** (1955) 214.
Gla 55 Glaubman, M. J.; Phys. Rev. **98** (1955) 645.
Go 46 Good, W. M., Peaslee, D., and Deutsch, M.; Phys. Rev. **69** (1946) 313.
Go 58 Goldhaber, M., Grodzins, L., and Sunyar, A. W.; Phys. Rev. **109** (1958) 1015.
Gr 42 Greuling, E.; Phys. Rev. **61** (1942) 568.
Gr 52 Graves, G. A., Langer, L. M., and Moffat, R. D.; Phys. Rev. **88** (1952) 344.

Ha 57 HAGEDOORN, H. L., and KONIJN, J.; Physica **23** (1957) 1069.
Ha 58 HAGEDOORN, H. L.; Thesis 1958, Technical University of Delft, Excelsior, The Hague 1958.
Har 58 HARMER, D. S., and PERLMAN, M. L.; unpublished values chosen in preference to the earlier values given by (Ko 55), the newer result being a direct measurement. (See also (Pe 58)).
He 44 HEITLER, W.; "The Quantum theory of Radiation", Oxford 1944.
Ho 49 HORNYAK, W. F., LAURITSEN, T., and RASMUSSEN, V. K.; Phys. Rev. **76** (1949) 731.
Ho 56 HOBSON, J. P., HUBBS, J. C., NIERENBERG, W. A., SILSBEE, H. B., and SUNDERLAND, R. J.; Phys. Rev. **104** (1956) 101.
Hu 52 HUDDLESTON C. M., and MITCHELL, A. C. G.; Phys. Rev. **88** (1952) 1350, Phys. Rev. **89** (1953) 903A.
Hu 56 HUISKAMP, W. J., STEENLAND, M. J., MIEDEMA, A. R., TOLHOEK, H. A., and GORTER, C. J.; Physica **22** (1956) 587.
Hy 51 HYDE, E. K., and O'KELLY, G. D.; Phys. Rev. **82** (1951) 944.
Hy 54 HYDE, E. K., FLORENCE, M. G., and STEPHENS, F. S.; UCRL-report No. 2813, University of California, Berkeley, (December 1954).
Jo 51 JOHANSSON, S., CAUCHOIS, Y., and SIEGBAHN, K.; Phys. Rev. **82** (1951) 275.
Jo 57 JOHNSON, N. R., and O'KELLY, G. D.; Phys. Rev. **108** (1957) 82.
Ka 56 KAFALAS, P., and IRVINE Jr., J. W.; Phys. Rev. **104** (1956) 703.
Ke 54 KEISTER, G. L.; Phys. Rev. **96** (1954) 855 I 6.
Ki 55 KILLION, L. E.; Thesis, Abstr. 15 858NSA9, 24B (1955).
Ko 41 KONOPINSKI, E. J., and UHLENBECK, G. E.; Phys. Rev. **60** (1941) 308.
Ko 55 KOERTS, L., MACKLIN, P., FARRELLY, B., VAN LIESHOUT, R., and WU, C. S.; Phys. Rev. **98** (1955) 1230.
Ko 56 KONIJN, J., VAN NOOIJEN, B., MOSTERT, P., and ENDT, P. M., Physica **22** (1956) 887.
Kr 54 KREGER, W. E.; Phys. Rev. **96** (1954) 1554.
La 56 LABERRIGUE-FROLOW, J., and RADVANYI, P.; J. Phys. Rad. **17** (1956) 944.

Le 54 LEWIS, I. A. D., and WELLS, F. H., "Millimicrosecond Pulse Techniques", London, Pergamon Press L.T.D. (1954).

Le 57 LEE, T. D.; "The Proc. Rehovoth Conf. Nucl. Structure 1957", North-Holland Publ. Co. (1958), Amsterdam.

Li 38 LIVINGOOD, J. J., and SEABORG, G. T.; Phys. Rev. **53** (1938) 765.

M 53 MARTY, N., LANGEVIN, H., and HUBERT, M. P.; J. Phys. Rad. **14** (1953) 663.

Ma 49 MAIENSCHEIN, F., and MEEM Jr., J. L.; Phys. Rev. **76** (1949) 899.

Ma 50 MACKLIN, P. A., LIDOFSKY, L. J., and WU, C. S.; Phys. Rev. **78** (1950) 318 C 5.

Ma 52 MAHMOUD, H. M., and KONOPINSKI, E. J.; Phys. Rev. **88** (1952) 1266.

Ma 53 MARQUEZ, L.; Phys. Rev. **92** (1953) 1511.

Ma 57 MAZARI, M., BUECHNER, W. W., and SPERDUTO, A.; Phys. Rev. **107** (1957) 1383.

Mo 51 MOSZKOWSKI, S. A.; Phys. Rev. **82** (1951) 35.

N 58 VAN NOOIJEN, B., KONIJN, J., and WAPSTRA, A. H.; Physica **24** (1958) 231.

Na 52 "Tables for the analysis of beta spectra", National Bureau of Standards, Applied Mathematics Series No. 13, U.S. Government Printing Office, Washington (1952).

No 50 NORDHEIM, L. W.; Phys. Rev. **78** (1950) 294.

No 57 VAN NOOIJEN, B., KONIJN, J., HEYLIGERS, A., VAN DER BRUGGE, J. F., and WAPSTRA, A. H.; Physica **23** (1957) 753.

No 58 VAN NOOIJEN, B.; Thesis 1958, Technical University of Delft, Erla, Amsterdam.

Nu 58 Nuclear Data Sheets, National Academy of Sciences—National Research Council, 2101 Constitution Ave., Washington U.S.A.

Os 47 OSBORNE, R. K., and DEUTSCH, M.; Phys. Rev. **71** (1947) 467 B 8.

Pe 46 PEACOCK, W. C., and DEUTSCH, M.; Phys. Rev. **69** (1946) 306.

Pe 54 PERLMAN, M. L., and WELKER, J. P.; Phys. Rev. **95** (1954) 133.

Pe 58 PERLMAN, M. L., WELKER, J. P., and WOLFSBERG, M.; Phys. Rev. **110** (1958) 381.

Pi 57 PIEPER, G. F., and HEYDENBERG, N. P.; Bull. Am. Phys. Soc. **2** No. 1 (1957) p. 69.

Po 56 PORTER, F. T., FREEDMAN, M. S., NOVEY, T. B., and WAGNER Jr., F.; Phys. Rev. **103** (1956) 921.

Ra 54 DE RAAD, B., MIDDELKOOP, W. C., VAN NOOIJEN, B., and ENDT, P. M.; Physica **20** (1954) 1278.

Ri 55 RIETJENS, L. H. TH., ARKENBOUT, G. J., WOLTERS, G. F., and KLUYVER, J. C.; Physica **21** (1955) 110.

Ro 49 ROSE, M. E., and JACKSON, J. L.; Phys. Rev. **76** (1949) 1540.

Ro 52 ROGGENKAMP, P. L., PRUETT, C. H., WILKINSON, R. G.; Phys. Rev. **88** (1952) 1262.

Ro 53 ROSE, M. E.; Phys. Rev. **91** (1953) 610.

Ro pr ROSE, M. E.; "Tables of internal conversion coefficients", private communication.

Ru 51 RUBY, L., and RICHARDSON, J. R.; Phys. Rev. **83** (1951)698.

Ru 56 RUDSTAM, G.; Thesis 1956, Uppsala, Sweden.

Sc 57 SCOBIE, J., and LEWIS, G. M.; Phil. Mag. **2** (1957) 1089.

Se 51 SELIGER, H. H.; Phys. Rev. **88** (1951) 408.

Se 54 SEHR, R.; Z. Phys. **137** (1954) 523.

Sh 54 SHERR, R., and MILLER, R. H.; Phys. Rev. **93** (1954) 1076.

Sh 56 SHERR, R., and GERHART, J. B.; Bull. Am. Phys. Soc. **1** (1956) 219.

Si 55 SIEGBAHN, K.; "Beta and gamma ray spectroscopy", North-Holland Publ. Co., Amsterdam, (1955).

Sl 55 SLACK, L., private communication in (Wa 55).

St 53 STERK, M. J., WAPSTRA, A. H., and KROPVELD, R. E. W.; Physica **19** (1953) 135.

Te 56 TEMMER, G. M., and HEYDENBURG, N. P.; Phys. Rev. **104** (1956) 967.

Ve 51 VERSTER, N. F.; Thesis 1951, University of Amsterdam.

Wa 50 WALTER, M., HUBER, O., and ZÜNTI, W.; Helv. Phys. Acta **23** (1950) 697.

Wa 55 WAY, K., KING, R. W., MCGINNIS, C. L., and VAN LIESHOUT, R.; "Nuclear Level Schemes A = 40 — A = 92", (June 1955), U.S. Atomic Energy Commission.

Wa 58 WAPSTRA, A. H., NIJGH, G. J., and VAN LIESHOUT, R., "Nuclear spectroscopy Tables", North-Holland Publ. Co., Amsterdam, in preparation.
We 55 WELKER, J. P., and PERLMAN, M. L.; Phys. Rev. **100** (1955) 74.
Wo 54 WONG, C.; Phys. Rev. **95** (1954) 765.
Wr 53 WRIGHT, B. T.; Phys. Rev. **90** (1953) 159.
Wu 49 WU, C. S., and FELDMAN, L.; Phys. Rev. **76** (1949) 697.
Wu 57 WU, C. S., AMBLER, E., HAYWARD, R. W., HOPPES, D. D., and HUDSON, R. P.; Phys. Rev. **105** (1957) 1413.

Zü 48 ZÜNTI, W.; Helv. Phys. Acta **21** (1948) 179.
Zw 57 ZWEIFEL, P. F.; Phys. Rev. **107** (1957) 329; Phys. Rev. **96** (1954) 1572.

STELLINGEN

I

De suggestie van MAZARI e.a. dat het 3161 keV niveau in ^{52}Cr gevoed wordt vanuit de grondtoestand van ^{52}Mn, is onjuist.

M. MAZARI, W. W. BUECHNER en A. SPERDUTO; Phys. Rev. **107** (1957) 1383. Hoofdstuk 3 van dit proefschrift.

II

De uit de metingen van (ε/β^+)-verhoudingen verkregen waarde van de fierz-term-parameter kan gebruikt worden voor een nauwkeurige berekening van de longitudinale polarisatie van elektronen.

Hoofdstukken 2 en 6 van dit proefschrift.

III

De (ε/β^+)-verhoudingen van eenmaal verboden, niet-unieke bêta-overgangen kunnen aanzienlijk afwijken van de waarden die de theorie voor toegestane bêta-overgangen voorspelt.

Hoofdstukken 2 en 6 van dit proefschrift.

IV

Bêta-gamma-coïncidentiemetingen zijn in vele gevallen in een proportionele teller nauwkeuriger uit te voeren dan in een magnetische bêtaspectrometer.

V

De waarde voor de totale desintegratie-energie van ^{113}Sn zoals gemeten door JUNG en POOL is in tegenspraak met de resultaten van GIRGIS en VAN LIESHOUT en van BHATKI e.a. Het is mogelijk een bevredigende verklaring voor het resultaat van de metingen van JUNG en POOL te geven.

R. G. JUNG en M. L. POOL; Bull. Am. Phys. Soc. **1** (1956) 172, E11; K. S. BHATKI, R. K. GUPTA, S. JHA en B. K. MADAN; Nuovo Cim. **6** (1957) 1461; R. K. GIRGIS en R. VAN LIESHOUT; Physica **24** (1958) in voorbereiding.

VI

De stralingsopbrengsten van de K-schil voor vanadium en mangaan zoals deze door JOHNSTON e.a. worden vermeld, zijn onjuist.

R. E. JOHNSTON, W. F. FREY en J. I. HOPKINS; Bull. Am. Phys. Soc. **3** (1958) 299, D4.

VII

De coëfficiënt van de Z^3-term in de semi-empirische formules van LABERRIGUE-FROLOW en RADVANYI en van BURHOP is nauwkeuriger te bepalen uit metingen van de Augeropbrengst dan uit die van de stralingsopbrengst.

E. H. S. BURHOP; J. Phys. Rad. **16** (1955) 625; J. LABERRIGUE-FROLOW en P. RADVANYI; J. Phys. Rad. **17** (1956) 944.

VIII

Er bestaat behoefte aan technische woordenboeken die periodiek worden aangevuld met een lijst van nieuwe woorden.

IX

Het verdient aanbeveling voor nieuwe buitenlandse technische termen zo spoedig mogelijk een passende Nederlandse vertaling vast te stellen.

X

Het is aan te bevelen bij het inbinden der tijdschriften in de bibliotheek van de afdeling voor Technische Fysica niet het laatst ingebonden exemplaar mee te geven als voorbeeld; het tijdstip van het inbinden van dezelfde tijdschriften bij de verschillende bibliotheken der T.H. dient bovendien te worden gecoördineerd.

XI

Verkeersborden met Nederlandse opschriften zoals „einde inhaalverbod" en „einde autoweg" dienen vervangen te worden door internationale verkeerstekens.

XII

Het verdient aanbeveling handenarbeid (slöjd voor jongens, huishoudelijk werk voor meisjes) verplicht te stellen bij het middelbaar onderwijs.

XIII

Daar de ingenieur over een grote taalvaardigheid moet beschikken, verdient het aanbeveling hem tijdens zijn studie de gelegenheid te bieden om een cursus in het juiste mondelinge en schriftelijke gebruik van zijn moedertaal te volgen.